

Skeletal Muscle Biomechanics Drives Intramuscular Transport
of Locally Delivered Drugs

by

Peter I-Kung Wu

B.S. Mechanical Engineering
University of California, Berkeley, 2000

SUBMITTED TO THE DEPARTMENT OF MECHANICAL ENGINEERING
IN PARTIAL FULFILLMENT OF THE REQUIREMENTS FOR THE DEGREE OF

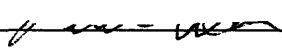
MASTER OF SCIENCE IN MECHANICAL ENGINEERING

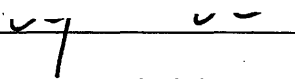
at the

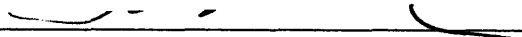
MASSACHUSETTS INSTITUTE OF TECHNOLOGY


September 2007

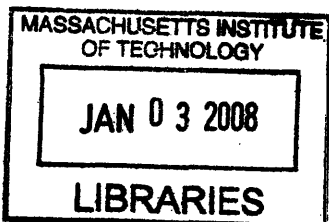
© 2007 Massachusetts Institute of Technology
All rights reserved

Signature of Author:  Department of Mechanical Engineering
August 30, 2007

Certified by:  Elazer R. Edelman
Thomas D. and Virginia W. Cabot Professor of Health Sciences and Technology
Thesis Supervisor

Certified by:  Peter T. C. So
Professor of Mechanical and Biological Engineering
Thesis Reader, Mechanical Engineering

Accepted by:  Lallit Anand
Professor of Mechanical Engineering
Chairman, Committee on Graduate Students



ARCHIVES

Skeletal Muscle Biomechanics Drives Intramuscular Transport of Locally Delivered Drugs

by

Peter I-Kung Wu

Submitted to the Department of Mechanical Engineering
on August 30, 2007 in Partial Fulfillment of the
Requirements for the Degree of
Master of Science in Mechanical Engineering

ABSTRACT

Introduction: Effective local drug delivery to contractile tissues such as skeletal muscle requires a thorough understanding of the impact of mechanical loads on intramuscular pharmacokinetics. Current preparations for studying skeletal muscle biomechanics typically use mounting techniques that lead to mechanical disruption of the tissue, which can create drug transport artifacts. In order to accurately study mechanical influences on drug transport, experimental techniques and setups need to meet the particular design requirements of both biomechanical testing setups and local drug delivery preparations. Studies of intramuscular pharmacokinetics require anatomically physiologic and functionally viable conditions for accurate drug transport. In this study, we invent a method for the surgical isolation and mounting of whole skeletal muscles of small rodents that maintains the physiologic configuration of the tissue. We also invent a mounting assembly and dynamic loading system designed appropriately for *in vitro* drug transport studies. We present an effective protocol for tissue processing and visually quantifying intramuscular distribution of drug. With the primary objective of investigating muscle pharmacokinetics, we use these techniques in a study to elucidate the influence of mechanical loading on the intramuscular transport and distribution of locally delivered drug.

Methods and Results: The dynamic loading system was characterized and used to investigate intramuscular transport of aqueous macromolecular drug. The loading system was designed to achieve a maximal force, velocity, and acceleration of up to 72N, 0.45m/s, and 8.5m/s², respectively, for imposing cyclic strain on soleus muscle samples. Total compliance of the series assembly from the motor to muscle mounting blocks was less than 0.0057 ± 0.002 mm/N. Under proportional-integral-derivative (PID) control with a positional resolution of 20 μ m, the loading system achieved a positional precision of $\pm 60\mu$ m or better for sinusoidal reference curves required in our studies. Tissue architectural and functional integrity as well as a technique for quantifying intramuscular fluorescent dextran were validated using the loading system. Histologic studies of rat soleus showed that interstitial porosity was consistent in tissues subjected to mechanical loading for 70 minutes, and changes in porosity were independent of the nature of imposed static (0-15% fixed strain) and cyclic (3Hz sinusoidal strain with amplitude of 2.5% oscillating about mean strains of 5-15%) loads. Permanent changes in architectural

integrity depended only on the duration of time spent *in vitro* after isolation, in which porosity increased at the tissue edge from $11.1 \pm 3.3\%$ to $21.0 \pm 6.1\%$ over the course of a 70-minute incubation. The source solution used for local delivery of drug (dextran) preserved tissue functional viability, allowing muscle samples to maintain isometric twitch contractile activity at a rate of 3Hz for at least 1 hour. The active twitch force-length characteristic of soleus samples showed $0.24 \pm 0.06\text{N}$ at 0% strain, a maximum of $0.35 \pm 0.06\text{N}$ at 10% strain, and a decrease to $0.19 \pm 0.06\text{N}$ at 20% strain. Isometric twitch contractile force was at least 0.19N when measured every 15 minutes over a 2 hour period. Fractional volume of distribution for dextran was 84% of the bulk source concentration over the range of $0.1\mu\text{M}$ -1mM bulk concentrations, and demonstrated the non-binding properties of dextran. Fluorescence intensity of FITC-dextran equilibrated in soleus tissue exhibited a linear dependence on dextran concentration. Dextran penetration and distribution in soleus muscles under either cyclic (3Hz, 0-20% peak-to-peak) or static (fixed at 0%) tensile strain for 80 minutes was quantified by fluorescent imaging. Penetration depth of 1mM 20kDa FITC-dextran at the planar surfaces of the soleus increased significantly from $0.52 \pm 0.09\text{mm}$ under static strain to $0.81 \pm 0.09\text{mm}$ under cyclic strain. Penetration at the curved margins of the soleus was significantly greater than at planar surfaces by a factor of 1.57 and 2.52 under static and cyclic strain, respectively. Penetration at curved surfaces increased to a greater extent, by a factor of 1.6, than at planar surfaces under cyclic strain.

Discussion: This investigation demonstrated that dynamic, or cyclic, tensile strain impacts the penetration and distribution of aqueous drug in skeletal muscle. In the course of this study, we established an effective and robust experimental system and protocol for studying mechanical influences on intramuscular pharmacokinetics. The innovation of our surgical isolation and mounting technique allowed for the investigation of an isolated soleus muscle without disrupting the muscle, tendons, or physiologic bone attachments. The mounting device enabled muscles to be secured in a physiologic *in situ* configuration, to undergo more physiologically distributed tensile stresses and strains, and to be mechanically loaded while incubated *in vitro* in drug. Thus, the method and device eliminated the artificial tissue stresses typically introduced by current tissue handling techniques that could result in drug transport artifacts. While effective as a standalone biomechanical testing preparation, characterization and validation of the dynamic loading system with a protocol for tissue processing and quantitative assessment of intramuscular fluorescent drug distribution demonstrated that it is a novel and robust preparation for investigating both tissue biomechanics and pharmacokinetics. With the finding from the present study that dynamic loading influences intramuscular drug transport in an architecturally dependent manner, we intend to investigate the isolated effects of different mechanical loading regimens on drug transport to establish a broader understanding of muscle pharmacokinetics. It is hoped that the insights from this work will guide the design and application of future local drug delivery strategies to mechanically active tissues.

Thesis Supervisor: Elazer R. Edelman

Title: Thomas D. and Virginia W. Cabot Professor of Health Sciences and Technology

TABLE OF CONTENTS

ABSTRACT	3
TABLE OF CONTENTS	5
TABLE OF FIGURES	8
1. INTRODUCTION	9
2. DESIGN OF A TISSUE HANDLING TECHNIQUE AND MECHANICAL LOADING SYSTEM	14
2.1 General Description	14
2.2 Surgical Isolation Protocol	14
2.3 Mounting Configuration	16
2.4 System Design Considerations	18
2.5 Mechanical Loading System	20
2.5.1 Mounting Blocks and Static Assembly	22
2.5.2 Dynamic Loading System	24
2.5.3 Motion Actuation and Control	27
3. METHODS	29
3.1 Characterization of Dynamic Loading System	29
3.1.1 System Compliance	29
3.1.2 Motor Tuning	29
3.2 Evaluation of Tissue Properties	30
3.2.1 Architectural Integrity	30
3.2.2 Functional Viability	31

3.2.3	Force-Length Relationships	33
3.3	Quantification of Drug Transport	33
3.3.1	Fractional Volume of Distribution	33
3.3.2	Drug Transport Under Mechanical Loading	35
3.3.3	Tissue Processing and Measurement of Drug	36
4.	RESULTS	38
4.1	System Compliance	38
4.2	Motor Tuning	39
4.3	Architectural Integrity	40
4.4	Functional Viability	41
4.5	Force-Length Relationships	42
4.6	Fractional Volume of Distribution	43
4.7	Measurement of Drug	45
4.8	Drug Transport Under Mechanical Loading	46
5.	DISCUSSION	49
5.1	Design of a New Biomechanics Preparation and Mechanical Loading System	50
5.1.1	Tissue Isolation and Mounting	51
5.1.2	Dynamic Loading System	53
5.2	System Validation	54
5.2.1	Dynamic Loading	54
5.2.2	Tissue Preservation	55

5.2.3	Quantification of Drug Transport	57
5.3	Intramuscular Pharmacokinetics	58
5.3.1	Equilibrium Distribution of Drug	58
5.3.2	Drug Penetration and Distribution Under Mechanical Influence	61
5.3.2.1	Validation of Experimental System	61
5.3.2.2	Drug Penetration and Distribution	62
5.3.2.3	Impact of Dynamic Loading	63
5.3.2.4	Interaction Between Loading and Architecture ...	64
5.4	Conclusions	66
6.	FUTURE STUDIES	68
6.1	Static Strain	68
6.2	Drug Physical Property	68
6.3	Dynamic Strain	68
6.4	Contraction	69
6.5	Computational Model	69
7.	REFERENCES	70
8.	ACKNOWLEDGMENTS	75
	APPENDIX A: MATLAB SOURCE CODE TO SIMULATE RESTING MUSCLE RESPONSES TO LENGTH PERTURBATIONS	76
	APPENDIX B: COMPONENT DESIGNS	79
	APPENDIX C: MOTOR SPECIFICATIONS	97

TABLE OF FIGURES

FIGURE 1: Mounting Configuration and Blocks	17
FIGURE 2: Model of Resting Muscle Response to Length Perturbations ...	19
FIGURE 3: Static Mounting Assembly	23
FIGURE 4: Dynamic Loading System	26-27
FIGURE 5: Mounting Configurations for Assessing Functional Integrity...	32
FIGURE 6: System Compliance	38
FIGURE 7: Motor Response Under Maximal Performance Requirements ..	39
FIGURE 8: Tissue Integrity	41
FIGURE 9: Force-Length Relationship of the Soleus	42
FIGURE 10: Incubation and Elution Equilibrium Times	43
FIGURE 11: Equilibrium Distribution Measurements	44
FIGURE 12: Fluorescence Intensity vs. Equilibrium Tissue Concentration ..	46
FIGURE 13: Quantification of Fluorescent Drug	47
FIGURE 14: Impact of Mechanical Loading on Drug Transport	48
FIGURE 15: Constant Drug Source	48
FIGURE 16: Equilibrium Distribution Model	59

1. INTRODUCTION

Muscle tissue presents an exclusive drug transport environment in which dynamic mechanical motion and loading may be a predominant influence on the pharmacokinetics of locally delivered agents. These motions and loads, which are shaped by both structure and function of the muscle, can present significant dynamic physical influences on aqueous drug transport by means of their effect on modulating extracellular space or fluid distribution [1].

The effects of mechanical loading on the transport of local agents have been investigated in a variety of mechanical tissues. Studies have examined the effects of tension-compression on solute and dextran transport in cartilage [2-4], static tensile loading on the diffusion of water in Achilles tendon [5, 6], and stretch on the transmural transport of albumin, LDL, and Evans Blue dye in the arterial wall [7, 8]. Similar studies in skeletal muscle have investigated the impact of contraction on the bulk uptake of substrates like glucose [9, 10]. However, no studies have investigated the effects of mechanical loading on the distribution and transport – not just the total uptake – of local agents in the interstitial space of skeletal muscle. With the advent of local drug delivery, and with the present clinically motivated need for effective strategies to locally deliver therapeutic angiogenic growth factors to ischemic muscles [11], a quantitative knowledge of the pharmacokinetics in muscle is critically important. Thus, the goal of this study is to elucidate a fundamental understanding of the impact of mechanical loading on drug transport in skeletal muscle.

Given that there are little data and prior experimental models in the literature on this topic, we present an innovative experimental approach and associated system of devices designed to determine the impact of mechanical loading on aqueous drug transport in muscle. The approach and devices integrate the specific design requirements of both biomechanical testing and *in vitro* drug delivery preparations.

Preparations for studying whole skeletal muscle biomechanics have involved invasive procedures using both *in situ* and *in vitro* preparations. However, the surgical isolation and muscle mounting methods typically used in these studies disrupt the physiologic anatomy and configuration of the intact muscle bundle. Most isolation techniques leave the tendons on a muscle, such as the soleus, intact so that they may be used for mounting. However, this also eliminates any support provided by bony attachments that helps to maintain the physiologic configuration of the muscle-tendon unit and thereby affects the physical dimensions and force transmission through the muscle bundle. While other isolation techniques leave a small piece of calcaneus attached to the distal tendon, the piece serves only as an anchoring point to prevent slippage of suture tying the tendon [12, 13] and is not used for mounting the muscle in a physiologic configuration. And, the few techniques that actually use the bony attachments for mounting do so without an adequate means of fixing the bone segment to secure the orientation of the tissue [14, 15].

Current mounting methods applied on the intact tendon or directly on the muscle itself rely mostly on suture thread or wires [12, 13, 16-19], chains [20], clamps [21-23], pins [24-26], hooks [14, 27, 28], or fixing rods [14] to hold the samples in place. However, few of these techniques maintain physiologic tendon or muscle bundle

configuration rigorously enough for studies of intramuscular drug transport, which require physiologic architecture and functional force transmission to be preserved. By their very mechanism, sutures, chains, and clamps distort tendon and muscle anatomy, hooks disrupt muscle integrity and mechanical continuity, and fixing rods do not insure that bone-tendon orientation is accurately recreated or maintained.

Such architectural disruption of the tissue during surgical isolation and mounting may result in drug transport artifacts because drug transport and distribution depend highly on the architectural state of the target tissue. In the case of a mechanically active tissue such as muscle, in which mechanical function and architectural configuration are intimately related [29], architectural disruption furthermore disrupts mechanical properties and performance, whose impact on drug transport and distribution is the primary focus of this study. Consequently, these traditional experimental preparations are inadequate for studies of intramuscular pharmacokinetics under mechanical loading. Pharmacokinetic studies that seek to quantify and visualize the intramuscular distribution, and not simply the total uptake, of drug require isolation and mounting methods that more rigorously maintain both the physiologic architecture and mechanical function of muscle.

Additionally, accurate drug transport requires functional viability of tissues. Because viability dictates both architectural integrity and mechanical function of muscles, a further requirement for pharmacokinetic studies is a local drug delivery setup that effectively maintains functionally viable and mechanically active tissue. *In situ* preparations for electrophysiological studies have been devised to immerse muscles in solution by forming a pocket out of overlying skin flaps [12, 15, 20, 30-32]. Such

preparations offer a feasible method to incubate tissues in drug as well as the advantage of maintaining muscle viability and physiologic configuration. However, they would be ineffective for local drug delivery as surrounding tissues forming the pocket would absorb drug and alter the concentration of the source bath. Moreover, *in situ* preparations typically require elaborate and inconvenient stereotaxic setups [12, 13, 15, 20, 30, 31, 33]. Therefore, a convenient and effective preparation for both mechanical testing and local drug delivery to muscles under architecturally physiologic and functionally viable conditions is required.

In the present study we invent a tissue handling approach and associated mechanical loading system designed suitably for drug transport studies and use this system to investigate the transport and distribution of locally delivered, aqueous macromolecular drug in skeletal muscle under mechanical loading. The study of accurate drug transport requires particular handling of tissue samples to avoid introducing disturbances to architectural integrity and functional viability that could result in transport artifact. Therefore, our tissue handling approach consists of a method for surgical isolation, explantation, and mounting of small rodent soleus muscles that allows for investigating tissue mechanics without disrupting the muscle, its tendons, or physiologic bone attachments, and without loss of physiologic dimensions and tone. The mechanical loading system consists of a mounting assembly and dynamic loading system for investigating intramuscular transport of locally delivered drugs in association with control of muscle biomechanics. The innovation of the technique and associated mounting assembly allows muscles to be held in a physiologic configuration. This enables muscles to undergo more physiologically distributed tensile strains and stresses

as they would experience in an *in situ* configuration, thereby eliminating artificial tissue stresses imposed by regular handling methods such as sutures, hooks, or clamps that could introduce drug transport artifacts. The loading system enables dynamic mechanical testing to be performed on physiologically mounted tissue samples while they incubate in an *in vitro* drug bath that maintains muscle functional viability. Along with this system, we present a protocol for tissue processing and visually quantifying intramuscular distribution of fluorescent drug. We validate and use the experimental approach and system in our primary aim to study muscle pharmacokinetics to determine whether cyclic tensile loading affects drug transport in soleus tissues.

2. DESIGN OF A TISSUE HANDLING TECHNIQUE AND MECHANICAL LOADING SYSTEM

2.1 General Description

This is a method for the surgical isolation and mounting of isolated, whole soleus muscles of small rodents, as well as the associated mounting assembly and dynamic loading system designed for investigating the intramuscular transport of locally delivered drugs under mechanical loading. The method and mounting device are uniquely designed for mounting isolated muscle in a physiologic *in situ* configuration without physical disruption to the soft tissues or bone attachments in order to eliminate experimentally imposed mechanical sources of drug transport artifacts. The method and mounting device are also robust enough to be incorporated into existing preparations or setups used in general studies of muscle biomechanics. The dynamic loading system enables biomechanical testing to be performed on muscle samples while they are immersed in a drug bath, under functionally viable conditions, and thereby delivers the diverse functional capabilities of both biomechanical testing and *in vitro* drug delivery preparations.

2.2 Surgical Isolation Protocol

Male Sprague-Dawley rats weighing 450-470g are administered 1000U of Heparin via intraperitoneal injection 5 minutes prior to euthanasia with inhaled carbon dioxide. Thoracotomy is performed immediately after euthanasia, and 60ml of Krebs-Henseleit-BDM (KH-BDM) solution (118.1mM NaCl, 4.7mM KCl, 2.5mM CaCl₂,

1.2mM MgSO₄, 1.2mM KH₂PO₄, 25mM NaHCO₃, 11.1mM Glucose, supplemented with 1mM Sodium Pyruvate, 1mM Isoleucine, 1mM Leucine, 1mM Valine, and 5mM butanedione monoxime (BDM) at pH 7.4) that is oxygenated with 95% O₂ / 5% CO₂ gas mixture is infused down the aorta to relax and preserve the tissues of the lower body of the rat during the surgery.

The soleus is surgically exposed in one of the distal hindlimbs. The skin is opened by sharp dissection. The overlying gastrocnemius and plantaris are separated from the soleus and excised by both sharp and blunt dissection. Fascial connections are dissociated from the soleus by blunt dissection. The tendon attachments of the overlying muscle bundles at the tuber calcanei and the head of the fibula are dissociated from the tendons of the soleus. The length of the soleus muscle is measured *in situ* between its proximal and distal myotendinous junctions while flexing the knee and ankle joints at 90°. In our study, this *in situ* length is referred to as the nominal length, and was measured using a Mitutoyo Digimatic caliper with a precision of ±0.01mm.

The calcaneus is then resected from the foot by separating it from its ligamentous attachments to the talus, cuboid, navicular, and 5th metatarsal. The tuberosities on the calcaneus are trimmed away using bone cutters. The soleus is gently lifted from underlying muscle bundles – the peroneus longus and flexor hallucis longus – as fascial connections to these muscles are cut by sharp dissection. This procedure also detaches the soleus from the diaphysis of the fibula. While holding the soleus away from the rest of the limb, the diaphysis and proximal epiphysis of the fibula are separated from surrounding muscle by sharp dissection. The head of the fibula is sheared from the lateral condyle of the tibia. The fibula is then broken at mid-diaphysis to complete the

resection of the soleus muscle along with its tendinous attachments, the head of the fibula, and the tuber calcanei still intact.

During surgical isolation and extraction, the soleus is superfused with KH-BDM to prevent drying. The surgical isolation procedure is then repeated for the soleus of the contralateral limb while the first excised soleus is held at its nominal length using the mounting assembly while sitting in regular Krebs-Henseleit (KH) loading solution (118.1mM NaCl, 4.7mM KCl, 2.5mM CaCl₂, 1.2mM MgSO₄, 1.2mM KH₂PO₄, 25mM NaHCO₃, 11.1mM Glucose, supplemented with 1mM Sodium Pyruvate, 1mM Isoleucine, 1mM Leucine, and 1mM Valine at pH 7.4) that is oxygenated with 95% O₂ / 5% CO₂ gas mixture and chilled on ice.

2.3 Mounting Configuration

The excised whole muscle bundle plus its tendons and bone segments are fixed onto the mounting blocks by inserting the bone segments into angled slots in the blocks (Figure 1). The slots secure the bone segments by mechanical fit and leverage, which holds the segments at an acute angle in relation to the axis of the muscle without the need for additional fastening mechanisms. The mechanical fit prevents slippage and rotation of the specimen, and leverage on the bones enables them to transmit tensile forces to the tendons and muscle. The blocks and mounting configuration maintain the *in situ* orientation of the myotendinous junctions and tendinous attachments with respect to the bone segments. The mounting blocks suspend the soleus muscle between its two ends in an *in situ* configuration via its own physiologic attachments, preserve the physical dimensions of the muscle, and eliminate any disruption or distortion to the muscle or

tendons. The mounting blocks enable tensile force to be applied to only the bones, and to be transmitted to the muscle through its tendinous attachments without the use of sutures, hooks, or clamps.

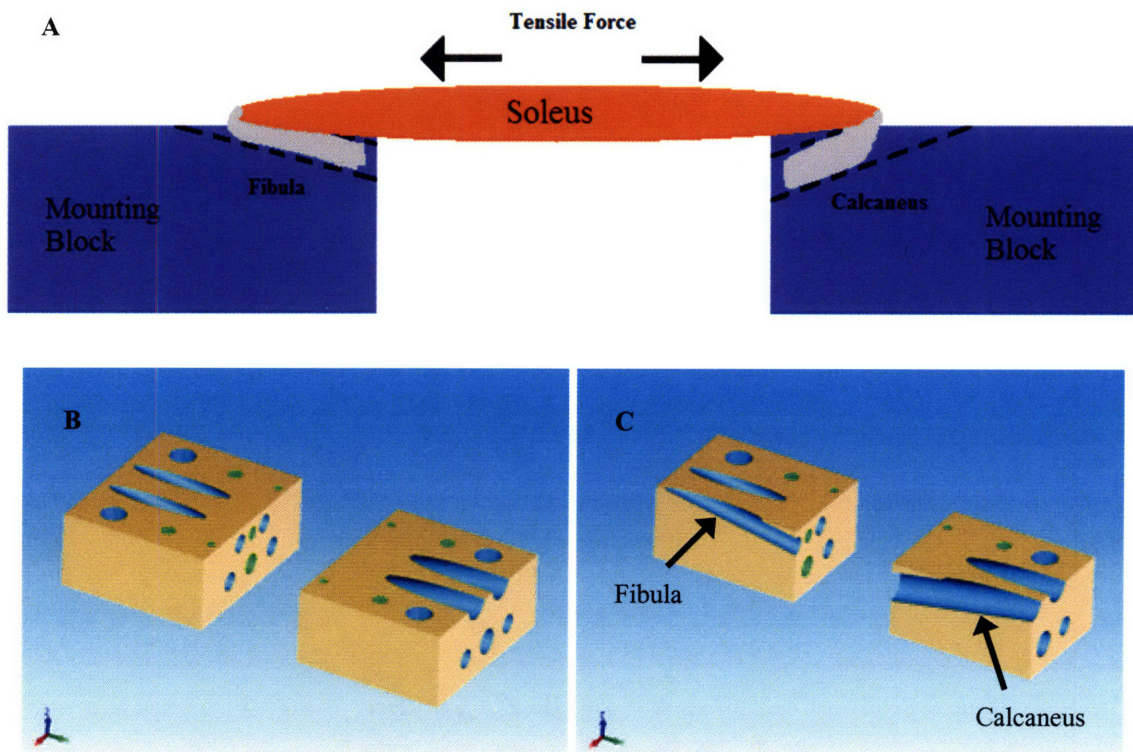


Figure 1. Mounting configuration and blocks. A) The mounting configuration of the isolated soleus and its natural bone attachments in the mounting blocks. The mounting blocks secure the bone segments at an acute angle in relation to the axis of the muscle without disruption to the muscle or tendons by sutures, hooks, or clamps. Tensile force is transmitted from the bone segments to the muscle in a physiologic manner to preserve tissue dimensions and configuration. B) The Solidworks design and rendering of the mounting blocks. The physical design and orientation of the slanted slots in the mounting blocks enables them to secure bone segments in place without the use of fixtures. C) A cross-sectional view of the mounting blocks showing the internal course of the slanted slots through the blocks (arrows).

2.4 System Design Considerations

Materials selection and motor sizing for the dynamic loading system were determined based on numerical simulations of the passive material properties of muscle in response to externally applied changes in length. A one-dimensional, lumped-parameter, viscoelastic model of resting muscle was used to simulate the passive force response to both step and cyclic uniaxial mechanical strain. The validity of a one-dimensional model is based on the uniformity of both the cross-sectional geometry and mechanical properties along the length of the uniaxial muscle (soleus) used experimentally.

The model consists of two viscoelastic units (K_1, C_1 and K_2, C_2) both coupled in parallel with an elastic element (K_0), and in series with an inertial mass (M) (Figure 2). Values from the literature for muscle length, 10mm ($20\text{mm} \div 2$ for symmetrical motion of the mounting blocks in the dynamic loading system) and cross-sectional area, 20mm^2 , as well as muscle mass plus estimated inertial mass of the mounting blocks, 200g, were used in the model along with the elastic and viscous parameter values from Loeffler, et. al. [34] In these simulations, length perturbations to no more than 20% of the muscle length were used for both the step and sinusoidal strain inputs to probe the properties of the resting muscle.

The lumped-parameter model was simulated in Matlab. The passive tension developed by the muscle in response to a step change in length was simulated in the time domain. The frequency response of the muscle to sinusoidal length perturbations was simulated using a state space characterization of the model. The Bode plot generated for the frequency response shows the magnitude conversion factor between the perturbation

input and force output of the muscle, as well as the phase response, over a range of frequencies (Figure 2D). Matlab source codes for these simulations are shown in Appendix A.

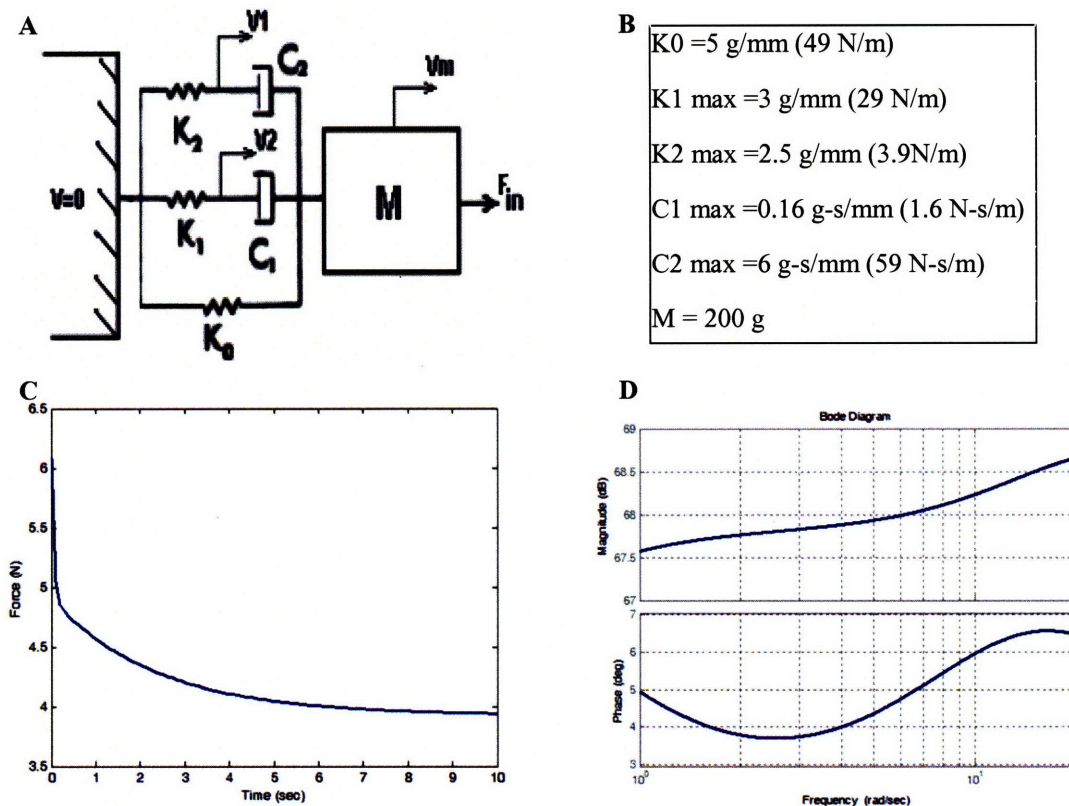


Figure 2. Model of resting muscle response to length perturbations. A) The one-dimensional, lumped-parameter, viscoelastic model of resting muscle used for materials selection and motor sizing of the dynamic loading system. B) The parameter values for the viscous, elastic, and mass elements used to simulate the model. C) Passive tension developed in response to a step in length change of 2mm. Peak passive force developed was 6N. D) Frequency response. The magnitude conversion factor at 3. Thus, a 2mm perturbation input at 3Hz yields a 5.4N force response.

The upper bound force requirements for the loading system were determined using the passive force response to a 2mm step in length change (20% strain of a 10mm length of muscle), and frequency response to a 2mm perturbation at 3Hz frequency (the maximum rate required in our loading experiments). These peak forces were 6N and

5.4N, for the static and cyclic strain conditions, respectively. Upper bound velocity and acceleration requirements were determined using a sinusoidal displacement profile with 3Hz frequency and 2mm amplitude. These forces, velocity, and acceleration were used with a factor of safety of 2 and sample number of 6 to specify peak performance requirements for the motor. The requirements for peak force, velocity, and acceleration were determined to be 72N, 0.45m/s, and 8.5m/s², respectively.

2.5 Mechanical Loading System

The mechanical loading system is designed to allow for the study of isolated muscle bundles in a physiologic *in situ* configuration, with intact myotendinous and tendinous-bony junctions. The system consists of two major components: 1) corrosion resistant mounting blocks and 2) a dynamic loading system. Designs and drawings of the components in the system were made using Solidworks and are shown in Appendix B.

The pair of conjugate mounting blocks suspends a pair of soleus muscles by their physiologic bone attachments while maintaining the muscles in an *in situ* configuration and preserving architectural dimensions. The mounting blocks provide an independent means for holding muscle specimens and are robustly designed to be applicable in general biomechanics studies and incorporated into existing setups or preparations. In this study, the mounting blocks can be secured in a “fixed,” or static, mounting assembly as a standalone device to provide an independent means to impose static tensile loading at user-defined fixed strains on muscle samples (Figure 3). Or, they can be disengaged from the fixed assembly and individually attached onto the dynamic loading system to

serve as mounting fixtures that hold samples for automated dynamic, or cyclic, tensile loading (Figure 4).

The static mounting assembly may be used on muscle samples for imposing static strain; investigating passive tensile force; or measuring isometric or isotonic contraction force, velocity, or displacement. The assembly allows for static tensile loading to be performed in either a horizontal or vertical orientation, and specifically enables the muscle samples to be immersed in select media and incubated in a well-stirred and oxygenated solution during loading. The assembly can also accommodate the attachment of weights (when orientated vertically) and load cells or force transducers.

The dynamic loading system imposes automated, cyclic or oscillatory, and high force loads on mounted samples. It features the full functionality of a biomechanical test instrument with the unique capability to implement its mechanical utilities while tissue samples are immersed in well-stirred and oxygenated media or maintained in a local drug delivery preparation. The system is driven by a linear motor but is designed to accommodate a range of driving sources, such as a linear motor, rotary motor with cam or belt drive, or ball screw drive for actuating the mechanical loading of samples. The loading arrangement can be configured to impose isotonic, isometric, eccentric, or concentric strain. Strain can be imposed either symmetrically or asymmetrically through independent control of the displacement and fixation of the two mounting blocks. These different configurations allow for potential measurement of tensile forces using a load cell that can be attached to the loading system or of strain of the sample by quantifying the displacement of the mobile block. The loading setup can be orientated for loading to be performed along either a horizontal axis (for drug delivery studies on incubated

samples) or a vertical axis (for applying dynamic loads with the option of attached weights on non-incubated samples).

2.5.1 Mounting Blocks and Static Assembly

The following descriptions with Roman numbering refer to the labels in Figure 3. Two Polycarbonate (Lexan) blocks of equal size are each machined with 2 primary through-holes that run at a 10° angle from the top surface of the block (i) to serve as the mounting holes for bone segments. These holes on each block are sized to fit the respective bone (fibula or calcaneus) that they secure to insure a proper mechanical fit with the bone. A pair of tapped through-holes (ii) on each block that run from the top to the bottom surface of the block offer the option of attaching clamping bars to secure the bones to the block. The use of bar clamps also serves as an option for further securing the samples but is unnecessary for most general purposes.

For use in the static mounting assembly, each block is machined with a pair of through-holes (iii) that run in the direction of the axis of the muscle samples. Stainless steel rods (iv) pass through these holes and co-align the two blocks. The rods serve as guide-rails for the two blocks to slide on during axial displacement. Set screws that engage the guide-rails are used to lock the Lexan blocks at user-defined fixed positions along the guide-rails. Each block is further machined with a center through-hole (v) that also runs in the direction of the axis of the samples. This hole is tapped in the fibula mounting block but untapped in the calcaneus mounting block. These two holes allow a #8-32 thread lead screw (vi) to be used to set and fix the separation distance of the blocks with respect to each other. The lead screw is held in place in the calcaneus block by

locknuts (vii) and adjusts the displacement of the fibula block with a resolution of 0.8mm per turn. The lead screw can also be locked in a fixed position by a set screw to fix the separation distance of the two blocks. A set of through-holes (viii) that run from top to bottom allow for the attachment of the mounting blocks to the motor-actuated, dynamic loading system. Figure 3 shows the mounting blocks in the static assembly and with soleus muscles mounted.

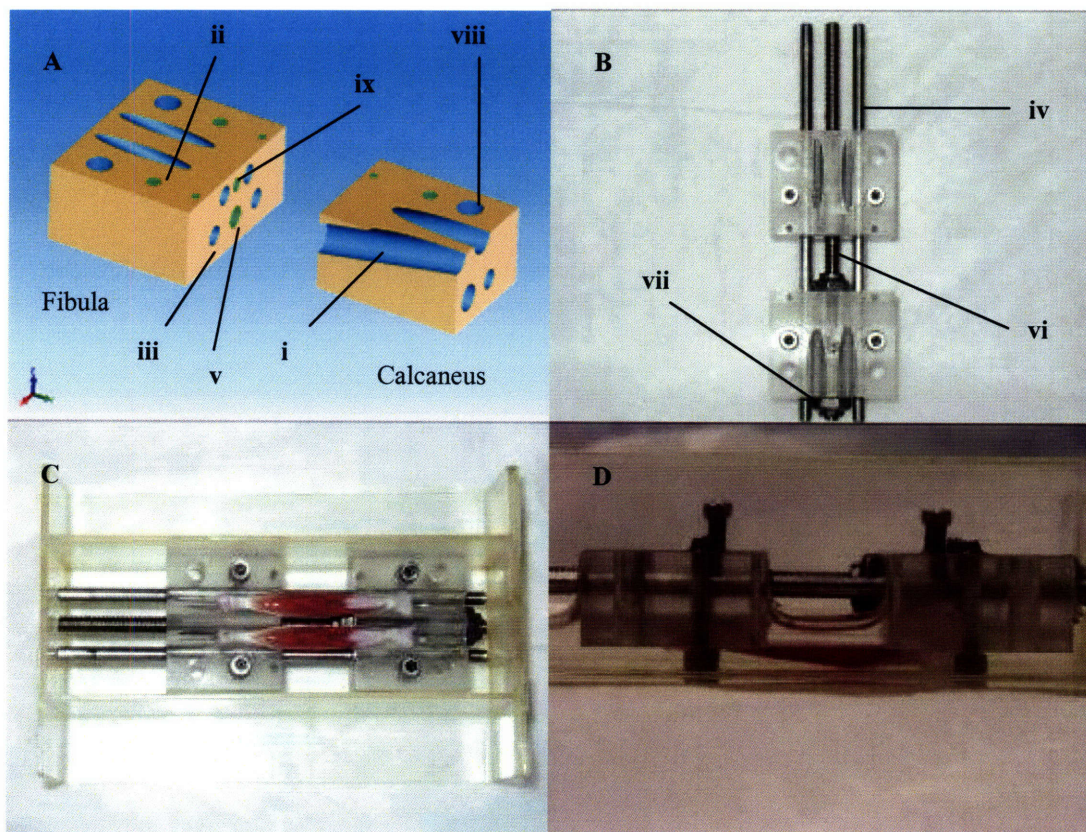


Figure 3. Static mounting assembly. The mounting blocks hold and maintain physiologic configuration of muscle samples using their natural bony attachments as strain transmitters rather than as restraining devices alone. A) Design of the mounting blocks. Slanted through-holes are sized appropriately for the bone segment (fibula or calcaneus) that they secure. B) The fixed, or static, mounting assembly applies static tensile strain on mounted muscle samples. C) Soleus muscles are mounted by securing the calcaneus and fibula without the use of fixtures. Strain can be applied while the samples are immersed in select media and incubated in a well-stirred and oxygenated solution. D) The simple mounting method allows muscles to incubate in a minimal volume of solution to conserve drug source and avoid the use of excessive, suprapharmacologic doses in transport studies. The fixed assembly can be disassembled and the mounting blocks used as the mounting fixtures in the dynamic system.

A tapped through-hole (ix) at the centerline of the fibula mounting block enables the block to be attached to a support (to a wall if aligned along a horizontal axis of displacement, or to an overhanging structure if aligned along a vertical axis of displacement), to a weight (for applying constant force along a vertical axis), or to a load cell.

2.5.2 Dynamic Loading System

The following descriptions with Roman numbering refer to the labels in Figure 4. Similar to the design of the fixed mounting assembly, 2 stainless steel guide-rails (i) co-align 2 equally sized Lexan sliding blocks (ii) that run on the rails by means of ceramic bearings (iii). The ceramic bearings reduce the kinetic friction of the sliding blocks to facilitate their cyclic motion during dynamic loading. The guide-rails are locked into support brackets (iv) at either end by means of slotted spring pins (v). This entire unit, consisting of sliding blocks, guide-rails, and support brackets, is mounted atop a platform base, on which is also fixed the linear motor (vi) that actuates the cyclic loading. The motor is mounted to the platform base by means of its mounting flange.

The rotor, or slider, of the linear motor runs through a center hole in one of the support brackets to attach to the outer side of one of the Lexan sliding blocks (vii). The sliding block is attached to end of the slider, which has a threaded borehole on its end, by means of a M8 hex screw (viii). An oversized screw hole is machined in the sliding block to compensate for any errors in axial alignment between the block and the end of the slider. Care was also taken to prevent or compensate for errors in parallelism

between the sliding blocks and the linear motor by means of precisely aligning the guide-rails and the linear motor during design, manufacture, and assembly of the system.

The opposite sliding block has a tapped through-hole (ix) that allows for it to be fixed to the support bracket or to a force transducer that may be attached to the support bracket. A rack and pinion assembly is situated at the midpoint of each guide-rail by set screws (x). The pinion rotates about a shaft fixed to the guide-rail and a rack is fixed to each sliding block on either side. This assembly enables the symmetric displacement of the sliding blocks about the midline of the guide-rails. It also actuates the coordinated and simultaneous motion of both sliding blocks while only one is driven by the linear motor. This rack and pinion assembly can be disengaged, and one sliding block can be fixed to the support bracket or a force transducer that is attached to the support bracket while the other sliding block is driven by the linear motor to enact asymmetric displacement of the sliding blocks. Each sliding block has a pair of tapped holes machined on its underside for the attachment of a mounting block. The mounting block can be attached to the sliding block either flush or offset by a connecting block (xi) and spacers. The offset configuration shown in Figure 4D and 4E enables the mounting blocks and suspended muscle sample to be immersed in superfusate solution during cyclic loading. When the mounting blocks are attached to the dynamic setup, the guide-rails and lead screw from the fixed assembly are removed, and displacement of the mounting blocks is driven by the linear motor.

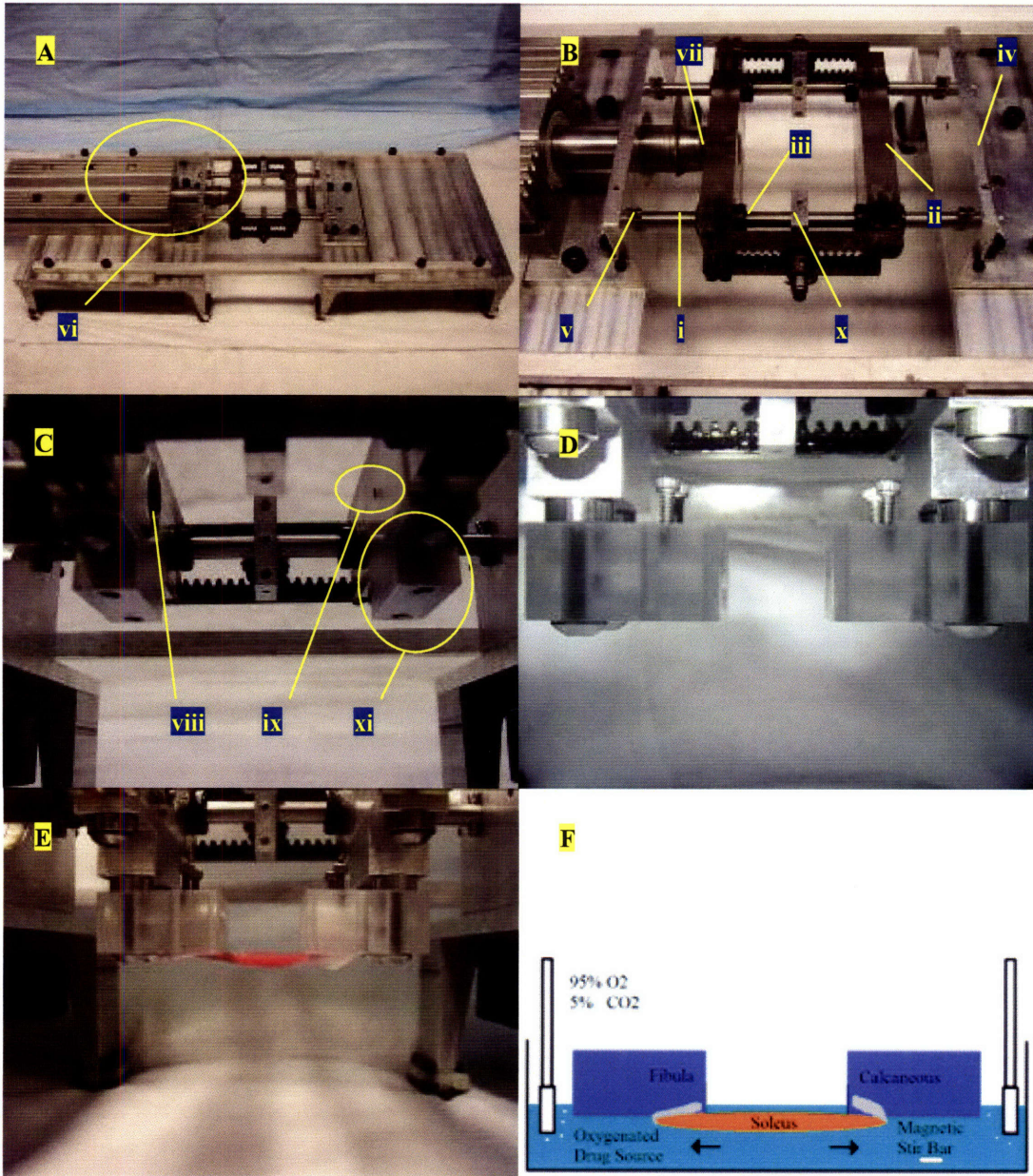


Figure 4 (A-F). Dynamic loading system. A) A PID-controlled linear servo motor actuates dynamic strains on mounted muscle specimens. B) The rack and pinion assembly for actuating symmetrical displacement of the sliding blocks. This can be disengaged to enable asymmetrical displacement of the blocks, and for the attachment of a load cell on one side so that force measurements can be made. C) Each sliding block has a connecting block for attaching and offsetting one of the individual mounting blocks shown in Figure 3. D) When attached to the sliding blocks via the connecting blocks, the mounting blocks are positioned in the same configuration as when they are in the static assembly. Without the guide-rails and lead screw of the static assembly, the mounting blocks are free to translate according to the motion executed by the motor. E) Mounted soleus muscles can be suspended in a superfusate bath while mechanical loading is performed. F) In the experimental setup for applying either static or dynamic loading, mounted samples are stretched while incubated in well-mixed and oxygenated drug solution at room temperature.

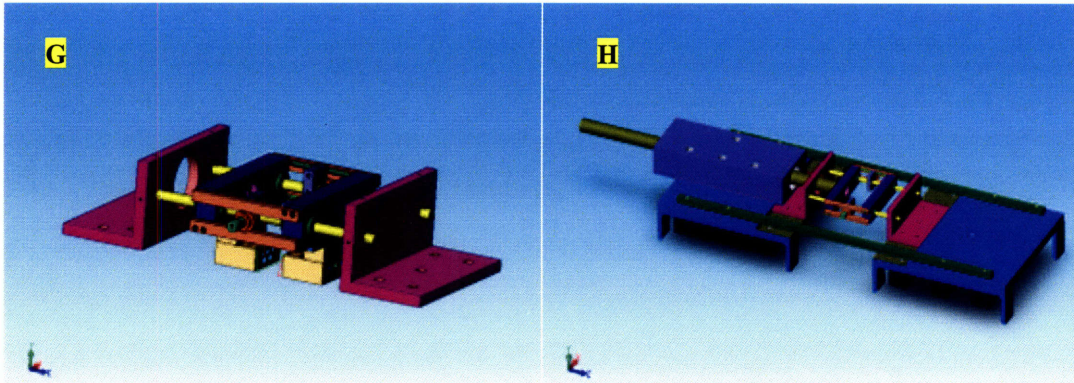


Figure 4 (G-H). G) Solidworks rendering of the dynamic mounting assembly with mounting blocks attached. This assembly is mounted atop the platform base. H) Solidworks rendering of the dynamic loading system.

2.5.3 Motion Actuation and Control

The cyclic mechanical loading of the sliding blocks is actuated by a *LinMot*® P01-37x240/60x260 linear servo motor that is controlled by a *LinMot*® E100-MT servo controller. A linear motor is used as the motion control element to simplify the design and enable linear stroke motion to be directly applied to the sliding blocks without the use of mechanical gears, belts, or ball screws; conventional pneumatic cylinders; or mechanical constructions based on levers, spindle drives, cam disks, belts, etc. The direct actuation provided by a linear drive improves accuracy and precision by minimizing mechanical play, reducing compliance, and avoiding wear of multiple additional elements. The *LinMot*® P motor consists of a fixed stator housing with 2 two-phase windings and a moveable slider containing neodymium magnets. This motor is an electromagnetic, direct, linear driver with fully integrated, contact-free, Hall effect, position sensors and bearings that enable it to execute dynamic, position-controlled, linear movements easily and directly to the load. Furthermore, because motion control of this mechatronic drive system is defined exclusively in the *LinMot*® software, a diverse

range of linear loading protocols can be selected, adjusted in real-time, and executed without the need for altering the physical setup.

Motion control – including actual machine functionality, loading protocol, and motion parameters – is performed by the *E100-MT* servo controller, which also supplies power to drive the motor. The controller regulates all control and monitoring actions necessary for controlling the motor. It saves and loads stored motion profiles and parameters from an overlaid control system. An integrated digital position control system enables the *E100-MT* to drive the motor smoothly to desired positional setpoints using proportional-integral-derivative (PID) controller logic and feed-forward anticipatory compensation. Feed-forward control includes three anticipatory parameters with which the control behavior and hence the attainable dynamics can be improved. These compensate for sliding friction, accelerating load, and decelerating load. Thus, PID control and feed-forward compensation enable the system to achieve very robust, repeatable, and accurate execution of a desired motion profile even in the presence of external disturbances, and corrects any static controller deviations.

Configuring and commissioning of the *LinMot*®-E servo controller is performed using *LinMot*® Talk, a Microsoft Windows-based software program. *LinMot*® Talk supports a modular graphical interface with menus that enable the user to define motion profiles and to configure, command, and monitor the linear motor in real-time. On-line measurements of motor data and movements made by the controller can be shown in graphical form and stored on the computer. The software thus enables complex test routines to be performed for biomechanics studies. In this study, a sinusoidal motion profile was defined and run continuously for dynamic loading of soleus samples.

3. METHODS

3.1 Characterization of Dynamic Loading System

3.1.1 System Compliance

Mounting blocks were attached to the sliding blocks of the dynamic loading system in the symmetric loading configuration. Stainless steel guide-rails were inserted into the mounting blocks as they would be in the static assembly and locked into place by their designated set screws, thereby fixing the positions and separation distance of the mounting blocks. The linear motor imposed sinusoidal positional profiles with amplitudes of 0.125mm, 0.25mm, and 0.5mm on this locked assembly. Displacement and force generated by the motor were recorded by the motor's internal position sensor and encoder and used to calculate the compliance of the loading system.

3.1.2 Motor Tuning

The dynamic performance and positional accuracy of the motor were optimized for applying cyclic strain profiles used our in transport experiments by tuning the PID controller under maximal performance conditions. With 2 soleus muscles of 28mm nominal length mounted in the symmetric loading configuration, the linear motor imposed a reference sinusoidal positional profile with 0.35mm amplitude and 3Hz frequency to simulate upper bound performance conditions in our transport studies. The PID controller parameters were tuned in real-time during continuous actuation such that proportional, integral, and derivative control were maximized to optimize motor response time, minimize tracking error and positional overshoot during acceleration and

deceleration, and eliminate steady state positional error while not causing motor oscillations or positional instabilities. The reference and actual position of the motor was monitored in real-time during continuous actuation using the internal position sensor of the motor, which has a 20 μ m resolution, and recorded using the oscilloscope utility included in *LinMot*® Talk to characterize performance. The optimal PID parameters found by this test were used in all subsequent loading experiments.

3.2 Evaluation of Tissue Properties

3.2.1 Architectural Integrity

Changes in the architectural integrity of soleus muscles developed *in vitro* under the range of loading regimens imposed by our transport experiments were assessed histologically. Because rats were selected in a narrow weight range, all soleus muscles used in the experiments in this investigation were of uniform size and measured 28mm in nominal length. Isolated muscles underwent mechanical loading for 70 minutes while they incubated in a superfusate bath of KH oxygenated with 95% O₂/ 5% CO₂ at room temperature. All experiments in this study were performed at room temperature, which is most favorable for the simultaneous investigation of both muscle biomechanics and drug transport. Room temperature is optimal for maintaining the viability and physiologic stability of muscles *in vitro* [35] without loss or inhibition of drug binding or transport properties. Room temperature furthermore enhances muscle endurance [36] and economy of substrate turn-over [37] during contractile performance, while maintaining the physiologic force-length relationship and contractile capacity of the muscle [37, 38]. Samples (n=6) underwent a range of magnitudes of static or dynamic straining

conditions. Static loading cases underwent 0%, 5%, 10%, or 15% strain. Dynamic loading cases underwent maximal loading conditions. Sinusoidal strain of 3Hz frequency and 2.5% strain amplitude was applied at mean strains of 5%, 10%, or 15%. In this study, 0% strain corresponds to the measured *in situ* nominal length, 5% strain corresponds to a muscle length that is 105% of the nominal length, etc. After mechanical loading, tissues were snap-frozen at nominal length while mounted on the static assembly in Isopentane chilled to -145°C in liquid nitrogen. 8µm thickness axial cross-sections from the midpoint of the soleus samples were cut using a Leica CM1850 cryotome and stained with Hematoxylin and Eosin. Light microscopy images of the sections were taken at 40X magnification. Image processing was performed using Matlab. The size and shape of soleus muscle fascicles were qualitatively assessed. The tissue porosity, or relative area of the interstitial space between muscle fibers and fascicles, was quantified as a percentage of the total area of the section and used as a measure of tissue structural integrity.

3.2.2 Functional Viability

The functional viability of soleus samples under *in vitro* conditions was assessed. Soleus samples (n=6) were held at their *in situ* nominal length by the static assembly and incubated in a KH bath oxygenated with 95% O₂/ 5% CO₂ at room temperature. Samples were continuously paced by electric field stimulation to induce isometric twitch contractions at a rate of 3Hz for 1 hour. This was done to assess the presence and persistence of contractile activity and functional viability under the maximal performance requirements and through the duration of a transport experiment. The electric stimulus

was a biphasic voltage output of 15V amplitude and 50ms pulse duration applied by 2 stainless steel foil plates situated at either end of the static assembly, spanning a separation distance of 10cm (Figure 5A). Electric stimulus was generated using a National Instruments DAQPAD-6062E data acquisition board and controlled by its Arbitrary Waveform Generator virtual instrument.

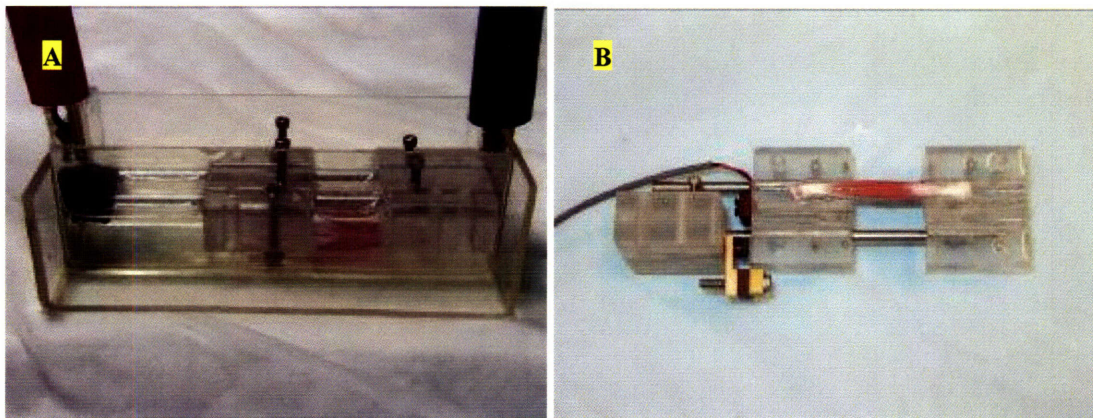


Figure 5. Mounting configurations for assessing functional integrity. A) Isometric twitch contractions were electrically paced at 3Hz for 1 hour by field stimulation to assess the presence and persistence of functional viability under the maximal performance requirements of transport studies. B) Active twitch and passive force-length relationships were quantified using a modified configuration of the static assembly that incorporated a force transducer.

Force measurements of soleus samples were separately recorded using a modified configuration of the fixed assembly (Figure 5B). A thin-beam load cell (Omega Engineering, Inc., LCL-227G, 0-227g) secured to one of the guide-rails was attached to the fibula mounting block, which was allowed to slide freely. The calcaneus block was fixed in position to the guide-rails by set screws. Soleus muscles (n=7) were individually mounted and stimulated to produce isometric twitch contractions at their *in situ* nominal length using a biphasic voltage output with 15V amplitude and 50ms duration applied to the tendons using stainless steel electrodes. Active twitch tension was measured every 15

minutes over a period of 2 hours. Between force recordings, muscle samples were kept fresh by incubating in KH superfusate oxygenated with 95% O₂/ 5% CO₂ at room temperature.

3.2.3 Force-Length Relationships

Muscles (n=7), 28mm in nominal length, were individually mounted on the force measurement configuration of the static assembly and stimulated to produce isometric twitch contractions using a biphasic voltage output with 15V amplitude and 50ms duration applied to the tendons using stainless steel electrodes. Each muscle was pre-strained over a range of fixed strains (0%, 5%, 10%, 15%, and 20%), and passive and total tension developed during contractions were measured at each strain. Developed active twitch force at each strain was calculated by subtracting passive from total tension. Between force recordings, samples were kept fresh by incubating in KH superfusate oxygenated with 95% O₂/ 5% CO₂ at room temperature.

3.3 **Quantification of Drug Transport**

3.3.1 Fractional Volume of Distribution

Fractional volume of distribution of FITC-dextran (Sigma, Catalog # FD4, 4kDa MW), our model drug, in soleus tissue was determined through equilibrium incubation studies. The time course of dextran equilibration, which was achieved when the time rate of increase or decrease of drug concentration in the incubated tissue reached zero, for incubation and elution was first determined. Equilibration time for elution of dextrans from pre-incubated soleus samples was first quantified. Soleus (n=5) samples of 50mg

mass and 4-5mm maximal thickness, which were pre-incubated in 10mL of 1mM concentration 4kDa FITC-dextran in PBS for 5 days, were incubated in 10mL volumes of fresh PBS for a range of time points (0, 0.5, 1, 3, 8, 13, 24, 50, 74, 98, or 130 hours). At each elution time point, 100 μ L of the bulk PBS was sampled and fluorescence was quantified using a ThermoLabsystems Fluoroskan Ascent® FL microplate fluorometer (ex: 485nm / em: 538nm) in order to determine the amount of dextran eluted out of the soleus sample by each time point. The time for elution concentration to reach equilibrium, or steady state, was determined when fluorescence intensity of the bulk no longer increased.

Equilibration time for uptake of dextran by soleus samples was then quantified. Soleus (n=5) samples of 50mg mass and 4-5mm maximal thickness were incubated in 10mL volumes of 1mM or 0.1mM concentration 4kDa FITC-dextran in PBS for a range of time points (0, 6, 8, 12, 24, or 60 hours). At each incubation time point, muscle samples were removed from the dextran solution, blotted on dry towels, and immersed in 10mL of fresh PBS until elution of dextran reached equilibrium, as determined by the elution experiment. Fluorescence of the eluate was quantified in order to calculate the total amount of dextran uptaken by the sample by each incubation time point. The time for uptake concentration in the tissue to reach equilibrium was quantified.

Based on the equilibration times for uptake and elution, the fractional volume of distribution for dextran in soleus muscle was determined for a range of bulk source concentrations of dextran. Soleus (n=6) samples of 20-30mg mass and 4-5mm maximal thickness were incubated to equilibrium in 10mL volumes of 0.1 μ M, 1 μ M, 0.01mM, 0.1mM, or 1mM bulk source concentrations of 4kDa FITC-dextran in PBS. After

equilibration, each specimen was blotted on dry towels and immersed in 10mL of fresh PBS until elution of dextran reached equilibrium. Fluorescence of the eluate was quantified and used to calculate the equilibrium tissue concentration achieved by uptake. An equilibrium distribution relationship, which characterizes the distribution of drug through tissues incubated to equilibrium in bulk phase concentrations of drug, was constructed by plotting the concentration of drug in the sample versus the concentration in the corresponding bulk source. Fractional volume of distribution of the muscle, which is the ratio of the tissue concentration to bulk concentration, was determined from the slope of the equilibrium distribution relationship.

3.3.2 Drug Transport Under Mechanical Loading

Soleus muscles were secured in pairs onto the mounting blocks and fixed in the dynamic loading setup. Samples (n=5) were cyclically loaded for 80 minutes by a sinusoidal positional profile with a peak-to-peak displacement that stretched the muscles between 0% and 20% strains at a frequency of 3Hz. Loading was performed while the samples incubated in 16mL of KH solution containing 1mM concentration 20kDa FITC-dextran (Sigma, Catalog # FD20). The drug source was oxygenated with 95% O₂/ 5% CO₂ at room temperature and kept well-mixed by a magnetic stir bar and the motion of the mounting blocks.

Samples in the control group were secured onto the mounting blocks in the fixed assembly and incubated for 80 minutes at nominal length in 16mL of KH solution containing 1mM concentration 20kDa FITC-dextran that was oxygenated with 95% O₂/ 5% CO₂ at room temperature. The source was kept well-mixed by a magnetic stir bar.

The fluorescence intensity of the dextran bulk source was sampled (100 μ l, n=6) at the beginning and end of a representative 80-minute incubation and quantified using a ThermoLabsystems Fluoroskan Ascent® FL microplate fluorometer (ex: 485nm / em: 538nm).

3.3.3 Tissue Processing and Measurement of Drug

Drug penetration and distribution in the soleus tissue was quantified using epifluorescence microscopy. After mechanical loading, tissue samples were removed from the dextran bath, rinsed twice in 15mL of fresh KH to remove surface drug, and snap-frozen at nominal length while mounted on the static assembly in Isopentane chilled to -145°C in liquid nitrogen. 8 μ m thickness axial cross-sections from the midpoint of the soleus samples were cut using a Leica CM1850 cryotome. FITC-dextran in tissue sections was visualized and imaged using an upright epifluorescence microscopy system (Leica DMRA2 Microscope, 50X magnification, Hamamatsu ORCA 286 Digital CCD Camera, Metamorph Version 6.3 Software), exciting with a 450-490nm bandpass filter and collecting with a 515nm longpass filter. Image intensity values were analyzed using Matlab. The intramuscular penetration depth of dextran from the planar and curved surfaces of the muscle was defined as the perpendicular distance from the surface at which fluorescence intensity in the muscle decreased to 5% of the intensity found at the muscle surface. An initial calibration curve correlating fluorescence intensity in images with equilibrium drug concentration in the tissue was generated prior to quantifying penetration depth. Tissue samples (n=6) were incubated to equilibrium in 0.01mM, 0.1mM, or 1mM bulk source concentrations of 20kDa FITC-dextran. Fluorescence

intensity measured in images of 8 μ m thickness sections of these incubated tissues were correlated to the drug concentration in the tissue. Tissue concentration was determined by calculating the product of the bulk source concentration and the fractional volume of distribution of dextrans in soleus muscle.

4. RESULTS

4.1 System Compliance

The displacement measured by the internal position sensor of the linear motor tracks one lateral side of the dynamic mounting assembly, which is half of the total displacement of the mounting blocks in the symmetric loading configuration. Thus, the total mechanical compliance of the series combination of motor, rack and pinion assembly, and mounting blocks is the ratio of twice the measured displacement over the measured force. Total compliance was less than 0.0057 ± 0.002 mm/N and linear over a broad force range (Figure 6).

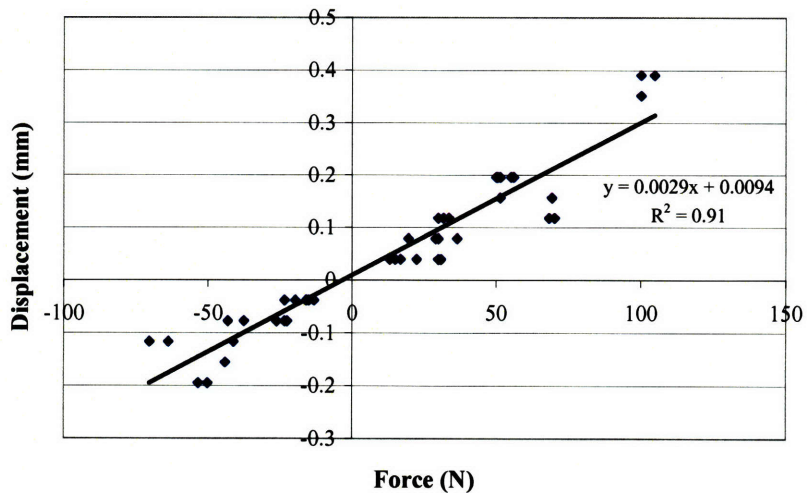


Figure 6. System compliance. Compliance is the slope of the relationship between the displacement and force produced by the motor. Total mechanical compliance of the dynamic loading assembly from motor to muscle sample is equal to twice the slope because of symmetrical displacement of the mounting blocks.

4.2 Motor Tuning

The peak sinusoidal displacement (0.35mm, 3Hz) used oscillates a single lateral aspect of the symmetrical mounting assembly with a peak-to-peak displacement of 2.5% strain for a soleus muscle that is 28mm in length. This corresponds to a total cyclic strain of 5%. The optimal PID parameters that gave the least positional tracking error and instability were, P: 3.5A/mm, I: 2.005A/(mm*s), and D: 4.005A*s/m. The feed-forward (FF) friction coefficient, which was programmed based on estimated friction coefficient of the system, was 0.234A. These settings enabled the muscle to track displacement in phase with the reference profile and without significant positional error (Figure 7). Over a 0.7mm peak-to-peak displacement of the motor, the positional error for our upper bound performance profile was $\pm 60\mu\text{m}$. These PID parameters and FF friction coefficient were used for all subsequent loading experiments.

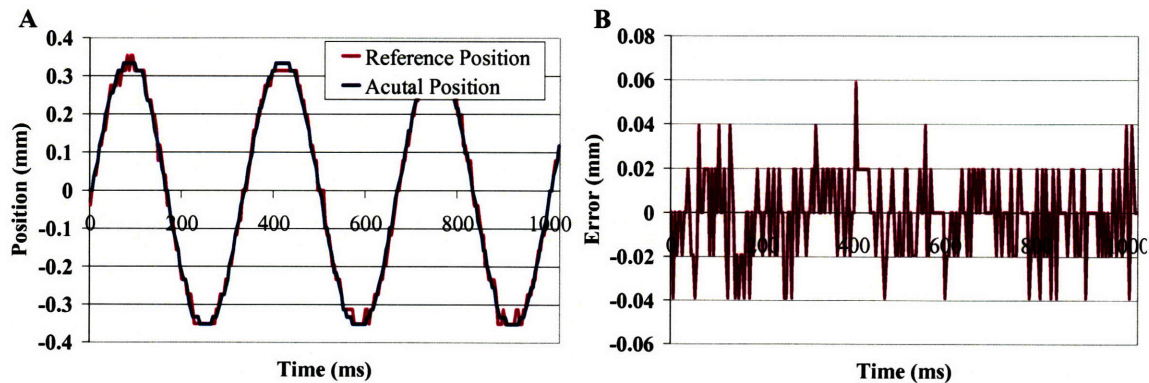


Figure 7. Motor response under maximal performance requirements. Dynamic performance of the motor was measured as it imposed a 0.35mm amplitude, 3Hz sinusoidal positional reference profile on a pair of mounted soleus samples. Response of the motor was optimized for this maximal performance reference profile by tuning the PID controller so that A) the actual position of the motor tracked closely to the reference profile and B) the error between the actual and reference positions was minimized.

4.3 Architectural Integrity

From preliminary incubation experiments, the interstitial space, or tissue porosity, as a percentage of the cross-sectional area of the tissue, was found to increase linearly with time up to 24 hours for muscle samples incubated *in vitro* without mechanical loading. One hour provided a duration of drug delivery long enough to enable drug penetration to be significant and quantifiable, as well as for differences in transport under different loading conditions to be differentiable. Thus, transport experiments were limited to one hour to limit the extent that structural integrity, and thus the drug transport environment, would be degraded from the physiologic state. Soleus muscle was assessed histologically to evaluate changes in tissue architecture as a result of different mechanical conditions applied *in vitro*. Control groups included tissues that were snap-frozen immediately after isolation (0 minutes) and tissues snap-frozen after 70 minutes of no mechanical loading (0% static strain, 70 minutes). Tissue porosity was quantified at both the superficial or peripheral edge of the tissue, where drug transport occurs, and at the central portion of the muscle cross-section (Figure 8).

Porosity of unloaded freshly excised tissue was ~11%. This value is in agreement with inulin distribution space, which characterizes the percentage volume of extracellular space, in rat soleus found by previous studies [39-41]. 70 minutes of *in vitro* exposure, whether in the presence or absence of mechanical loads, did not significantly increase porosity in the central portion of the muscle above the $11.6 \pm 5.7\%$ found in the 0-minute control ($p > 0.82$, Single Factor ANOVA), but it significantly increased porosity at the tissue edge. Porosity at the tissue edge increased by 1.5-2.2 fold above the $11.1 \pm 3.3\%$ found in the 0-minute control ($p < 0.015$, t-Test) to an average of $21.0 \pm 6.1\%$ for all 70-

minute groups. The porosity respective to each region of the muscle was statistically identical in all mechanically strained groups, which were loaded for 70 minutes ($p>0.46$ and $p>0.92$ at the edge and center, respectively, Single Factor ANOVA).

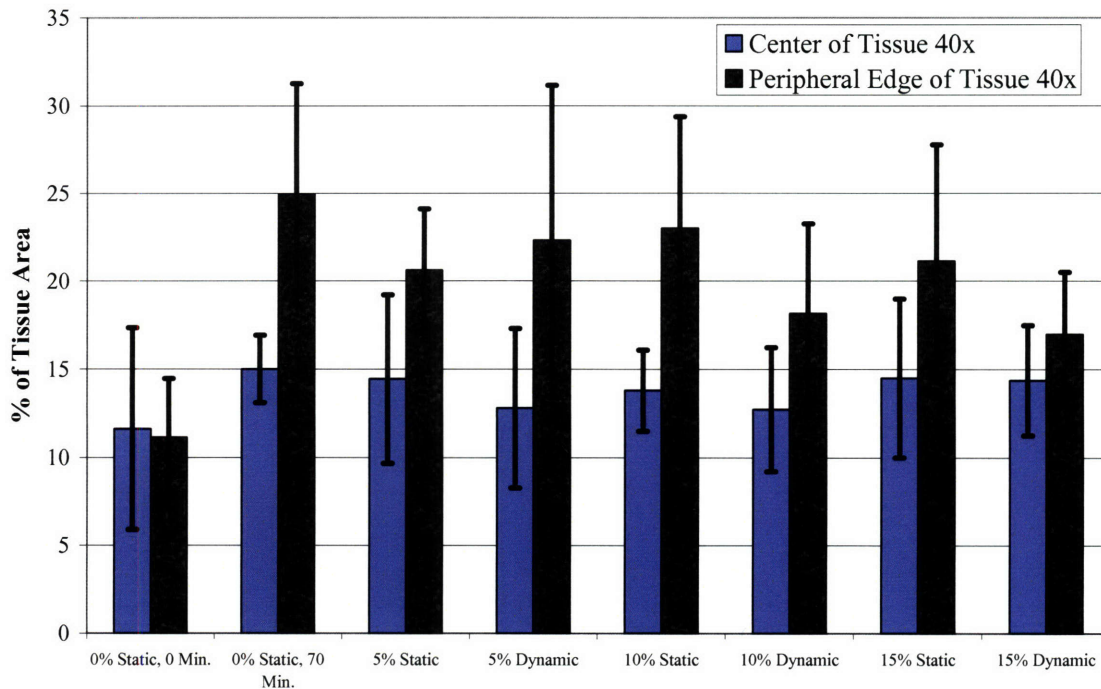


Figure 8. Tissue integrity. Porosity was measured after different incubation times and various regimens of static and dynamic strain. Static strain held muscles at 0%, 5%, 10%, and 15% strain for 70 minutes. Dynamic loading cyclically imposed $\pm 2.5\%$ strain at 3Hz about 5%, 10%, and 15% mean strains for 70 minutes. Porosity respective to the tissue edge or center was consistent among all samples incubated *in vitro* for the same duration, regardless of the nature of imposed strain, demonstrating that time was the predominant factor in affecting changes in porosity. Porosity increased at the edge of the tissue relative to the central portion of the tissue after 70 minutes *in vitro*.

4.4 Functional Viability

Muscle samples fixed at nominal length maintained isometric twitch contractile activity at a rate of 3Hz for at least 1 hour. Isometric twitch force from a single soleus measured every 15 minutes yielded a minimum of 0.19N for at least 2 hours.

4.5 Force-Length Relationships

The classic curvilinear, or exponential, increase in passive tension with increasing stretch that characterizes the passive extensibility of skeletal muscle was observed (Figure 9). When the soleus was mounted on the fixed assembly, the nominal length of the muscle was the length at which the first passive resistance to stretch could be measured. Developed active force, or twitch tension, was obtained as the difference between the total and passive forces and demonstrated the classic parabolic force-length relationship.

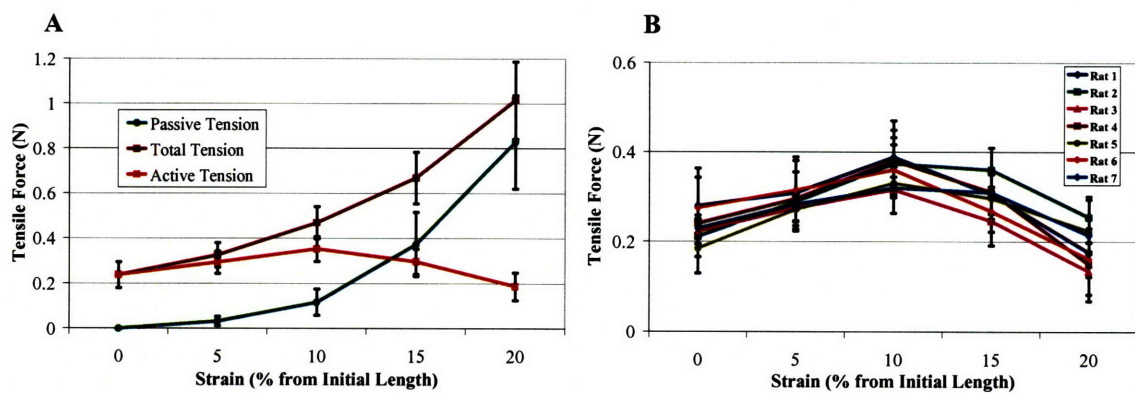


Figure 9. Force-length relationships of the soleus. Passive and total forces of the soleus were measured at 0%, 5%, 10%, 15%, and 20% strain. A) Total, active, and passive tension of a single soleus muscle (n=7). Active force is produced by isometric twitch contraction. It is the difference between total and passive force. B) Isometric twitch tension of 7 different single soleus samples.

Active twitch tension developed in single soleus samples averaged across 7 rats increased with increasing strain from $0.24 \pm 0.06\text{N}$ at nominal length, to a maximum of $0.35 \pm 0.06\text{N}$ at 10% strain, and thereafter decreased with further increase in length to $0.19 \pm 0.06\text{N}$ at 20% strain. Twitch tensions developed at different strains in both the increasing and decreasing halves of the parabolic force-length relationship were

statistically significantly different from each other (Single Factor Anova). Peak twitch tension was in agreement with values obtained in prior *in vitro* and *in situ* studies using rats of similar size [42, 43]. The passive force of $0.12 \pm 0.06\text{N}$ developed at the optimal muscle length where peak twitch tension occurs also agrees with that determined previously by others [43].

4.6 Fractional Volume of Distribution

The time for both uptake and elution of FITC-dextran (Figure 10) in soleus samples to reach equilibrium was approximately 28 hrs. Subsequently, incubation and elution equilibration times used in determining fractional volume of distribution were limited to 28 hours.

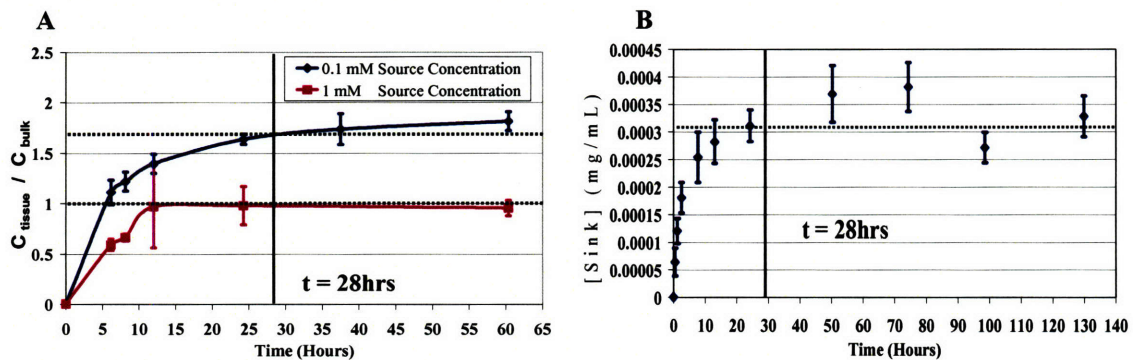


Figure 10. Incubation and elution equilibrium times. A) Plot of tissue concentration vs. time quantifies the uptake of drug in soleus samples incubated in bulk dextran sources of 0.1mM and 1mM concentration. B) Concentration of the bulk phase vs. time during the elution of dextran from soleus samples pre-incubated in 1mM dextran source. Incubation and elution equilibration times were both approximately 28 hours.

Fractional volume of distribution of dextran in the soleus was quantified over bulk source concentrations of 0.1 μM , 1 μM , 0.01mM, 0.1mM, and 1mM 4kDa FITC-dextran (Figure 11). Across this range of bulk concentrations, the equilibrium distribution

relationship showed a linear trend with a slope of 0.84, indicating a fractional volume of distribution of 84% available in the tissue for the source concentration of drug. Using an equilibrium distribution analysis [44], bound fraction of dextran was calculated by subtracting the product of (slope \times bulk phase concentration) from the tissue concentration. This demonstrated a spread about zero across the entire range of source concentrations, indicating that binding site density in the soleus was lower than the scatter in the data at high bulk phase concentrations, and therefore insignificant.

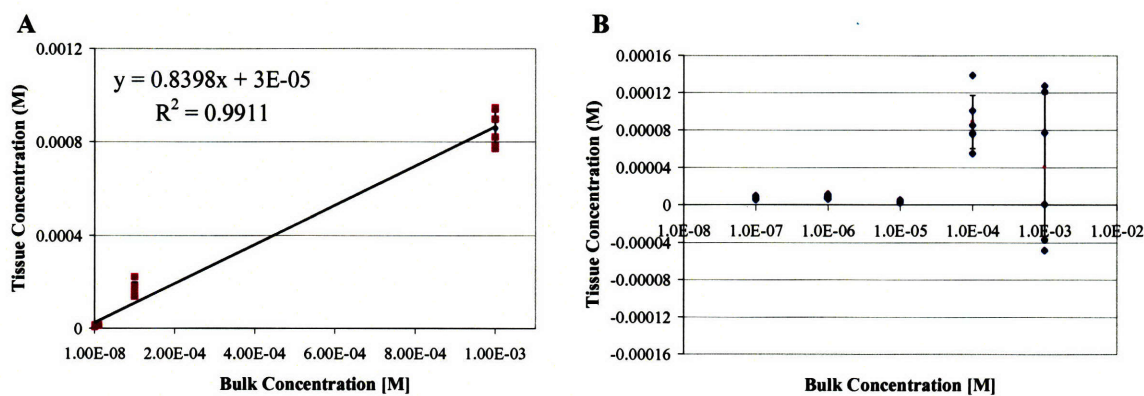


Figure 11. Equilibrium distribution measurements. Equilibrium tissue concentration is plotted against bulk source concentration. A) The measured equilibrium distribution relationship for dextran in soleus muscle. The equilibrium concentration of 4kDa FITC-dextran in the tissue over a range of bulk source concentrations (0.1 μ M – 1mM) follows a linear trend. Fractional volume of distribution, determined by the slope of the equilibrium relationship, is 0.84. B) Bound concentration of dextran in the soleus. A spread about zero across the range of source concentrations suggests that binding site density in the soleus for dextran is insignificant.

Individual ratios of tissue to bulk concentration that are higher than 0.84, as found in incubation studies (Figure 10), may be attributed to loss of tissue integrity, and therefore increase in porosity, over 28 hours. Since all samples in this study were incubated for 28 hours, and therefore tissue integrity was consistent among all samples across the range of bulk source concentrations, elevation of individual ratios may

uniformly offset the entire distribution relationship to higher tissue concentrations but does not affect the slope of the relationship or the fractional volume of distribution of 84%.

4.7 Measurement of Drug

A calibration curve relating fluorescence intensity to equilibrium drug concentration in soleus tissue was generated from epifluorescence images of soleus samples that equilibrated in 0.01mM, 0.1mM, 1mM bulk concentrations of 20kDa FITC-dextran. Tissue concentration was calculated based on the finding that fractional volume of distribution in the soleus was 84% of the bulk source concentration of dextran. An exposure rate for imaging was chosen that eliminated tissue autofluorescence and avoided saturation of the intensity detection ability of the imaging system by the source concentration of drug. Drug source concentrations and intensities represented the range used in our drug transport studies. The relationship between fluorescence intensity and tissue concentration was linear over this range of bulk source concentrations (Figure 12). This is in accordance with the linear relationship between fluorescence intensity and concentration described by Beer's Law for very low concentrations, $I=\epsilon CQ$, in which I is fluorescence intensity, ϵ is the molar absorption coefficient, C the molar concentration, and Q the quantum yield [45].

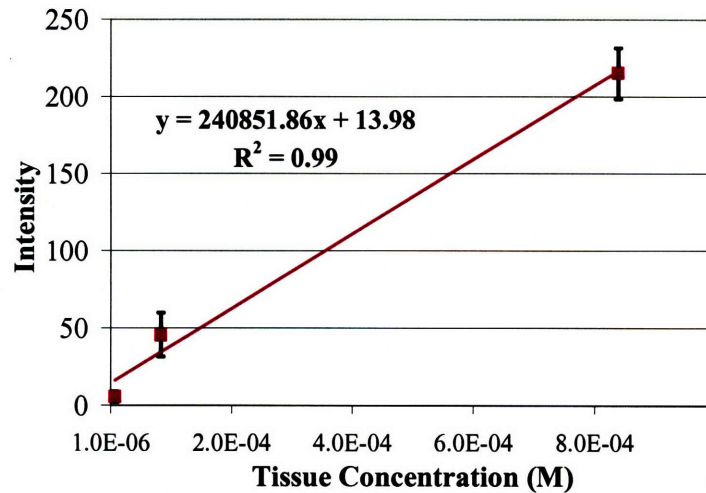


Figure 12. Fluorescence intensity vs. equilibrium tissue concentration. Tissues were equilibrated in 0.01mM, 0.1mM, and 1mM bulk concentrations of 20kDa FITC-dextran and imaged by epifluorescence microscopy. The fluorescence intensity vs. tissue concentration follows a standard linear relationship.

4.8 Drug Transport Under Mechanical Loading

In impact of mechanical loading on dextran penetration and distribution in soleus muscle was investigated by applying either static or cyclic strains on samples while they incubated in a 1mM concentration 20kDa FITC-dextran bath. Epifluorescence images of axial cross-sections from the midsection of the soleus muscle were taken, and drug penetration depth was measured at the planar and curved surfaces of the muscle (Figure 13). Planar surfaces are the dorsal and ventral surfaces of the tissue, and curved surfaces are the medial and lateral margins of the muscle. Surfaces are referred to as top, bottom, left, and right based on their location in fluorescent images. Penetration was equivalent at the opposing planar surfaces (top and bottom) for each loading condition. Penetration at the planar surfaces averaged $0.52 \pm 0.09\text{mm}$ under static strain and $0.81 \pm 0.09\text{mm}$ under dynamic strain (Figure 14). Similarly penetration was equivalent at the opposing curved surfaces (left and right) for each loading condition, averaging $0.82 \pm 0.19\text{mm}$

under static strain and 2.1 ± 0.24 N mm under dynamic strain. Penetration at curved surfaces was significantly higher than at planar surfaces by a factor of 1.57 and 2.52 under static and dynamic strain, respectively. Penetration at both groups of surfaces was significantly higher under dynamic loading than under static strain. Dynamic strain increased penetration at curved surfaces to a greater extent than at planar surfaces by a factor of 1.6 – while penetration increased by a factor of 1.56 at planar surfaces, it increased by a factor of 2.51 at curved surfaces. Bulk source concentration, quantified by the fluorescence intensity of bulk source samples taken at the beginning and end of the incubation period, remained the same throughout the experiment (Figure 15).

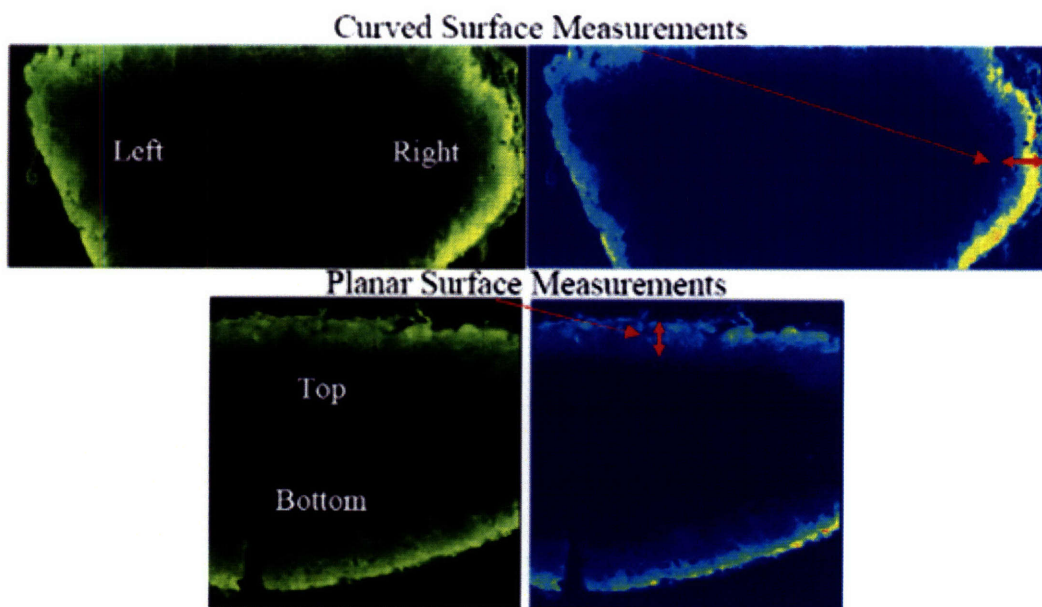


Figure 13. Quantification of fluorescent drug. Distribution of drug in soleus muscle was qualitatively assessed. Penetration of 1mM concentration 20kDa FITC-dextran into soleus muscle was quantified in axial cross-sections of the soleus using epifluorescence imaging. Raw images of fluorescence (images on the left) were converted to intensity values (images on the right) and analyzed in Matlab. Penetration depth from the surface of the muscle was quantified as the distance into the tissue at which fluorescence intensity decreased to 5% of the source intensity at the surface. Penetration was measured at the curved surfaces (designated Left and Right) and planar surfaces (designated Top and Bottom).

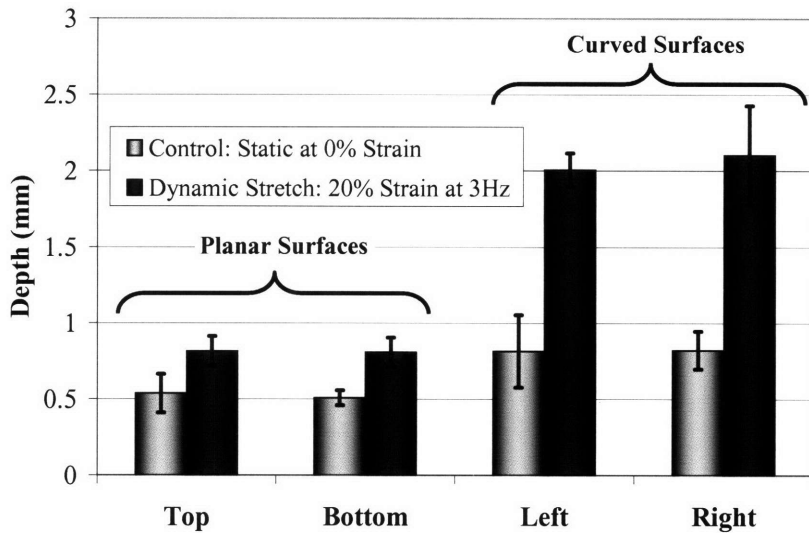


Figure 14. Impact of mechanical loading on drug transport. The effects of static and dynamic stretch on the penetration of FITC-dextran in soleus muscle were measured. Samples were loaded for 80 minutes while incubating in 1mM bulk concentration 20kDa FITC-dextran. Drug penetrates further into the muscle at curved (left, right) surfaces than at planar (top, bottom) surfaces. Dynamic strain increases the penetration of drug at both planar and curved surfaces. Penetration at curved surfaces increases to a greater degree, by a factor of 1.6, than at planar surfaces under dynamic loading.

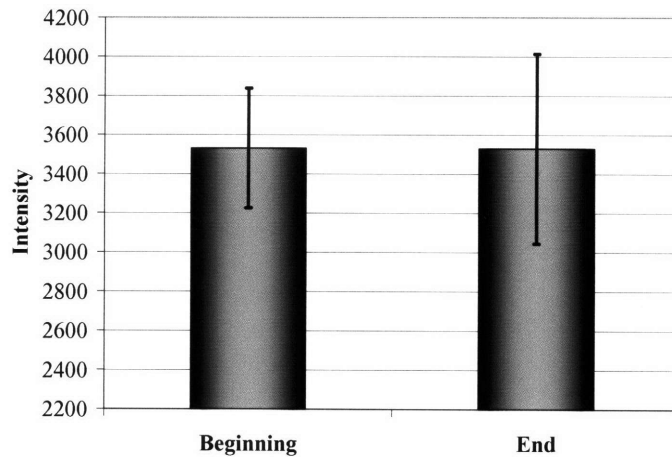


Figure 15. Constant drug source. Fluorescence intensity of the bulk source measured at the beginning and end of an 80-minute incubation of a pair of soleus muscles undergoing mechanical loading. Fluorescence intensity, and therefore drug source concentration, remained the same throughout the incubation of the specimens.

5. DISCUSSION

The aim of this work was to determine whether dynamic mechanical strain affects the intramuscular transport of locally delivered drug. To date much of the work on transport through muscles has focused on measuring changes in interstitial water distribution, total tissue volume, or extracellular space induced by strain or contraction using tritiated water [39]; molecular markers like inulin [39, 46, 47]; albumin [48, 49]; or solutes like EDTA [48], sodium, and potassium [1, 50]. A few studies have measured contraction-induced diffusion of water [51] or myoglobin [52] in single muscle fibers. And many other studies have focused on how strain or contraction in whole muscles affects the total uptake of metabolic substrates like glucose [9, 10, 23, 53-55], lactate [56], phosphate [57], calcium [26, 58], and sodium [59]. However, no investigations to date have quantified the isolated effects of different mechanical loading regimens on the extracellular spatial distribution and transport, not just total uptake, of a drug in muscle tissue. With the advent of local drug delivery to contracting structures, the impact of static as well as cyclic and dynamic strain is critical to a complete understanding of intramuscular pharmacokinetics and pharmacodynamics. Our current studies investigated the local pharmacokinetics of muscle under static and cyclic mechanical loading. These studies required careful preservation of natural muscle dimensions and contractile function, the ability to apply controlled strain and variable concentrations of drugs within pharmacologic ranges directly to the target tissue, and continued maintenance of tissue integrity and viability. We therefore designed and implemented a

surgical isolation and mounting technique, as well as a mechanical loading system, that achieved these goals.

5.1 Design of a New Biomechanics Preparation and Mechanical Loading System

Most preparations used in current studies of passive material properties or contraction mechanics of muscle disrupt the physiologic anatomy and mechanical function of the tissue specimen. The method for securing muscle samples in a biomechanics preparation, especially one for investigating drug transport, is critical for the investigation of accurate mechanical properties and drug transport. Strain conditions applied to a muscle bundle during mounting or suspension can introduce various loading artifacts that alter the structure and function of the muscle, as well as disrupt drug transport. Suture ties or piercings, using thread or steel wire, may quickly grip and suspend tissue in a diverse set of configurations, but do so without constraint of axial rotation of the muscle. Such rotational freedom allows unwanted torsional distortion of muscle architecture during tensile strain or contraction. Sutures also increase the compliance of a tensile system, which affects both force transmission and measurements. Moreover, as with the application of clips or clamps, compression and disruption of the extremities of the tissue by suture ties or piercings introduce stress concentrations and local disruption of muscle architecture that can create drug transport artifacts. Hooks and pins employed at either the tendon or muscle body are even simpler to apply than sutures, but they more significantly physically disrupt the tissue and interrupt the integrity of the architecture and the normal distribution of transmitted forces. Fixing rods provide more stable support if used with an intact bone segment and can potentially fix the ends of the

muscle without distortion of the soft tissues but do not provide secure fastening points to constrain the muscle in a physiologic orientation. To our knowledge, few studies have considered more rigorous techniques of securing muscle by bone attachments [60-62], and none have presented a preparation specifically designed to maintain an isolated muscle in an architecturally physiologic configuration for appropriate force transmission throughout the entire muscle unit, from muscle to bone. In this study, we presented a surgical technique and loading preparation that secures whole soleus samples, eliminates loading artifacts, and preserves physiologic architecture, configuration, and architecturally dependent force transmission – all of which directly influence intramuscular drug transport.

5.1.1 Tissue Isolation and Mounting

Our isolation and mounting methods are robust enough to extend to examination of general biomechanics. The tissue isolation, explantation, and preservation protocol can be applied to any study or preparation investigating mechanical, physiological, biochemical, or molecular properties of muscle. The mounting technique and device are applicable in any setup or preparation in which isolated muscle is to undergo either static or cyclic tensile strains or forces. These include studies of not only externally applied loads, but also contractile function under electrical as well as chemical stimulation in which muscles generate force, displacement, or velocity. Our mounting blocks can be used independently in a dedicated fixed, or static, assembly for applying static strain or load, securing tissue, or tracking electrophysiologic responses. The static assembly can be configured for force measurements with the attachment of a load cell or force

transducer. The mounting technique, and even the blocks themselves, can be incorporated as the fixturing method in existing *in vitro* or *in situ* physiology, biomechanics, or electrophysiology preparations for applying dynamic loads; or measuring passive and active tensile force, strain displacement, or velocity under external loading or stimulated contraction.

With their robust design, the isolation and mounting methods especially enable effective local drug delivery and transport studies to be performed. In any application, the surgical isolation protocol eliminates trauma to the soft tissues and maintains intact muscle, tendons, and bone attachments to allow more physiologic mechanical properties to be preserved. By the nature of their design, the mounting blocks can be applied to muscle specimens as quickly as, or quicker than, applying sutures, hooks, or clamps, but without the risk of slippage of the specimen. Angled slots in the blocks secure specimens by mechanical fit and leverage of the bone segments, which eliminate the need for additional fastening mechanisms. Mechanical fit prevents slippage and rotation of the specimen, and leverage on the bones enables them to transmit tensile forces to the tendons and muscle. By the mechanical mechanisms they use to restrain the bone, the mounting blocks maintain the physiologic configuration of suspended muscle specimens, and thereby eliminate artificial stresses and trauma to the muscle and tendons that are typically introduced by current mounting methods and are potential sources of drug transport artifact. In this manner, these techniques are optimal for the rigorous tissue handling requirements of studying accurate drug transport. Whether used in primary biomechanics studies or within the context of a another muscle physiology investigation, the ability of these techniques to accurately load samples in a physiologic mechanical

configuration is a valuable tool for investigating muscle in an *in vitro* or *in situ* setting, separate from *in vivo* work.

5.1.2 Dynamic Loading System

The dynamic loading system, which can incorporate the individual mounting blocks of the static assembly as its mounting fixtures to secure muscles in a physiologic configuration, enables mechanical loading of muscles with a broad range of dynamic functionality. The test instrument combines precise, feedback-controlled, mechanical loading that is driven by a linear motor at 20 μ m positional resolution, with versatile, computer-automated loading profiles that span a diverse range, from continuous cyclic strains to user-defined displacement profiles. The setup can be oriented either vertically or horizontally, incorporate force transducers or load cells, and accommodate different motors.

The loading system was designed as a means to examine drug delivery and transport. The device allows for either static or dynamic mechanical loading to be conducted on mounted samples while they are immersed in a media bath under physiologic conditions. This functionality enables biomechanics testing to be performed *in vitro* without loss of tissue integrity or mechanical function. Moreover, this functionality enables the preservation of muscle structural dimensions and functional viability, control of the local environment, and effective investigation of intramuscular transport of agents locally delivered directly to the samples by the bath. The compact design of the system makes it suitable for incubator use to perform *in vitro* testing under more precise temperature and environmental control. The ability for the system to

effectively perform biomechanics testing on muscle samples that are suspended under mechanically and environmentally physiologic conditions not only introduces a new realm for investigations of tissue pharmacokinetics, but also opens up new opportunities for biomaterials testing under axial loading. With the incorporation of proper mounting fixtures, these studies could be expanded beyond skeletal muscle to include arterial or myocardial tissues, as well as ligament, tendon, cartilage, and engineered tissue constructs.

5.2 System Validation

We validated the dynamics of our loading system, tissue preservation capacity of our drug delivery preparation, and ability to track drug transport after local drug delivery to soleus muscles under mechanical loading.

5.2.1 Dynamic Loading

As the total compliance of the loading system is less than 0.0057 ± 0.002 mm/N, our system can apply a greater range of static or dynamic load without loss of strain or displacement compared to other systems developed to apply high frequency vibrations concurrent with larger amplitude elongation, or small length perturbations, which have 2.5 to 116 times greater compliance [13, 34, 63, 64]. In return, the lower compliance of our system enables examination of a greater range of static or dynamic strain without loss of force transmission to the specimen. Linearity of the relationship between force and displacement demonstrates a constant compliance in the system and allows for simple correction for “series compliance” during biomaterials characterization.

5.2.2 Tissue Preservation

Along with characterizing the performance of the loading system, we examined the tissue preservation capacity of our drug delivery preparation. As a measure of tissue preservation, we assessed architectural integrity of soleus muscle samples. Architectural integrity is particularly important for drug transport studies because porosity, or interstitial space, defines the intramuscular accessible space available for transport of soluble dextran, which exhibits bulk uptake (i.e. the uptake increases linearly with bulk source concentration) and transports in the extracellular space [65-67]. Thus, changes in tissue porosity would dramatically affect drug transport.

Characterization of tissue porosity in the soleus suggests that changes in structural integrity experienced by the muscle *in vitro* during our transport studies occur at the peripheral edge of the specimens and are consistent among all samples incubated for the same duration, independent of the nature or range of mechanical loading. While mechanical loading expectedly influences structural configuration when applied on a specimen, it is the duration of time the specimen spends *in vitro* that is the predominant factor affecting progressive and permanent changes in tissue integrity and porosity. This finding suggests a time-dependent degradation of the tissue, starting at the peripheral edge, which progresses linearly with time, based on preliminary findings, throughout the incubation period. Peripheral changes may arise from a multitude of effects including greater exposure and loss of protein substrate to the superfusate and absence of circumferential support from adjacent muscle fibers. Anoxic degradation is common for *in vitro* preparations but is unlikely in this case as the peripheral edge of the muscle was

in direct contact with oxygenated solution, and architectural integrity of the deeper, central region was approximate to freshly excised specimens, suggesting that there was adequate oxygenation throughout the entire tissue. Consequently, as all specimens in our transport experiments are incubated for the same duration, the peripheral tissue architecture where drug transport occurs can be considered consistent among specimens across all loading groups, whether loading is static or dynamic. Any differences observed in transport can be attributed to the influences and dynamics of mechanical loading rather than differences in porosity resulting from tissue injury or degradation.

Despite porosity changes at the tissue edge, tissue viability was still preserved as architectural integrity at the center of the tissue remained intact, and functional integrity was still retained as demonstrated by continuous twitch activity for 1 hour under maximal performance conditions (3Hz contraction rate) and the preservation of active force production (at least 0.19N) for at least 2 hours.

The force-length characteristics of the intact muscle-tendon unit were measured. However, tendons, which consist of dense connective tissues, exhibit minimal length extensibility characteristics and can be considered to have constant length within a physiological range of strain [22, 68, 69]. Thus, the measured passive force-length relationship of the muscle-tendon unit reflects the passive viscoelastic material property of the muscle, which is well described in the classic biomechanics literature. As a comment on nomenclature used in these studies, because the peak of active force developed by stretched muscles occurs at 10% strain, the muscle length referred to in this study as 10% strain is equivalent to what is traditionally defined as the *optimal* or *resting length*, L_0 , the length at which maximal active force is developed. Furthermore, because

the nominal *in situ* length, or 0% strain, is the length at which passive force developed during stretch can first be measured, the muscle length referred to in this study as nominal length is equivalent to what is traditionally defined as the *initial length*, the length at which the first passive resistance to stretch occurs. Accordingly, 0% to 20% strains in this study span the mid-range muscle length, or the physiologic range of muscle extensibility, and do not approach the muscles' *maximum length*, the length beyond which further stretch results in rupture of muscle fibers. Thus, transport studies conducted within this range of strain will accurately capture the target tissue environment under physiologic lengths and active forces.

5.2.3 Quantification of Drug Transport

Linearity of the relationship between fluorescence intensity and tissue concentration demonstrates a range of drug source concentrations that enables accurate detection of drug in the tissue that is unaffected by tissue autofluorescence, fluorescence quenching, or intensity saturation of the fluorescence imaging system. Furthermore, linearity enables easy conversion between dimensionless fluorescence intensity values and drug concentration in the tissue. As a result, quantification of drug penetration depth in the muscle can be performed using the actual fluorescence intensity values directly from an image without the prior need to convert such values to tissue concentrations, which could introduce conversion deviations. Thus, this quantification method is an effective and direct way to not only measure drug uptake, but also to visualize the intramuscular spatial distribution of fluorescent drug.

5.3 Intramuscular Pharmacokinetics

5.3.1 Equilibrium Distribution of Drug

Dextrans are hydrophilic polysaccharides characterized by high water solubility, stability in solution, extracellular transport, inertness, and non-protein-binding properties [65, 67, 70]. Furthermore, dextrans are stably conjugated with fluorescent labels like fluorescein isothiocyanate (FITC) under *in vivo* and *in vitro* conditions [71]. Our tissue incubation studies validate the bulk uptake characteristics of FITC-dextran transport in soleus muscle. Equilibration time for both incubation and elution of dextran from soleus samples was 28 hours. Equivalent uptake and elution times suggest that any interaction or binding between dextran and cell surface or extracellular matrix binding sites in the target tissue has equivalent tissue-average association and dissociation kinetics, and is therefore non-specific and likely insignificant in nature.

The absence of significant specific binding allows soluble dextran to diffuse or convect through the intramuscular accessible space without the impediment of drug-tissue interactions. This characteristic is verified by our finding of an equilibrium distribution relationship that is linear over 4 orders of magnitude of bulk phase source concentrations (0.1 μ M - 1mM). A linear relationship signifies bulk uptake of dextran, or uptake that increases linearly with bulk source concentration.

The presence of a significant binding density, however, would present a saturable component to the uptake characteristic that would introduce a noticeable nonlinearity in the equilibrium distribution relationship at low source concentrations (Figure 16). A significant binding capacity that sequesters soluble drug would not only increase total drug uptake by a capacity equivalent to the density of binding sites in the tissue, but also

increase the fractional volume of distribution, or slope of the equilibrium distribution relationship, starting at low drug concentrations until saturation of the binding sites is reached. Linearity of our measured distribution relationship across a broad range of concentrations demonstrates that specific binding is not present. Moreover, the bound fraction of dextran that is calculated using the equilibrium distribution analysis is spread about zero across the entire range of bulk source concentrations. This indicates that the binding site density for dextran in the soleus, which is lower than the scatter in the data at high bulk phase concentrations, is insignificant.

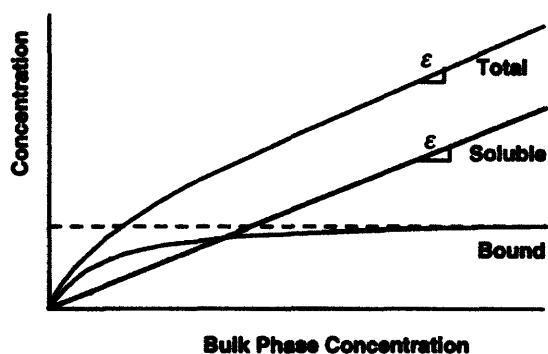


Figure 16. Equilibrium distribution model. This is a model of drug distribution through tissues incubated to equilibrium in bulk phase concentrations of drug [44]. The total concentration, which is measured empirically, is the sum of the bound and soluble fractions. The soluble concentration increases linearly, at a rate or slope of ϵ , with increasing source or bulk phase concentration. The bound fraction increases the capacity of total drug uptake. Binding increases the slope of the total equilibrium relationship at low concentrations up to the saturation density of binding sites in the tissue, as shown by the dashed line. A significant binding capacity will therefore introduce nonlinearity in the total equilibrium distribution relationship.

A linear relationship further signifies that the highest bulk source concentrations used in our studies do not saturate the total uptake capacity of the tissue for soluble dextran. Excessively high bulk concentrations would result in a total equilibrium relationship that asymptotes to a saturation limit at high bulk concentrations. Therefore,

linearity of the measured distribution relationship over the range of source concentrations used in our studies enables us to investigate drug transport that is unaffected by either specific drug-tissue interactions or capacity limitations of the tissue, which could potentially impede drug transport through sequestration or influence the driving force for drug penetration through tissue-induced gradients in drug concentration.

A fractional volume of distribution of 84% further supports the uninhibited transport characteristic of dextran in the tissue. Based on the equilibrium distribution model [44], the fractional volume of distribution is the empiric ratio between the concentration of soluble drug per unit total tissue volume and the concentration of the bulk phase. This relationship reflects the influences of steric interactions in the tissue that may exclude soluble drug and any charged partitioning in the accessible space that may reduce the concentration of soluble drug in the tissue. The fact that fractional volume of distribution is near 100% suggests that there is minimal inhibition, in the form of steric hindrance or partitioning, of dextran to freely diffuse through the muscle. Therefore, the concentration of dextran that transports within the accessible volume of the muscle closely approximates the concentration of dextran from the bulk source. This inert characteristic of dextran makes it an ideal, fluorescently labeled molecule to use in our experiments to investigate drug transport that is independent of specific binding.

As a matter of clarification, the fractional volume of distribution is distinct from the fractional volume, which is the ratio of accessible volume in the tissue to total tissue volume. Whereas fractional volume of distribution defines an effective drug transport space, fractional volume is a literal, physical space reflected more appropriately by tissue porosity. As a result, the soleus can have a fractional volume, or porosity, of 11%, as

shown by our tissue integrity studies, and also have a fractional volume of distribution of 84% for drug transport.

5.3.2 Drug Penetration and Distribution Under Mechanical Influence

5.3.2.1 *Validation of Experimental System*

Visual quantification of intramuscular drug transport gave us insight into the penetration and distribution of drug in soleus muscle and enabled us to evaluate the utility of our experimental system and measurement protocol. Drug penetration and distribution in incubated muscles was directly quantifiable from fluorescent images (Figure 13). Measurements made using these images had enough precision and consistency over multiple samples to show statistically significant differences in transport between loading groups.

Equivalent penetration at opposing planar and curved surfaces suggests that there is no directional preference to transport imposed by tissue architecture in either the dorsal-ventral or medial-lateral orientation. It suggests homogeneity of morphology with respect to each orientation, but not necessarily an overall isotropy for drug transport in the entire tissue. However, an isotropic transport environment may be assumed based on histological assessment. Additionally, equivalent penetration at opposing surfaces, or symmetry of penetration into the tissue, simplifies quantification of drug penetration in tissue images and serves as a measure of consistency of drug transport in each sample. Penetration can be quantified using either one of the opposing surfaces from either orientation. However, transport at the planar surfaces proceeds unidirectionally into the muscle and exemplifies transport into a semi-infinite medium as penetration does not

reach the half-thickness of the tissue within the duration of our experiments. Thus, drug penetration can be more consistently quantified and analyzed if measured from the planar surface.

Lastly, as drug source concentration was constant throughout the duration of the experiment there was no significant depletion of drug by the mass of the exposed muscles (Figure 15). Consequently, the driving force for drug penetration into the tissues was constant throughout the incubation period. These findings validate the precision and repeatability of the isolation and mounting technique, loading system, drug delivery preparation, and fluorescence quantification protocol.

5.3.2.2 Drug Penetration and Distribution

Muscle architecture and geometry play an important role in the intramuscular distribution of drug. Penetration at the curved margins of the soleus was greater than at planar surfaces by a factor of 1.57 under static strain and 2.52 under dynamic strain (Figure 14). Assuming an isotropic transport environment in the muscle, greater penetration at the curved margins may result from both the geometry of the curved surface itself and the spatial edge effect of drug distribution and penetration occurring at the margins of a nearly flat muscle cross-section. Substantial curvature of the marginal surface results in a semi-circumferential exposure to drug, which increases the surface area for drug to enter at this region and enables penetration to proceed in a multi-direction manner. Furthermore, drug transporting from these curved margins readily encounters drug penetrating at the planar surfaces due to the flatness and elliptical geometry of the muscle cross-section. Thus, drug penetration at the planar surfaces can

contribute significantly to the distribution of drug at the curved ends, especially when penetration is enhanced at all surfaces by mechanical loading.

5.3.2.3 Impact of Dynamic Loading

Dynamic loading impacts the penetration and distribution of drug in skeletal muscle. Cyclic strain significantly increased penetration of dextran into the tissue, by a factor of 1.56 at planar surfaces and 2.51 at curved surfaces. It is likely that dynamic loading, which cyclically stretches muscle through a range of strains from 0%-20%, both modifies the extracellular space available for drug distribution and alters the transport kinetics of the drug. From our assessment of architectural integrity, permanent changes to tissue porosity are independent of loading condition. Therefore, it is unlikely that drug penetration under dynamic loading increases due to progressive and lasting changes in extracellular space caused by straining the tissue. However, applying cyclical stretch between 0% and 20% strain may transiently expose drug to strain-dependent architectural configurations that have a larger accessible volume compared to that of the un-stretched configuration. Drug access to these larger volumes during a portion of each cycle of stretch may create spatially and temporally heterogeneous concentration gradients that increase the diffusional driving force for drug penetration. Moreover, mere exposure to a larger distribution space during a portion of the loading cycle may result in a greater time-averaged porosity for drug transport.

Perhaps not only mere exposure to architectural configurations with larger distribution space, but also the dynamic physical process of transitioning between different configurations has a great influence on drug transport. The dynamic forces

generated by oscillatory loading may impact transport kinetics and enhance drug penetration. Oscillatory loading can create dispersive influences [72] on soluble or aqueous drug that increase transport beyond molecular diffusion alone. Cyclic transitions between structural configurations during dynamic loading can compress and expand extracellular space. Such cyclic displacement and deformation of muscle fibers can impose normal and shear forces on interstitial fluid, resulting in pulsatile movement and agitation of soluble drug in the absence of bulk convective fluid flow. Such pulsatile agitation can disperse or spread drug over a greater volume of the available extracellular space, thereby driving it further into the tissue from the bulk source. As dispersion relies on the dynamics of structural displacement, it is dependent on the rate of oscillation. Therefore, dispersion is distinct from the mechanism of transient exposure to different architectural configurations, which yields the same time-averaged porosity for a single loading profile regardless of the rate of oscillation. For example, imposing a regular sinusoidal loading profile that strains the tissue between 0% and 20% would yield the same time-averaged porosity, whether the frequency was 1Hz, 2Hz, or 3Hz, because the tissue spends the same portion of each cycle at each strain regardless of the rate at which it occurs. However, rate of oscillation would modify the dynamics of loading and create progressively greater dispersive effects with greater loading frequencies.

5.3.2.4 Interaction Between Loading and Architecture

The fact that penetration at the curved margins increases to a greater degree, by a factor of 1.6, than at planar surfaces with dynamic loading may be attributed to the combined influence of static structural geometry, as discussed in Section 5.3.2.2, and the

spatially distinct dynamics of strain and extracellular space changes during stretch that are shaped by such geometry. While no biomechanics studies to our knowledge have quantified this effect, it is likely that changes in extracellular space and fractional volume of distribution inside a muscle developed during stretch are spatially heterogeneous and influenced by the local geometry of the muscle.

The uni-pennated, parallel-fibered rat soleus muscle has an elliptical axial cross-section that is observed to flatten and widen when the muscle is stretched. Studies of uni-pennated muscle have revealed that they experience changes in geometry during isometric contractions at various initial muscle lengths that are comprised of spatially heterogeneous changes in aponeurosis length, angle of pennation of muscle fibers, and fiber length [73]. One study observed transverse (perpendicular to the muscle surface) strains in superficial muscle fibers as the muscle body flattens during isometric contraction, and that aponeurosis surface area decreases with increasing initial muscle length [62]. It can be extrapolated from these studies, which assessed strains and changes in geometry only from the muscle surface, that flattening and widening of the soleus during stretch translate into similarly heterogeneous internal fiber rearrangements and intramuscular forces that can alter local drug distribution space and dispersion effects. This is especially the case when considering that conservation of muscle volume results in both widening and flattening of the muscle during elongation. While superficial muscle fibers at the planar surfaces tighten with muscle flattening, those at the curved margins of the soleus may experience increased outward transverse strains with muscle widening during stretch. Furthermore, because superficial fibers at the curved margins of the muscle occur more peripheral to the center of the tissue, they have more obtuse angles

of insertion relative to the muscle axis at the aponeuroses compared to fibers at planar surfaces, which are located towards the midline. These differences in local muscle geometry, fiber arrangement, and angle of insertion likely dictate heterogeneous local strain dynamics and changes in extracellular space during stretch or contraction. These architectural and dynamic heterogeneities may play a dominant role in producing greater enhancement of drug penetration at the curved surfaces under dynamic stretch.

Our findings suggest that mechanical loading influences drug transport through modulating and potentially superposing dispersive effects on the existing framework of drug transport established and dictated by tissue architecture.

5.4 Conclusions

This study presented a surgical isolation and muscle mounting method that preserves physiologic architecture of small rodent soleus muscles. A robust mechanical loading system and intramuscular fluorescent drug measurement protocol were also presented. These techniques were applied and validated through an experiment that investigated intramuscular transport of soluble macromolecule drug under mechanical loading of the tissue. The results from this experiment demonstrated the influence of not only architectural geometry and configuration, but also mechanical loading on intramuscular drug transport and distribution. Consequently, this work demonstrates the power and necessity of careful tissue isolation and mounting to maintain the physiologic configuration of samples. Significant findings from our work are that dynamic mechanical loading increases drug penetration into muscle above that achieved by static suspension of the muscle at nominal length, and it impacts drug distribution in muscle.

These findings yield important implications for pharmacokinetics investigations and clinical drug delivery strategies. Such studies should rightly consider the motion and contraction of a target tissue as drug transport is investigated. In particular, such studies should be conscious of the pharmacokinetic impact of mechanical loading and architectural physical activity of muscle target tissues, whose physiologic operational domain is mechanical activity.

6. FUTURE STUDIES

The influence of mechanical loading on transport is a new insight into tissue pharmacokinetics that requires further investigation. Further pharmacokinetics investigations using this test system and protocol have been planned to determine the isolated effects of different mechanical loading regimens on drug penetration and drug distribution profile.

6.1 Static Strain

These studies intend to quantify the effect of various degrees of static tensile strain on drug penetration to identify the distinct influence of architectural configuration and strain-dependent extracellular space on transport. Muscle morphology at these various strains will be quantified and correlated to drug penetration.

6.2 Drug Physical Property

In addition to studying target tissue structure, the influence of drug physical properties on transport will be investigated by comparing penetration of dextrans of various molecular weights at various static strains.

6.3 Dynamic Strain

The distinct contribution of oscillatory forces, independent of architectural configuration, will be investigated by quantifying drug penetration under various frequencies and durations of cyclic loading over a range of mean tensile strains.

6.4 Contraction

In contrast to elongating strain, the influence of contraction on drug transport will be assessed by quantifying penetration under various rates of isometric twitch contraction.

6.5 Computational Model

Ultimately, these investigations seek to establish a quantitative understanding of the influence of mechanical loading on transport by synthesizing the findings from these experiments into a computational model that describes these pharmacokinetic phenomena.

7. REFERENCES

1. Sreter, F.A., *Distribution of water, sodium, and potassium in resting and stimulated mammalian muscle*. Can J Biochem Physiol, 1963. **41**: p. 1035-45.
2. Huang, C.Y. and W.Y. Gu, *Effects of tension-compression nonlinearity on solute transport in charged hydrated fibrous tissues under dynamic unconfined compression*. J Biomech Eng, 2007. **129**(3): p. 423-9.
3. Quinn, T.M., V. Morel, and J.J. Meister, *Static compression of articular cartilage can reduce solute diffusivity and partitioning: implications for the chondrocyte biological response*. J Biomech, 2001. **34**(11): p. 1463-9.
4. Quinn, T.M., P. Dierickx, and A.J. Grodzinsky, *Glycosaminoglycan network geometry may contribute to anisotropic hydraulic permeability in cartilage under compression*. J Biomech, 2001. **34**(11): p. 1483-90.
5. Han, S., et al., *Changes in ADC caused by tensile loading of rabbit achilles tendon: evidence for water transport*. J Magn Reson, 2000. **144**(2): p. 217-27.
6. Helmer, K.G., et al., *Water movement in tendon in response to a repeated static tensile load using one-dimensional magnetic resonance imaging*. J Biomech Eng, 2006. **128**(5): p. 733-41.
7. Fry, D.L., R.W. Mahley, and S.Y. Oh, *Effect of arterial stretch on transmural albumin and Evan's blue dye transport*. Am J Physiol, 1981. **240**(4): p. H645-9.
8. Meyer, G., R. Merval, and A. Tedgui, *Effects of pressure-induced stretch and convection on low-density lipoprotein and albumin uptake in the rabbit aortic wall*. Circ Res, 1996. **79**(3): p. 532-40.
9. Ihlemann, J., et al., *Effect of stimulation frequency on contraction-induced glucose transport in rat skeletal muscle*. Am J Physiol Endocrinol Metab, 2000. **279**(4): p. E862-7.
10. Ihlemann, J., T. Ploug, and H. Galbo, *Effect of force development on contraction induced glucose transport in fast twitch rat muscle*. Acta Physiol Scand, 2001. **171**(4): p. 439-44.
11. Epstein, S.E., et al., *Therapeutic interventions for enhancing collateral development by administration of growth factors: basic principles, early results and potential hazards*. Cardiovasc Res, 2001. **49**(3): p. 532-42.
12. Marcil, M., et al., *Glucose infusion attenuates fatigue without sparing glycogen in rat soleus muscle during prolonged electrical stimulation in situ*. Eur J Appl Physiol, 2005. **93**(5-6): p. 569-74.
13. Ettema, G.J., *Mechanical behaviour of rat skeletal muscle during fatiguing stretch-shortening cycles*. Exp Physiol, 1997. **82**(1): p. 107-19.
14. Overgaard, K. and O.B. Nielsen, *Activity-induced recovery of excitability in K(+)-depressed rat soleus muscle*. Am J Physiol Regul Integr Comp Physiol, 2001. **280**(1): p. R48-55.
15. Monti, R.J., et al., *Mechanical properties of rat soleus aponeurosis and tendon during variable recruitment in situ*. J Exp Biol, 2003. **206**(Pt 19): p. 3437-45.
16. Bensamoun, S., et al., *Macroscopic-microscopic characterization of the passive mechanical properties in rat soleus muscle*. J Biomech, 2006. **39**(3): p. 568-78.

17. Vedsted, P., et al., *Muscle performance following fatigue induced by isotonic and quasi-isometric contractions of rat extensor digitorum longus and soleus muscles in vitro*. Acta Physiol Scand, 2003. **178**(2): p. 175-86.
18. Sakamoto, K., et al., *Akt signaling in skeletal muscle: regulation by exercise and passive stretch*. Am J Physiol Endocrinol Metab, 2003. **285**(5): p. E1081-8.
19. Wretman, C., et al., *Differential activation of mitogen-activated protein kinase signalling pathways by isometric contractions in isolated slow- and fast-twitch rat skeletal muscle*. Acta Physiol Scand, 2000. **170**(1): p. 45-9.
20. MacIntosh, B.R. and S.N. Bryan, *Potentiation of shortening and velocity of shortening during repeated isotonic tetanic contractions in mammalian skeletal muscle*. Pflugers Arch, 2002. **443**(5-6): p. 804-12.
21. Ai, H., et al., *Disruption of microtubules in rat skeletal muscle does not inhibit insulin- or contraction-stimulated glucose transport*. Am J Physiol Endocrinol Metab, 2003. **285**(4): p. E836-44.
22. Roeleveld, K., et al., *Role of tendon properties on the dynamic performance of different isometric muscles*. J Appl Physiol, 1993. **74**(3): p. 1348-55.
23. Ihlemann, J., et al., *Effect of tension on contraction-induced glucose transport in rat skeletal muscle*. Am J Physiol, 1999. **277**(2 Pt 1): p. E208-14.
24. Hunt, D.G., Z. Ding, and J.L. Ivy, *Propranolol prevents epinephrine from limiting insulin-stimulated muscle glucose uptake during contraction*. J Appl Physiol, 2002. **93**(2): p. 697-704.
25. Harrison, A.P. and J.A. Flatman, *Measurement of force and both surface and deep M wave properties in isolated rat soleus muscles*. Am J Physiol, 1999. **277**(6 Pt 2): p. R1646-53.
26. Armstrong, R.B., et al., *Elevations in rat soleus muscle [Ca²⁺] with passive stretch*. J Appl Physiol, 1993. **74**(6): p. 2990-7.
27. van Emst, M.G., et al., *Reducing chloride conductance prevents hyperkalaemia-induced loss of twitch force in rat slow-twitch muscle*. J Physiol, 2004. **561**(Pt 1): p. 169-81.
28. Ettema, G.J. and P.A. Huijing, *Skeletal muscle stiffness in static and dynamic contractions*. J Biomech, 1994. **27**(11): p. 1361-8.
29. Lieber, R.L. and J. Friden, *Functional and clinical significance of skeletal muscle architecture*. Muscle Nerve, 2000. **23**(11): p. 1647-66.
30. Devrome, A.N. and B.R. MacIntosh, *The biphasic force-velocity relationship in whole rat skeletal muscle in situ*. J Appl Physiol, 2007. **102**(6): p. 2294-300.
31. Roy, R.R., et al., *Mechanical properties of the electrically silent adult rat soleus muscle*. Muscle Nerve, 2002. **26**(3): p. 404-12.
32. Talmadge, R.J., et al., *Mechanical properties of rat soleus after long-term spinal cord transection*. J Appl Physiol, 2002. **93**(4): p. 1487-97.
33. Campbell, C.B., D.R. Marsh, and L.L. Spriet, *Anaerobic energy provision in aged skeletal muscle during tetanic stimulation*. J Appl Physiol, 1991. **70**(4): p. 1787-95.
34. Loeffler, L., 3rd and K. Sagawa, *A one-dimensional viscoelastic model of cat heart muscle studied by small length perturbations during isometric contraction*. Circ Res, 1975. **36**(4): p. 498-512.

35. Segal, S.S. and J.A. Faulkner, *Temperature-dependent physiological stability of rat skeletal muscle in vitro*. Am J Physiol, 1985. **248**(3 Pt 1): p. C265-70.
36. Petrofsky, J.S. and A.R. Lind, *The influence of temperature on the isometric characteristics of fast and slow muscle in the cat*. Pflugers Arch, 1981. **389**(2): p. 149-54.
37. Blomstrand, E., L. Larsson, and L. Edstrom, *Contractile properties, fatiguability and glycolytic metabolism in fast- and slow-twitch rat skeletal muscles of various temperatures*. Acta Physiol Scand, 1985. **125**(2): p. 235-43.
38. Close, R. and J.F. Hoh, *Influence of temperature on isometric contractions of rat skeletal muscles*. Nature, 1968. **217**(5134): p. 1179-80.
39. Cappelli, V., et al., *Tritiated water (HTO) and inulin spaces in isolated skeletal and cardiac muscles: influence of contractile activity*. Experientia, 1981. **37**(8): p. 849-50.
40. Kobayashi, N. and K. Yonemura, *The extracellular space in red and white muscles of the rat*. Jpn J Physiol, 1967. **17**(6): p. 698-707.
41. Sreter, F.A. and G. Woo, *Cell Water, Sodium, And Potassium In Red And White Mammalian Muscles*. Am J Physiol, 1963. **205**: p. 1290-4.
42. Ryall, J.G., et al., *Beta 2-agonist fenoterol has greater effects on contractile function of rat skeletal muscles than clenbuterol*. Am J Physiol Regul Integr Comp Physiol, 2002. **283**(6): p. R1386-94.
43. Rankin, L.L., et al., *Coexistence of twitch potentiation and tetanic force decline in rat hindlimb muscle*. J Appl Physiol, 1988. **65**(6): p. 2687-95.
44. Lovich, M.A. and E.R. Edelman, *Tissue average binding and equilibrium distribution: an example with heparin in arterial tissues*. Biophys J, 1996. **70**(3): p. 1553-9.
45. Pringsheim, P., *Fluorescence and Phosphorescence*. 1963, New York: Interscience Publishers, Inc. p. 347.
46. Creese, R., J.L. D'Silva, and S.E. Hashish, *Inulin space and fibre size of stimulated rat muscle*. J Physiol, 1955. **127**(3): p. 525-32.
47. Cappelli, V., et al., *Inulin uptake and washout in contracting and quiescent rat papillary muscle*. Arch Int Physiol Biochim, 1982. **90**(4): p. 231-6.
48. Ward, D.S., M.T. Hamilton, and P.D. Watson, *Measurement of tissue volume during non-steady state high-intensity muscle contraction*. Am J Physiol, 1996. **271**(6 Pt 2): p. R1682-90.
49. Baker, C.H. and D.L. Davis, *Isolated skeletal muscle blood flow and volume changes during contractile activity*. Blood Vessels, 1974. **11**(1-2): p. 32-44.
50. Sreter, F.A., *Cell Water, Sodium, And Potassium In Stimulated Red And White Mammalian Muscles*. Am J Physiol, 1963. **205**: p. 1295-8.
51. Trombitas, K., et al., *Contraction-induced movements of water in single fibres of frog skeletal muscle*. J Muscle Res Cell Motil, 1993. **14**(6): p. 573-84.
52. Papadopoulos, S., K.D. Jurgens, and G. Gros, *Protein diffusion in living skeletal muscle fibers: dependence on protein size, fiber type, and contraction*. Biophys J, 2000. **79**(4): p. 2084-94.
53. Holloszy, J.O. and H.T. Narahara, *Studies of tissue permeability. X. Changes in permeability to 3-methylglucose associated with contraction of isolated frog muscle*. J Biol Chem, 1965. **240**(9): p. 3493-500.

54. Aslesen, R., et al., *Glucose uptake and metabolic stress in rat muscles stimulated electrically with different protocols*. J Appl Physiol, 2001. **91**(3): p. 1237-44.
55. Constable, S.H., et al., *Muscle glucose transport: interactions of in vitro contractions, insulin, and exercise*. J Appl Physiol, 1988. **64**(6): p. 2329-32.
56. McDermott, J.C. and A. Bonen, *Lactate transport in rat sarcolemmal vesicles and intact skeletal muscle, and after muscle contraction*. Acta Physiol Scand, 1994. **151**(1): p. 17-28.
57. Abraham, K.A. and R.L. Terjung, *Phosphate uptake in rat skeletal muscle is reduced during isometric contractions*. J Appl Physiol, 2004. **97**(1): p. 57-62.
58. Gissel, H. and T. Clausen, *Excitation-induced Ca²⁺ uptake in rat skeletal muscle*. Am J Physiol, 1999. **276**(2 Pt 2): p. R331-9.
59. Gissel, H. and T. Clausen, *Excitation-induced Ca(2+) influx in rat soleus and EDL muscle: mechanisms and effects on cellular integrity*. Am J Physiol Regul Integr Comp Physiol, 2000. **279**(3): p. R917-24.
60. Verburg, E., et al., *Muscle contractile properties during intermittent nontetanic stimulation in rat skeletal muscle*. Am J Physiol Regul Integr Comp Physiol, 2001. **281**(6): p. R1952-65.
61. Schachar, R., W. Herzog, and T.R. Leonard, *The effects of muscle stretching and shortening on isometric forces on the descending limb of the force-length relationship*. J Biomech, 2004. **37**(6): p. 917-26.
62. van Donkelaar, C.C., et al., *Skeletal muscle transverse strain during isometric contraction at different lengths*. J Biomech, 1999. **32**(8): p. 755-62.
63. Ettema, G.J., J.T. Goh, and M.R. Forwood, *A new method to measure elastic properties of plastic-viscoelastic connective tissue*. Med Eng Phys, 1998. **20**(4): p. 308-14.
64. Templeton, G.H., et al., *Dynamic stiffness of papillary muscle during contraction and relaxation*. Am J Physiol, 1973. **224**(3): p. 692-8.
65. Elmquist, S., et al., *Dextrans as markers for endocytosis in innervated and denervated skeletal muscle*. Muscle Nerve, 1992. **15**(8): p. 876-84.
66. Osman, F.H., J.L. Munson, and D.M. Paton, *Estimation of extracellular space in rabbit detrusor muscle*. Comp Biochem Physiol A, 1971. **40**(1): p. 45-54.
67. Rutili, G. and K.E. Arfors, *Fluorescein-labelled dextran measurement in interstitial fluid in studies of macromolecular permeability*. Microvasc Res, 1976. **12**(2): p. 221-30.
68. Hawkins, D. and M. Bey, *Muscle and tendon force-length properties and their interactions in vivo*. J Biomech, 1997. **30**(1): p. 63-70.
69. Stolov, W.C. and T.G. Weilepp, Jr., *Passive length-tension relationship of intact muscle, epimysium, and tendon in normal and denervated gastrocnemius of the rat*. Arch Phys Med Rehabil, 1966. **47**(9): p. 612-20.
70. Mehvar, R., *Dextrans for targeted and sustained delivery of therapeutic and imaging agents*. J Control Release, 2000. **69**(1): p. 1-25.
71. Schroder, U., K.E. Arfors, and O. Tangen, *Stability of fluorescein labeled dextrans in vivo and in vitro*. Microvasc Res, 1976. **11**(1): p. 57-66.
72. McCarthy, M.J., D.S. Soong, and E.R. Edelman, *Control of Drug Release From Polymer Matrices Impregnated with Magnetic Beads - A Proposed Mechanism*

- and Model for Enhanced Release. Journal of Controlled Release, 1984. 1: p. 143-147.*
73. Zuurbier, C.J. and P.A. Huijing, *Changes in geometry of actively shortening unipennate rat gastrocnemius muscle. J Morphol, 1993. 218(2): p. 167-80.*

8. ACKNOWLEDGMENTS

These studies were supported in part by graduate fellowships from the Department of Defense and the Whitaker Foundation for Biomedical Engineering to Peter I-Kung Wu, and a research grant from the National Institutes of Health (GM/HL 49039, HL 60407) to Elazer R. Edelman.

Special thanks to Gerry Wentworth of the M.I.T. Laboratory of Manufacturing and Productivity for his technical advice on the manufacturing process and machining of the dynamic loading device.

APPENDIX A: MATLAB SOURCE CODE TO SIMULATE RESTING MUSCLE RESPONSES TO LENGTH PERTURBATIONS

Simulation of Step Response

```
clear
clc

%___Parameter Values for Inertial Mass, Muscle Stiffnesses, and Damping
Coefficients___
%___In SI Units, Newton, Kg, Meter, Seconds_____

%___Amplitude of length perturbation_____
A=.002; %m

k0=10*9.80665*20; %N/m      conversion from g/mm to N/m multiplied by
k1=3*9.80665*20; %N/m      cross sectional area of 20 mm^2
k2=2.5*9.80665*20; %N/m
c1=.1625*9.80665*20; %N.s/m
c2=6*9.80665*20; %N.s/m

%___Time-Domain
Equations_____
t=linspace(0,10,100);

first=A*k0;
second=A*k1*exp(-t/(c1/k1));
third=A*k2*exp(-t/(c2/k2));

fp=first+second+third;

max(fp)
plot(t,fp)
title('Passive Tension Response of Muscle to Step Displacement of 0.002m')
xlabel('Time (sec)')
ylabel('Force (N)')
```

Simulation of Frequency Response

```
clear
clc
```

```
%___ Parameter Values for Inertial Mass, Muscle Stiffnesses, and Damping
Coefficients___
%___ In SI Units, Newton, Kg, Meter,
Seconds_____
```

```
%___ Total Mass Estimate of muscle and loading assembly components
m=0.2;      %kg
```

```
%___ Model
```

```
Parameters_____
```

```
k0=10*9.806658*20; %N/m      conversion from g/mm to N/m multiplied by
k1=3*9.80665*20; %N/m      cross sectional area of 20 mm^2
k2=2.5*9.80665*20; %N/m
c1=.1625*9.80665*20; %N.s/m
c2=6*9.80665*20; %N.s/m
```

```
%_____
```

```
%___ State Space
```

```
Model_____
```

```
A=[0 (-1/m) (-1/m) (-1/m); k1 (-k1/c1) 0 0; k2 0 (-k2/c2) 0; k0 0 0 0];
B=[(1/m); 0;0;0];
C=[1 0 0 0];
D=[0];
sys=ss(A,B,C,D);
```

```
%_____
```

```
%___ Vm/Fin Transfer
```

```
Function_____
```

```
sys2=tf(sys);
```

```
%___ Creation of the Fin/Xm Transfer
```

```
Function_____
```

```
den=[5 94.39 38.46 0];
num=[1 18.88 1.521e004 2.316e005 7.544e004 0];
```

```
%___ Maximum
```

```
Estimate_____
```

```
%Transfer function
```

```
% 5 s^3 + 94.39 s^2 + 38.46 s
```

```
%-----  
%s^4 + 18.88 s^3 + 1.521e004 s^2 + 2.316e005 s + 7.544e004
```

```
% Bode Plot of Displacement Input and Force  
Output
```

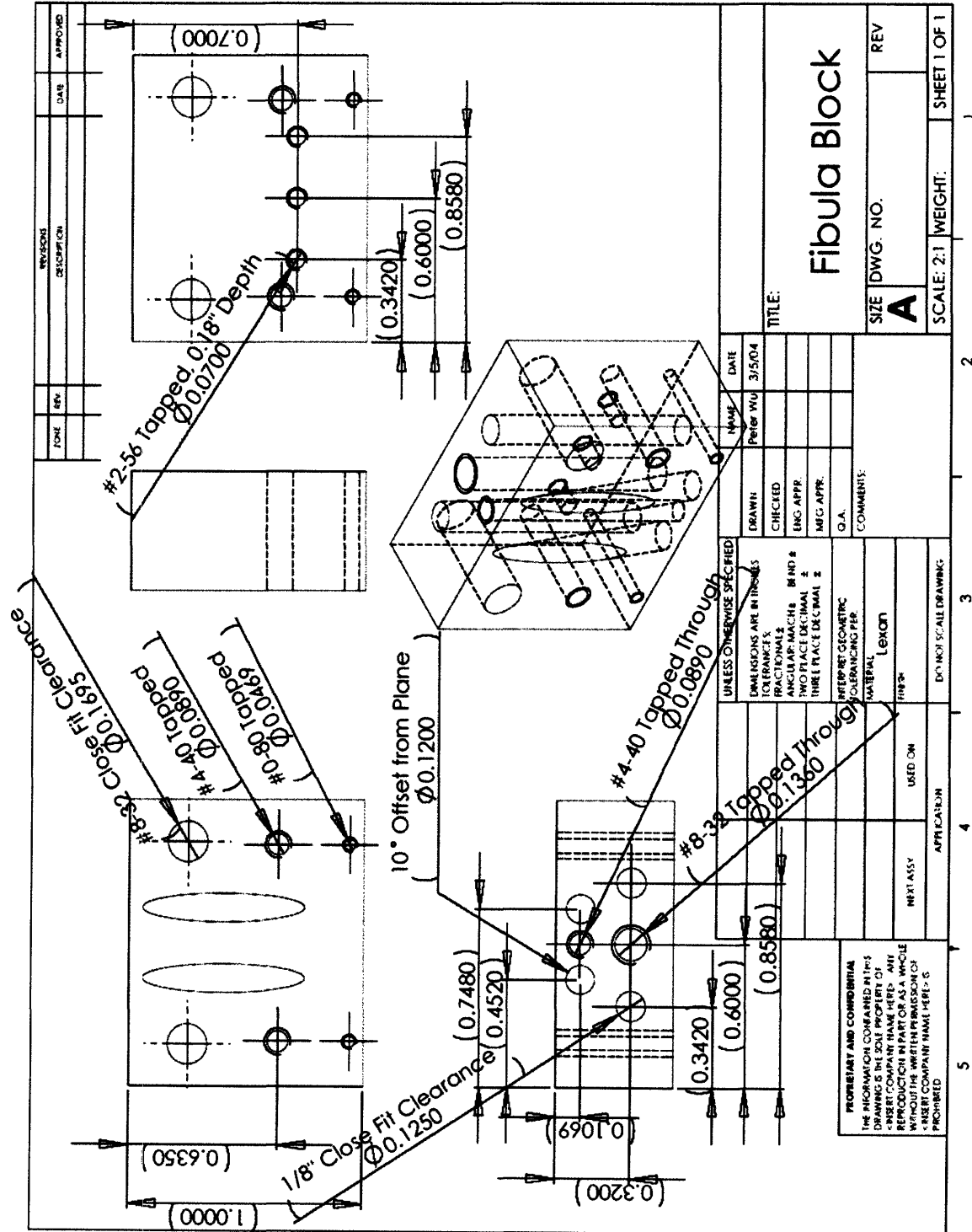
```
w=logspace(0,1.3,1000);  
bode(num,den,w)  
[MAG,PHASE,W] = BODE(num,den,w);
```

```
%-----
```

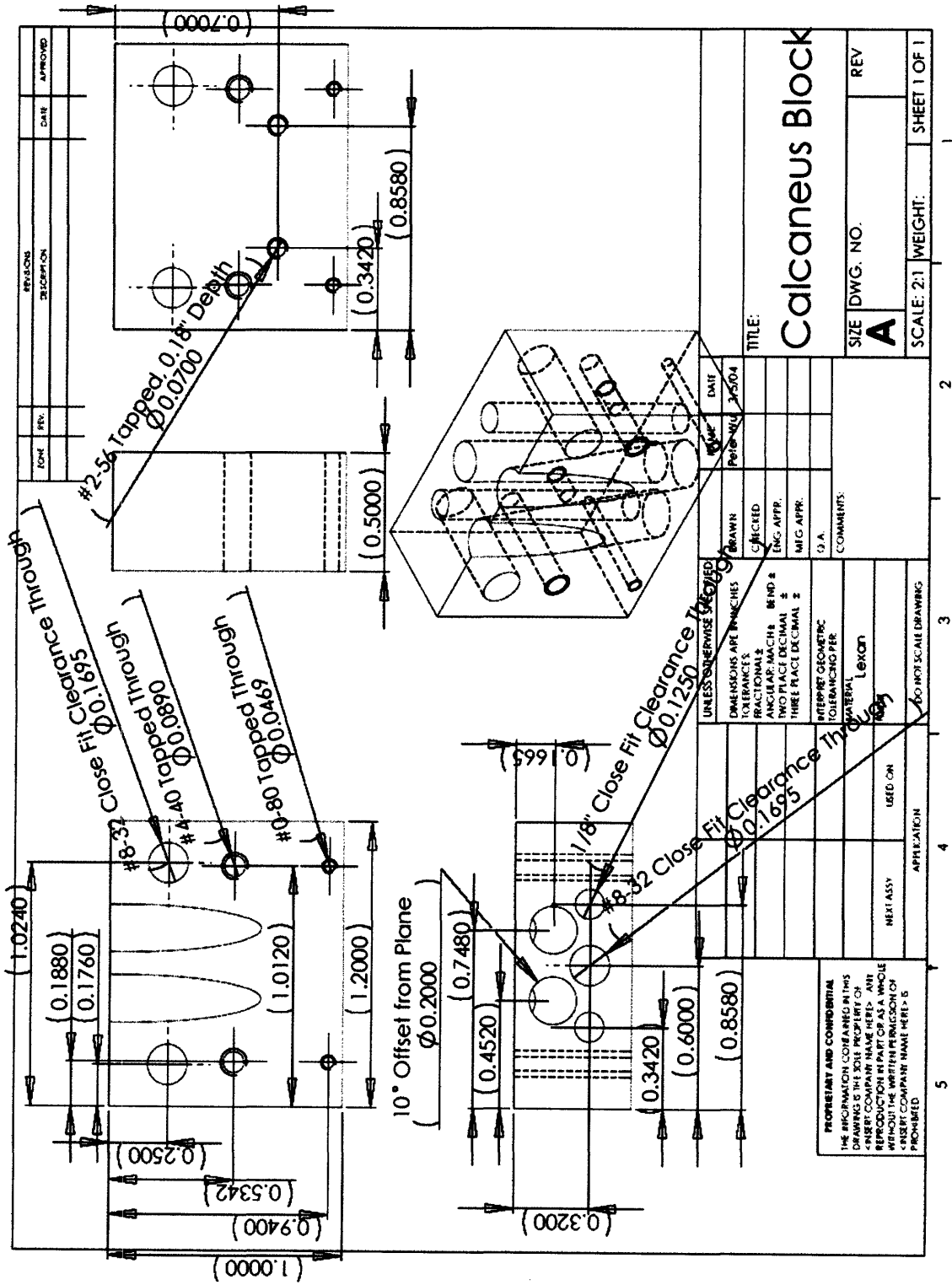
```
%Multiply the Force by a 20% displacement for a 10mm length of muscle  
%or a 2mm length perturbation
```

APPENDIX B: COMPONENT DESIGNS

Fibula Mounting Block (all units are in inches)



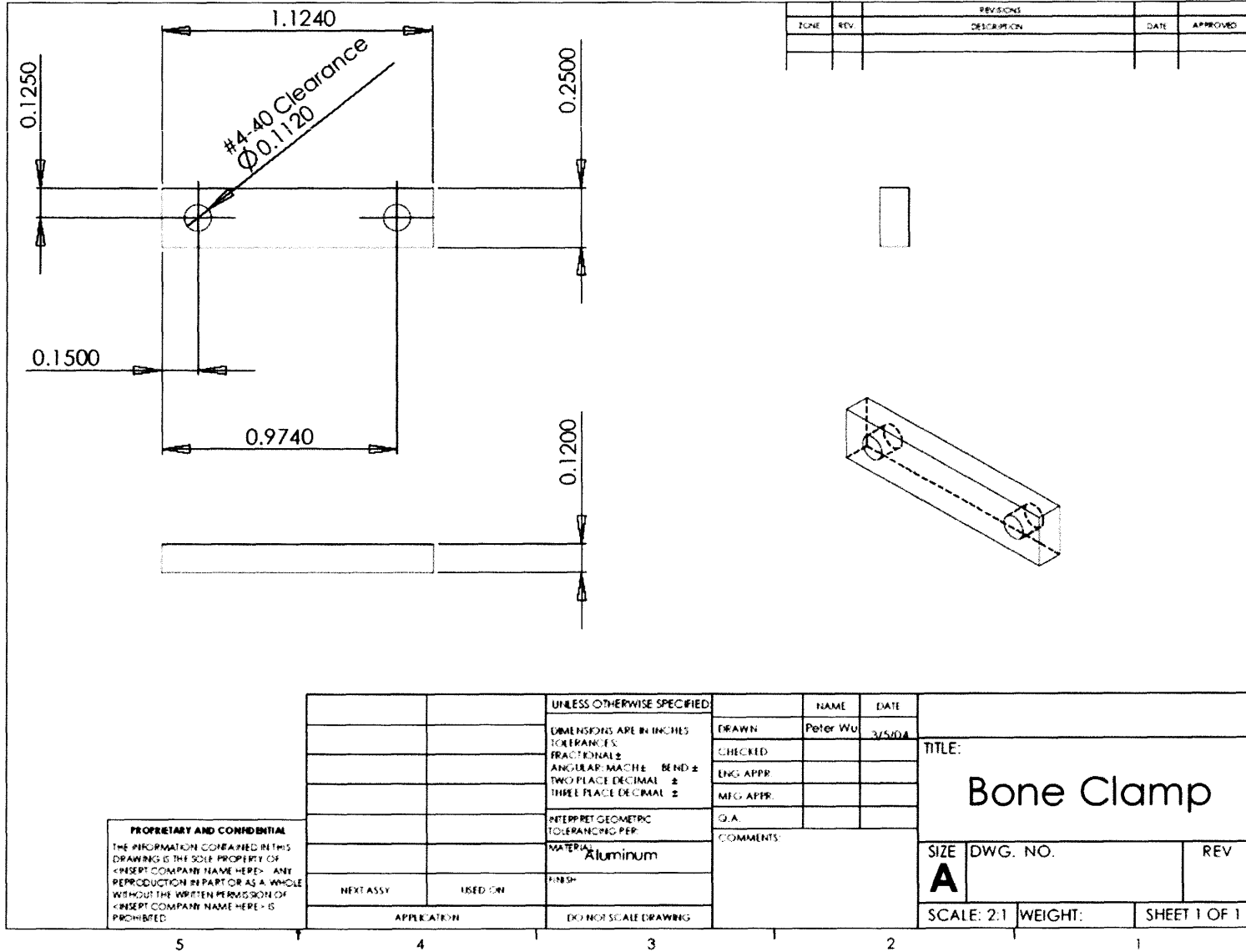
Calcaneus Mounting Block



REV.	DATE	DESCRIPTION	APPROVED

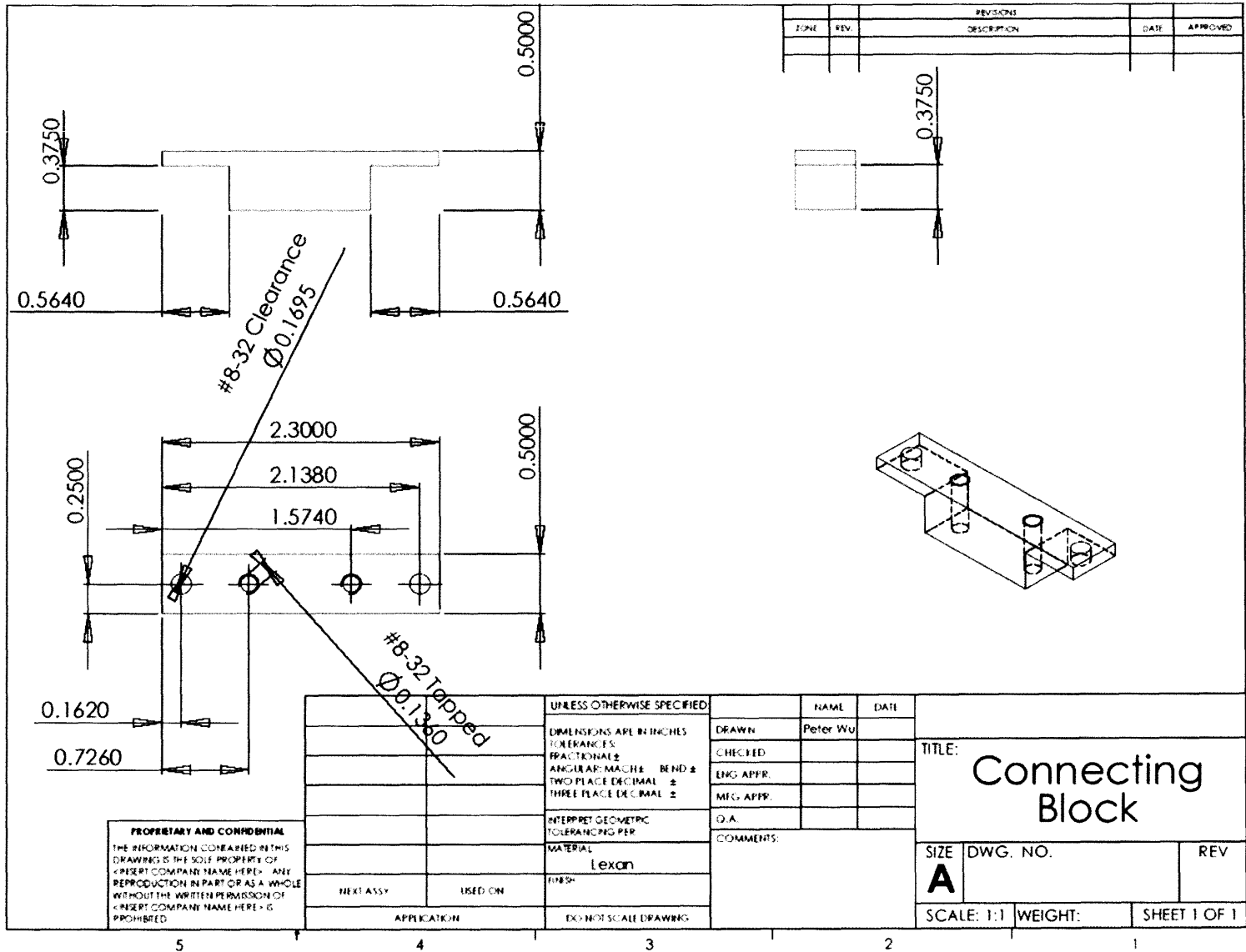
DRAWN		CHECKED		DATE	
ENG. APPR.		MIC. APPR.		PART-NUM 35504	
S.P.A.		COMMENTS:		TITLE: Calcaneus Block	
MATERIAL: Lexan		HEAT ASSY: USED ON:		SIZE DWG. NO. A	
APPLICATION:		TOLERANCE PER:		SCALE: 2:1	
ADD NOT SCALE DRAWING		UNLESS OTHERWISE SPECIFIED		WEIGHT: SHEET 1 OF 1	
DIMENSIONS ARE IN INCHES		FRACTIONS		1	
ANGULAR DIMENSIONS		DECIMALS		2	
HOLE LOCATIONS		THREE PLACE DECIMALS		3	
HOLE DIAMETERS		TWO PLACE DECIMALS		4	
HOLE PITCHES		THREE PLACE DECIMALS		5	

PROPRIETARY AND CONFIDENTIAL
 THE INFORMATION CONTAINED IN THIS
 DRAWING IS THE SOLE PROPERTY OF
 THE COMPANY. ANY REPRODUCTION
 WITHOUT THE WRITTEN PERMISSION OF
 THE COMPANY IS PROHIBITED.

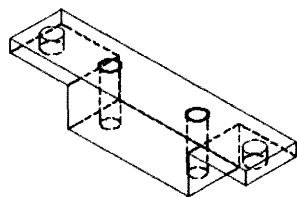


Bone Clamp

PROPRIETARY AND CONFIDENTIAL
 THE INFORMATION CONTAINED IN THIS DRAWING IS THE SOLE PROPERTY OF <INSERT COMPANY NAME HERE>. ANY REPRODUCTION IN PART OR AS A WHOLE WITHOUT THE WRITTEN PERMISSION OF <INSERT COMPANY NAME HERE> IS PROHIBITED.



REVISIONS		DATE	APPROVED
ZONE	REV.	DESCRIPTION	

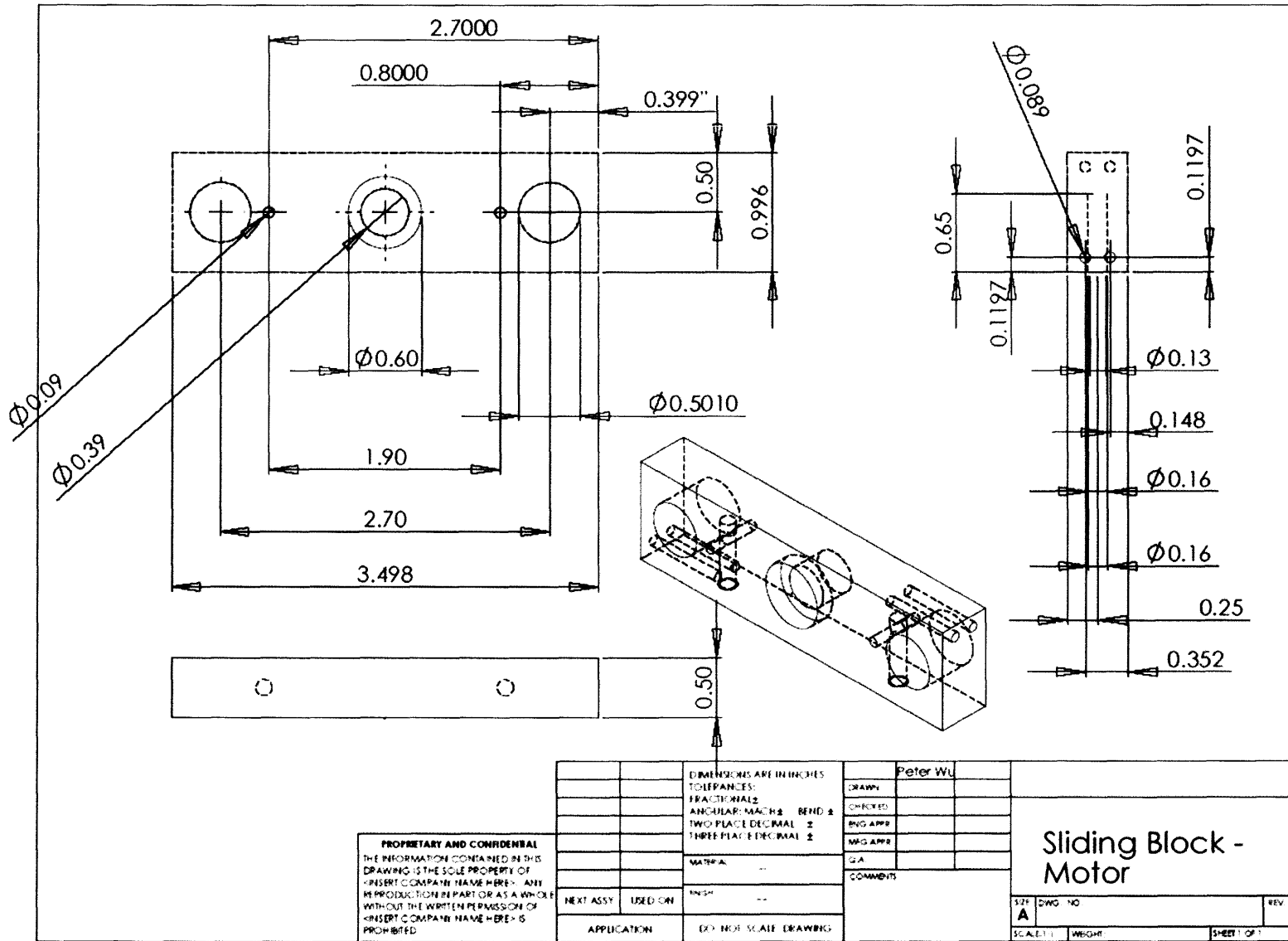


PROPRIETARY AND CONFIDENTIAL
 THE INFORMATION CONTAINED IN THIS DRAWING IS THE SOLE PROPERTY OF [INSERT COMPANY NAME HERE]. ANY REPRODUCTION IN PART OR AS A WHOLE WITHOUT THE WRITTEN PERMISSION OF [INSERT COMPANY NAME HERE] IS PROHIBITED.

UNLESS OTHERWISE SPECIFIED:	DRAWN	NAME	DATE
DIMENSIONS ARE IN INCHES	Peter Wu		
TOLERANCES:	CHECKED		
FRACTIONAL ±	ENG APPR.		
ANGULAR: MACHINE BEND ±	MFG APPR.		
TWO PLACE DECIMAL ±	D.A.		
THREE PLACE DECIMAL ±	COMMENTS:		
INTERPRET GEOMETRIC TOLERANCING PER			
MATERIAL			
Lexan			
FINISH			
APPLICATION			
DO NOT SCALE DRAWING			

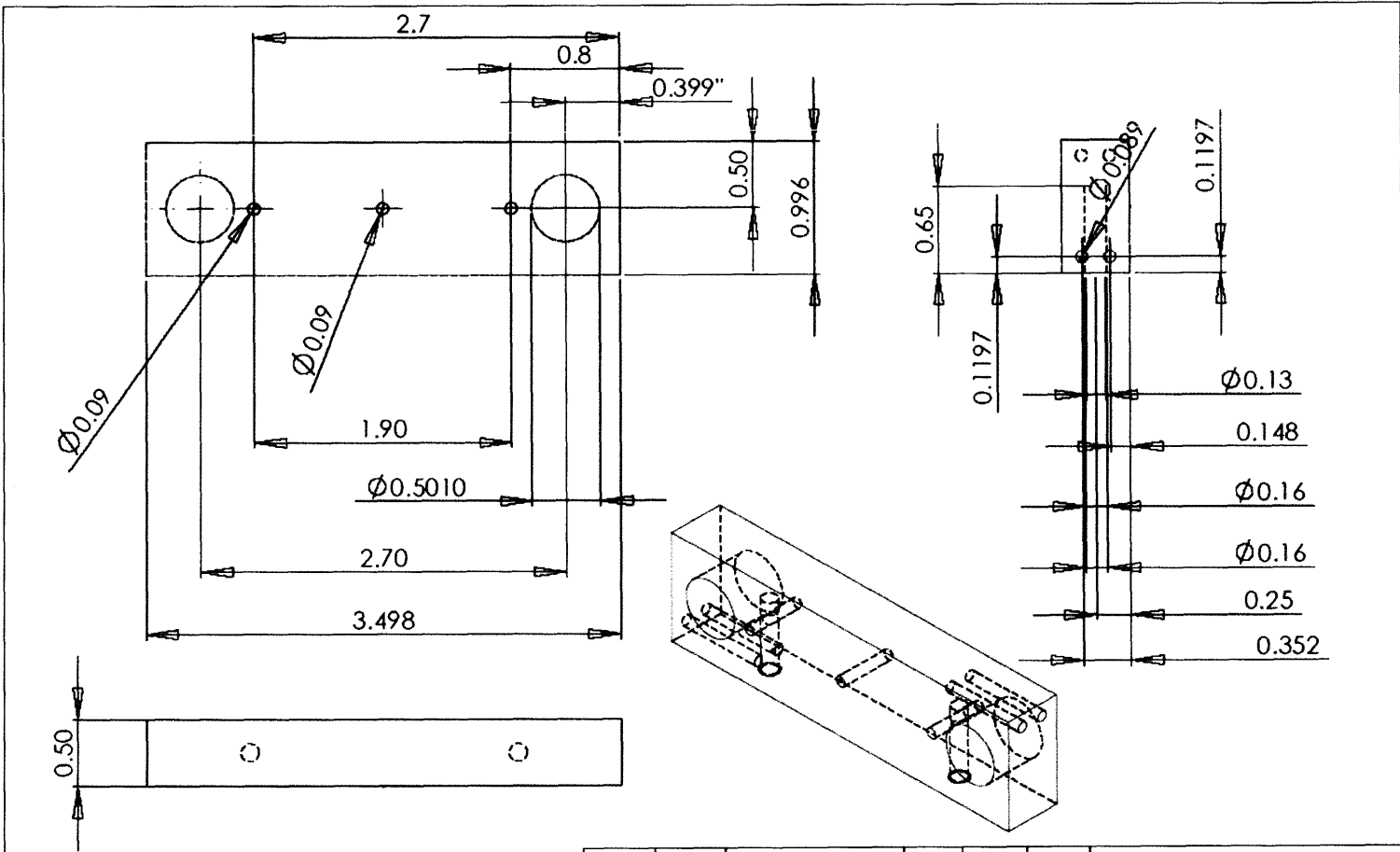
TITLE:		
Connecting Block		
SIZE	DWG. NO.	REV
A		
SCALE: 1:1	WEIGHT:	SHEET 1 OF 1

Connecting Block



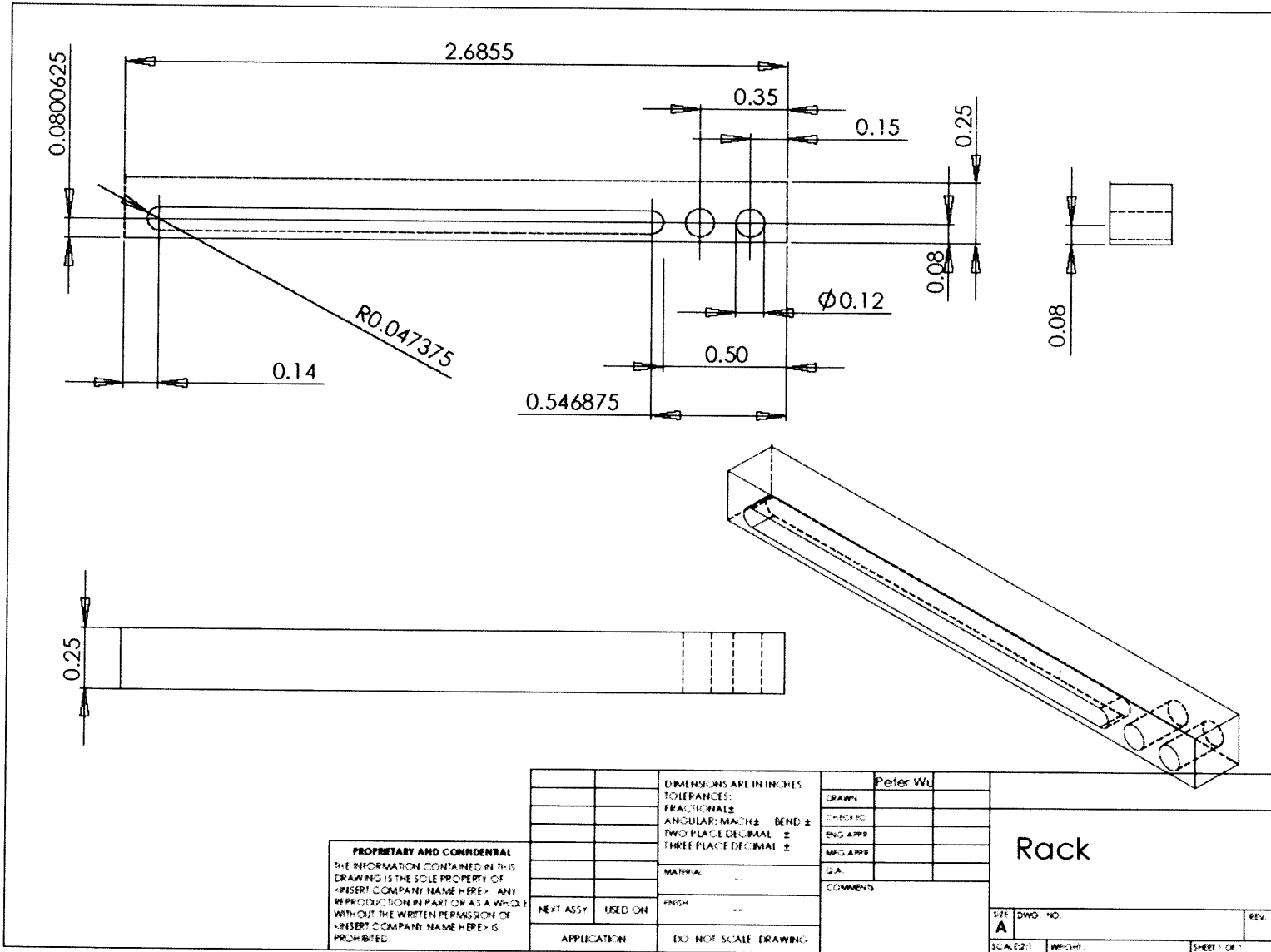
Sliding Block - Motor

Sliding Block – Load Cell



PROPRIETARY AND CONFIDENTIAL
 THE INFORMATION CONTAINED IN THIS DRAWING IS THE SOLE PROPERTY OF <INSERT COMPANY NAME HERE>. ANY REPRODUCTION IN PART OR AS A WHOLE WITHOUT THE WRITTEN PERMISSION OF <INSERT COMPANY NAME HERE> IS PROHIBITED.

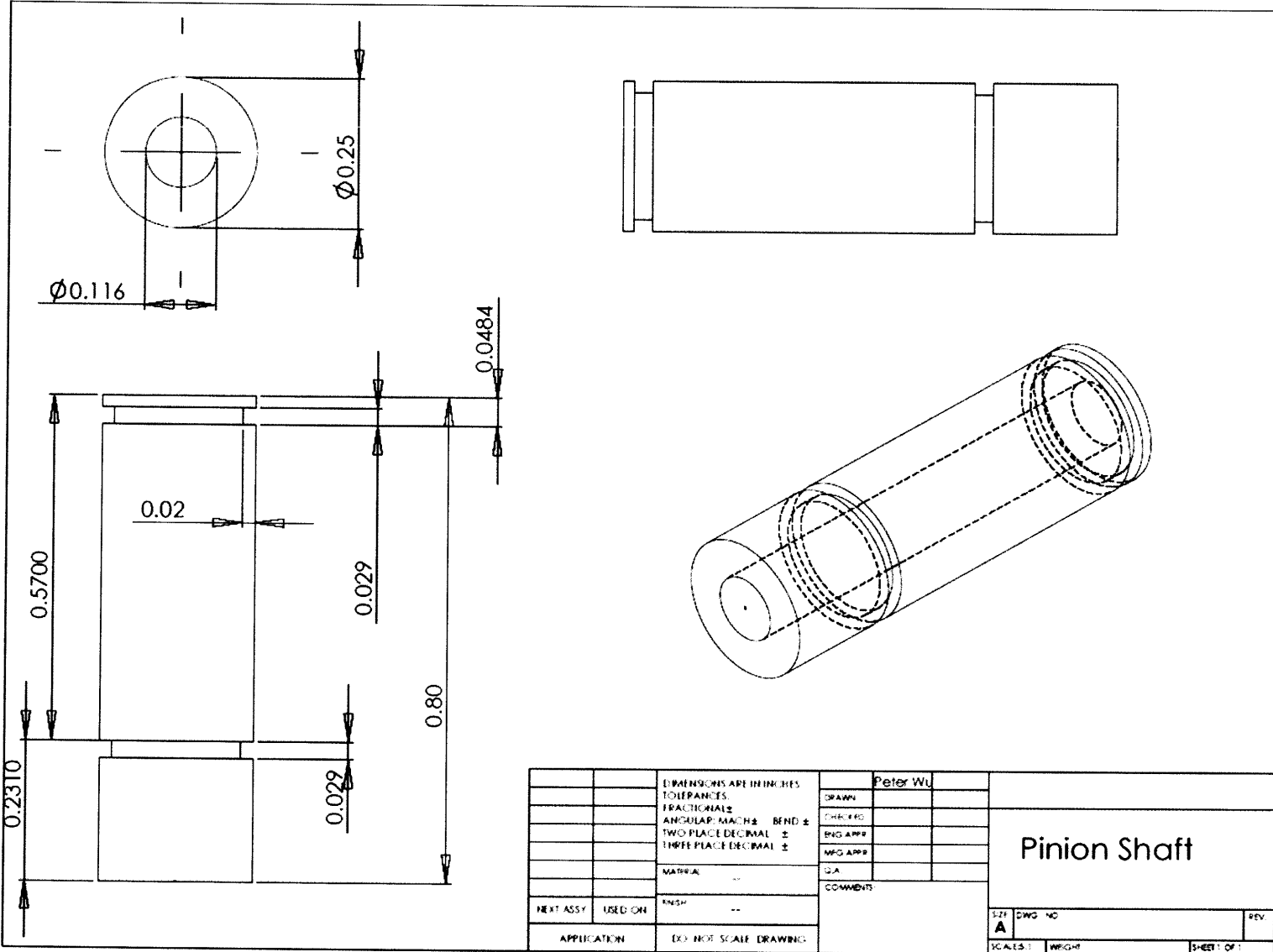
		DIMENSIONS ARE IN MILLIMETERS TOLERANCES: FRACTIONAL ± ANGULAR: MACH ± BEND ± TWO PLACE DECIMAL ± THREE PLACE DECIMAL ±		Peter Wu	
		MATERIAL: --		DRAWN: []	
		FINISH: --		CHECKED: []	
NEXT ASSY		USED ON		ENG APPR: []	
APPLICATION		DO NOT SCALE DRAWING		MFG APPR: []	
				QA: []	
				COMMENTS: []	
				Sliding Block - Load Cell	
				SIZE: A DWG NO: [] REV: []	
				SCALE: 1:1 WEIGHT: [] SHEET OF: []	



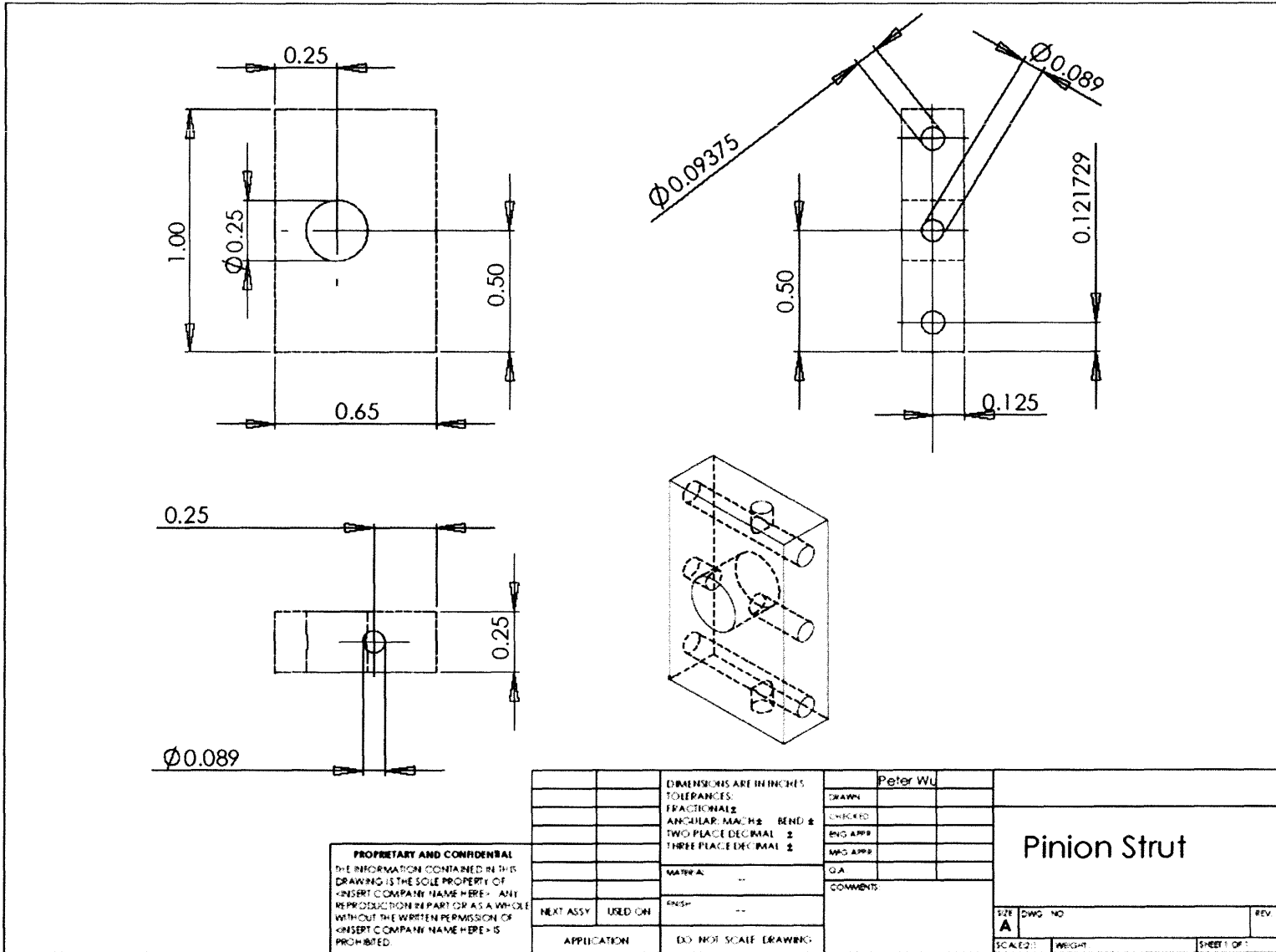
Rack

PROPRIETARY AND CONFIDENTIAL
 THE INFORMATION CONTAINED IN THIS
 DRAWING IS THE SOLE PROPERTY OF
 <INSERT COMPANY NAME HERE>. ANY
 REPRODUCTION IN PART OR AS A WHOLE
 WITHOUT THE WRITTEN PERMISSION OF
 <INSERT COMPANY NAME HERE> IS
 PROHIBITED.

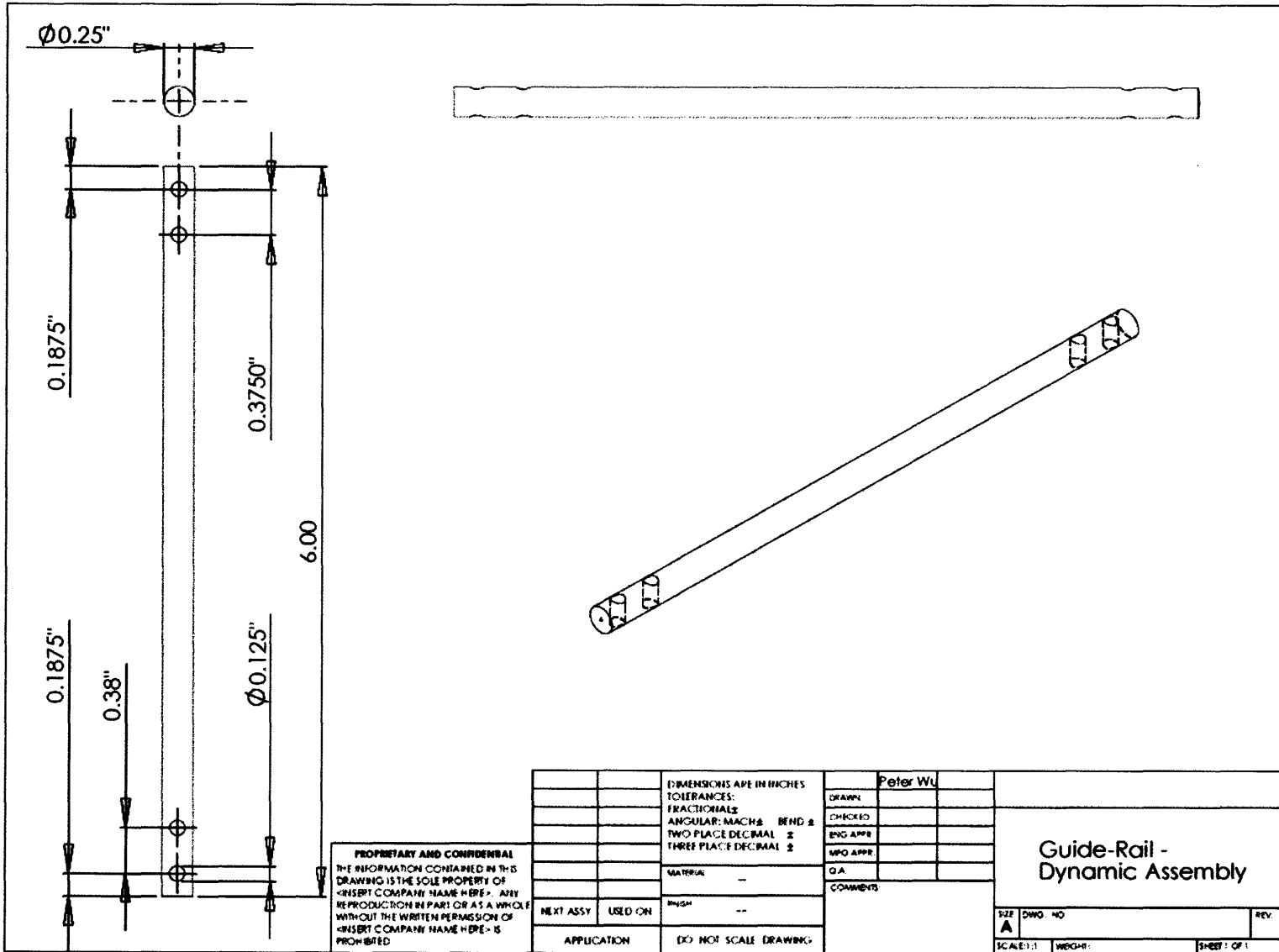
		DIMENSIONS ARE IN INCHES TOLERANCES: FRACTIONAL ± ANGULAR: MACH ± BEND ± TWO PLACE DECIMAL ± THREE PLACE DECIMAL ±		Peter Wu		<p>Rack</p> <table border="1"> <tr> <td>SIZE</td> <td>DWG NO</td> <td>REV</td> </tr> <tr> <td>A</td> <td></td> <td></td> </tr> <tr> <td>SCALE: 1</td> <td>WGT</td> <td>SHEET OF 1</td> </tr> </table>		SIZE	DWG NO	REV	A			SCALE: 1	WGT	SHEET OF 1
SIZE	DWG NO	REV														
A																
SCALE: 1	WGT	SHEET OF 1														
		MATERIAL: --		DRAWN												
		FINISH: --		CHECKED												
NEXT ASSY		USED ON		ENG APPR												
APPLICATION		DO NOT SCALE DRAWING		MFG APPR												
				QA												
				COMMENTS												



Pinion Shaft

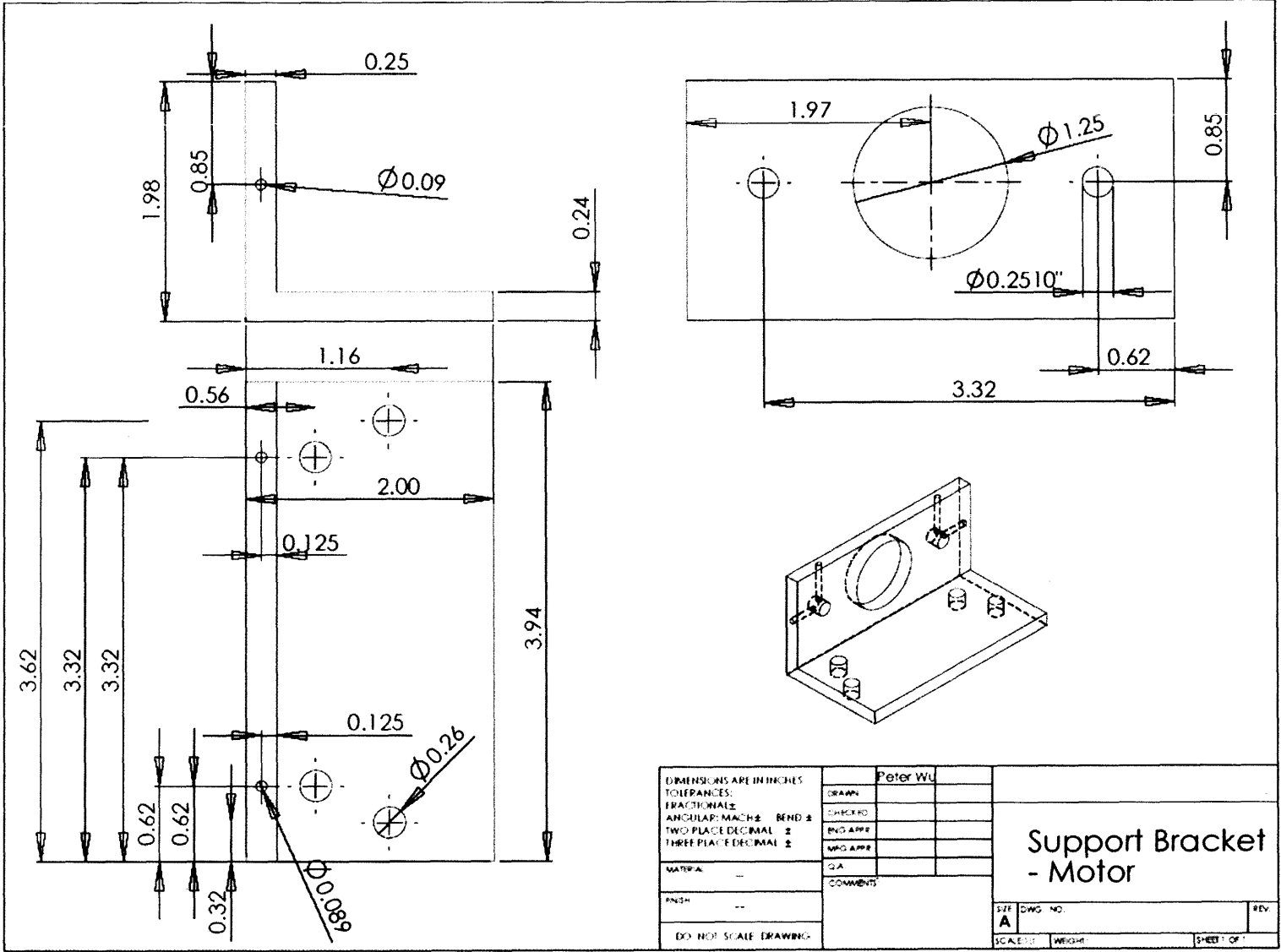


Pinion Strut

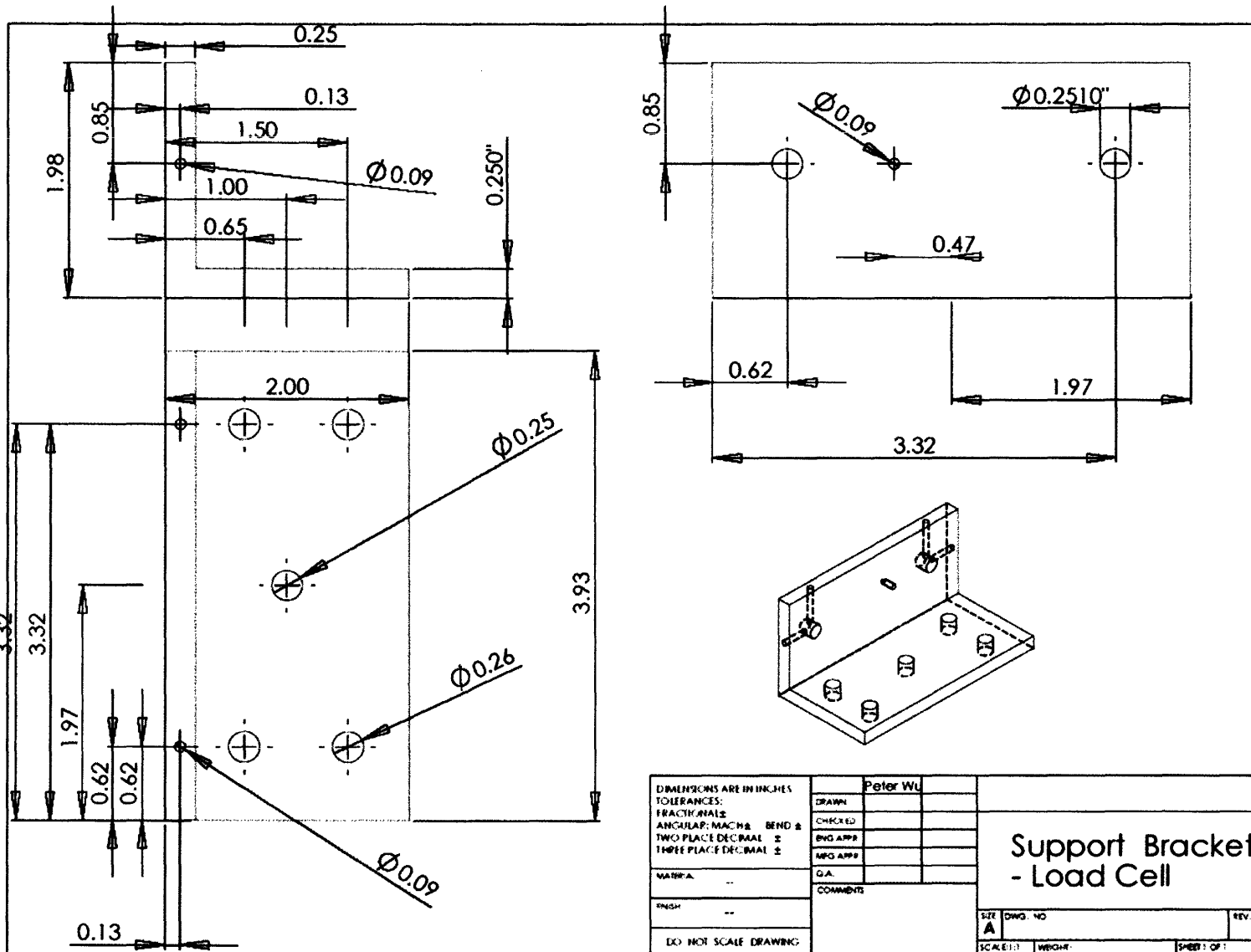


PROPRIETARY AND CONFIDENTIAL
 THE INFORMATION CONTAINED IN THIS
 DRAWING IS THE SOLE PROPERTY OF
 <INSERT COMPANY NAME HERE>. ANY
 REPRODUCTION IN PART OR AS A WHOLE
 WITHOUT THE WRITTEN PERMISSION OF
 <INSERT COMPANY NAME HERE> IS
 PROHIBITED

		DIMENSIONS ARE IN INCHES		Peter Wu	
		TOLERANCES:		DRAWN	
		FRACTIONALS:		CHECKED	
		ANGULAR: MACH ± BEND ±		ENG APPR	
		TWO PLACE DECIMAL ±		MFG APPR	
		THREE PLACE DECIMAL ±		QA	
		MATERIAL: --		COMMENTS	
NEXT ASSY	USED ON	FINISH	--		
APPLICATION	DO NOT SCALE DRAWING				
				Guide-Rail - Dynamic Assembly	
SIZE	DWG. NO			REV.	
A					
SCALE: 1:1	WEIGHT:		SHEET 1 OF 1		



Support Bracket - Motor



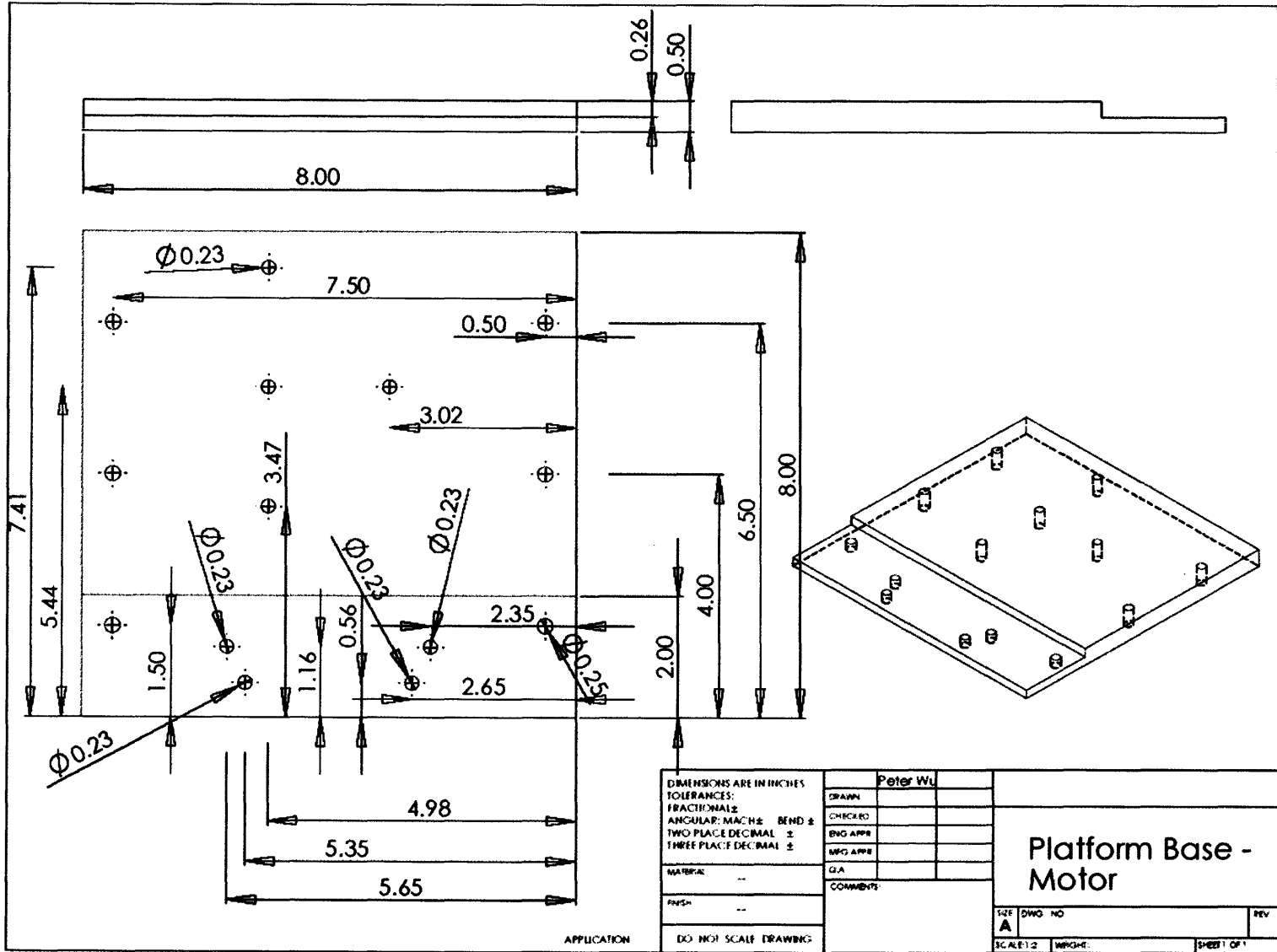
DIMENSIONS ARE IN INCHES
 TOLERANCES:
 FRACTIONAL: ±
 ANGULAR: MACH & BEND ±
 TWO PLACE DECIMAL ±
 THREE PLACE DECIMAL ±

MAT'RIA: ...
 FINISH: ...
 DO NOT SCALE DRAWING

DRAWN	Peter Wu
CHECKED	
ENG APPR	
MFG APPR	
Q.A.	
COMMENTS	

Support Bracket - Load Cell		SIZE	DWG. NO	REV.
		A		
SCALE: 1:1	WEIGHT:	SHEET 1 OF 1		

Support Bracket - Load Cell



Platform Base - Motor

DIMENSIONS ARE IN INCHES
 TOLERANCES:
 FRACTIONAL ±
 ANGULAR: MACHINE BEND ±
 TWO PLACE DECIMAL ±
 THREE PLACE DECIMAL ±

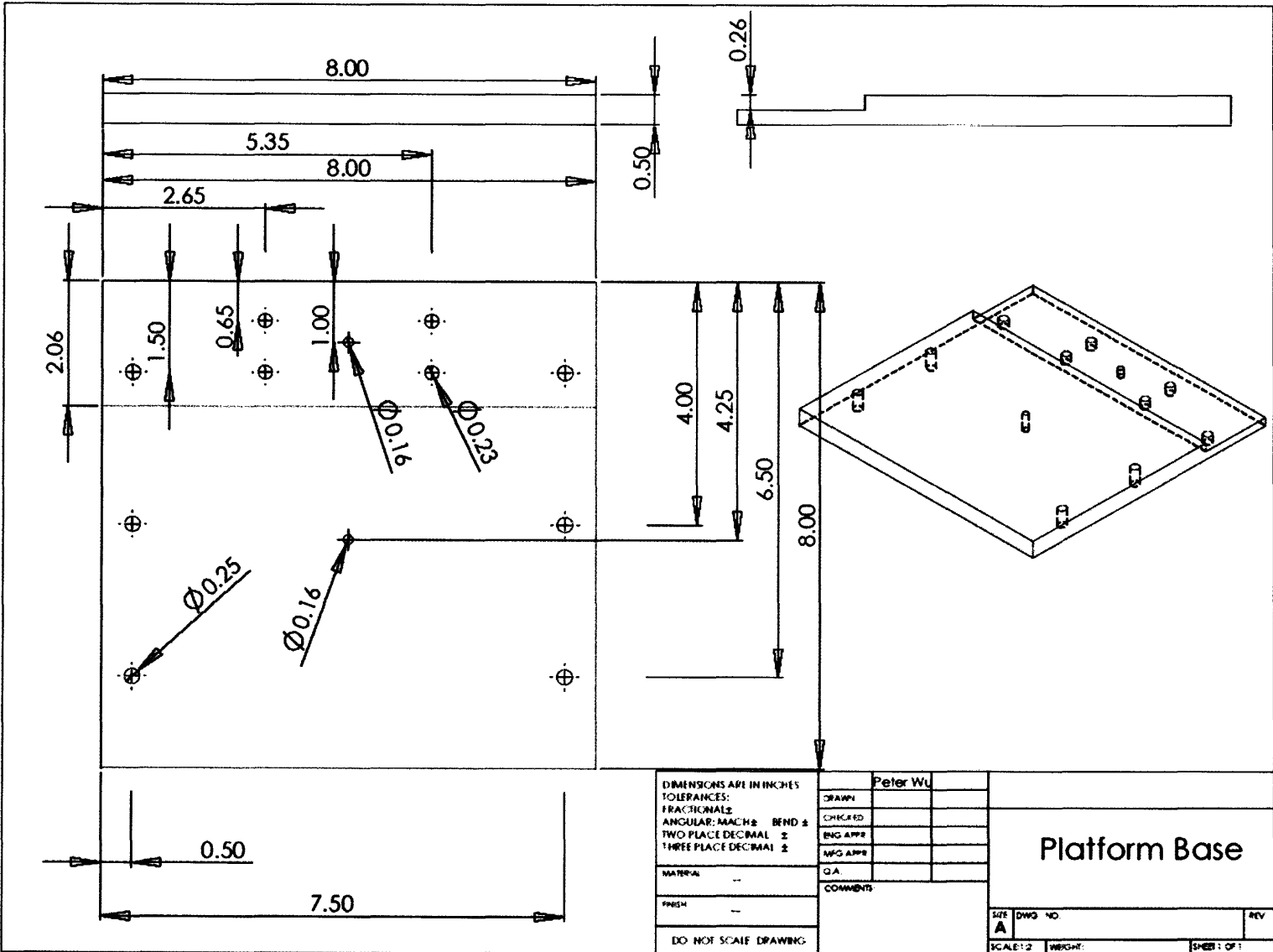
MATERIAL: --
 FINISH: --

DO NOT SCALE DRAWING

DRAWN	Peter Wu
CHECKED	
ENG APPR	
MFG APPR	
QA	
COMMENTS	

Platform Base - Motor	
SIZE	DWG NO
A	
SCALE: 1:2	INCHES
	SHEET 1 OF 1

Platform Base

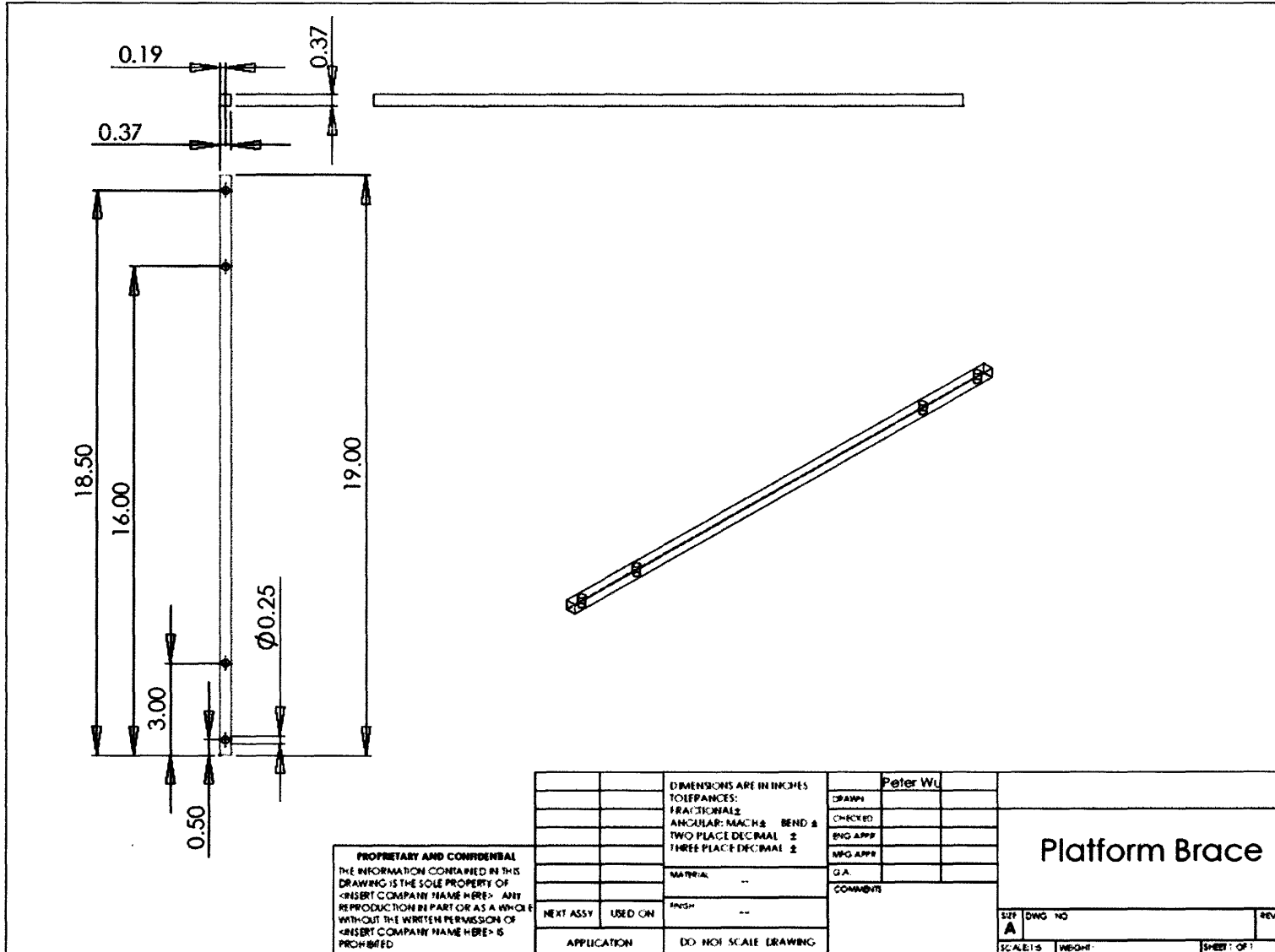


DIMENSIONS ARE IN INCHES
 TOLERANCES:
 FRACTIONALS: FRACTIONALS
 ANGULAR: MACH & BEND ± TWO PLACE DECIMAL &
 THREE PLACE DECIMAL &

DRAWN	Peter Wu	
CHECKED		
ENG APPR		
MFG APPR		
Q.A.		
COMMENTS		

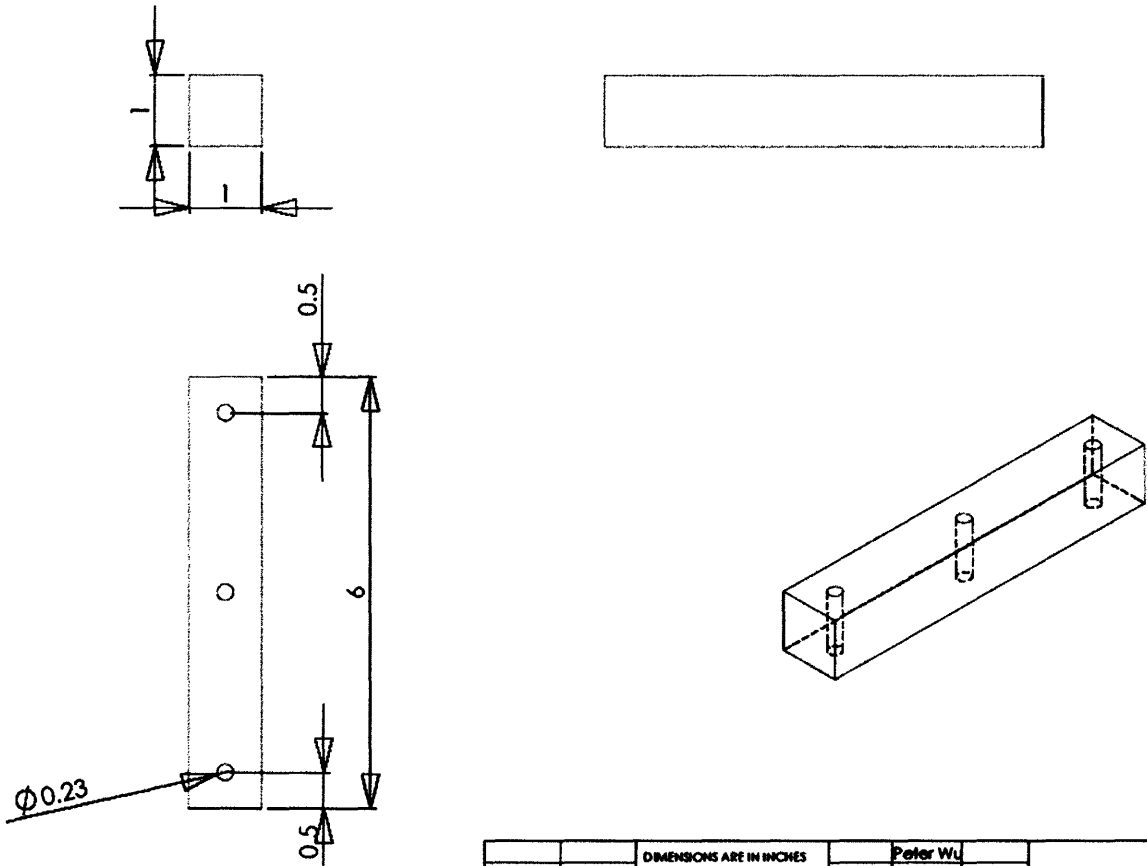
MATERIAL: --
 FINISH: --
 DO NOT SCALE DRAWING

Platform Base		
SIZE A	DWG NO.	REV
SCALE: 1:2	WEIGHT:	SHEET: OF 1



Platform Brace

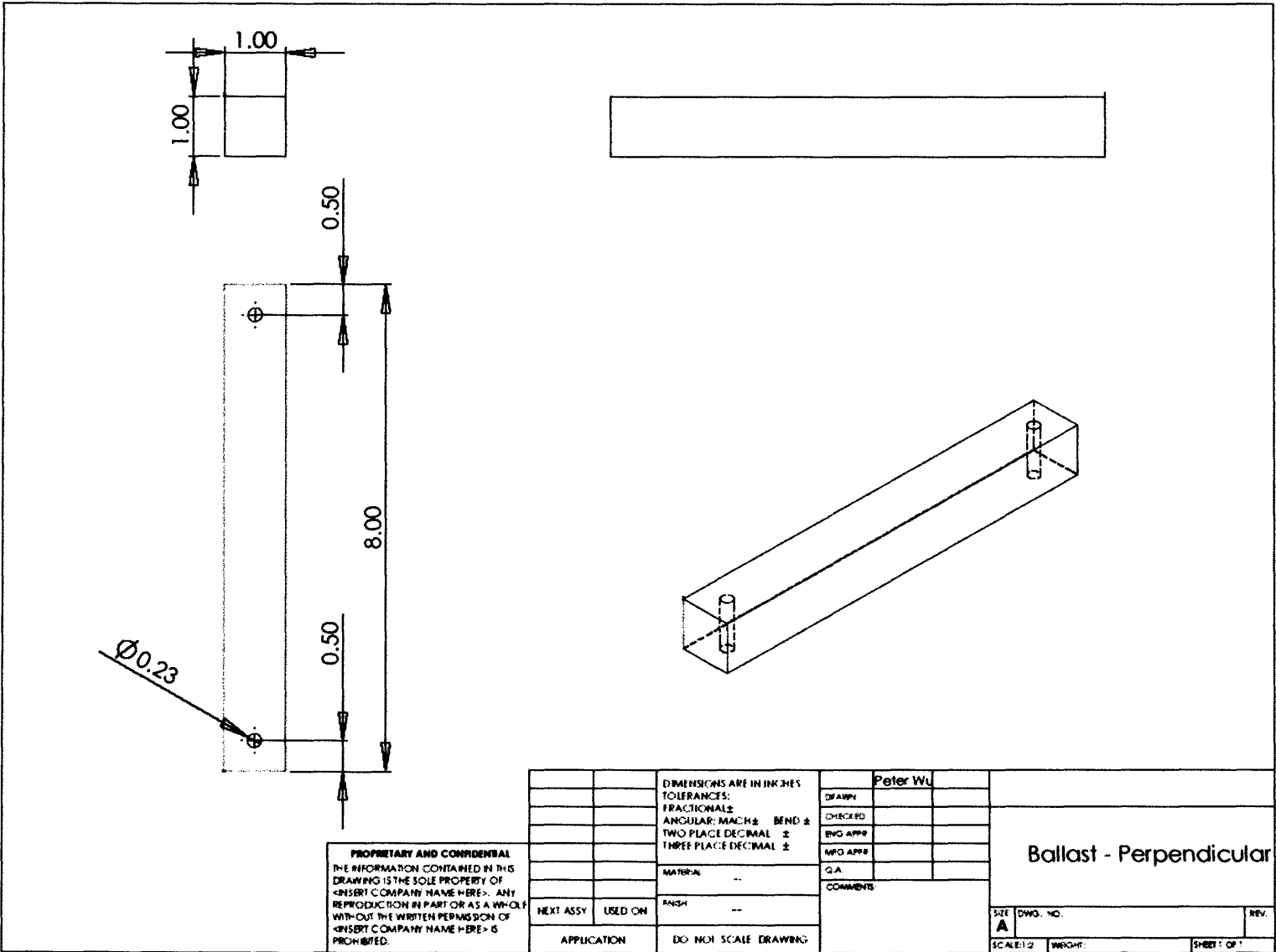
Axial Ballast on Dynamic Loading System



PROPRIETARY AND CONFIDENTIAL
 THE INFORMATION CONTAINED IN THIS
 DRAWING IS THE SOLE PROPERTY OF
 <INSERT COMPANY NAME HERE>. ANY
 REPRODUCTION IN PART OR AS A WHOLE
 WITHOUT THE WRITTEN PERMISSION OF
 <INSERT COMPANY NAME HERE> IS
 PROHIBITED.

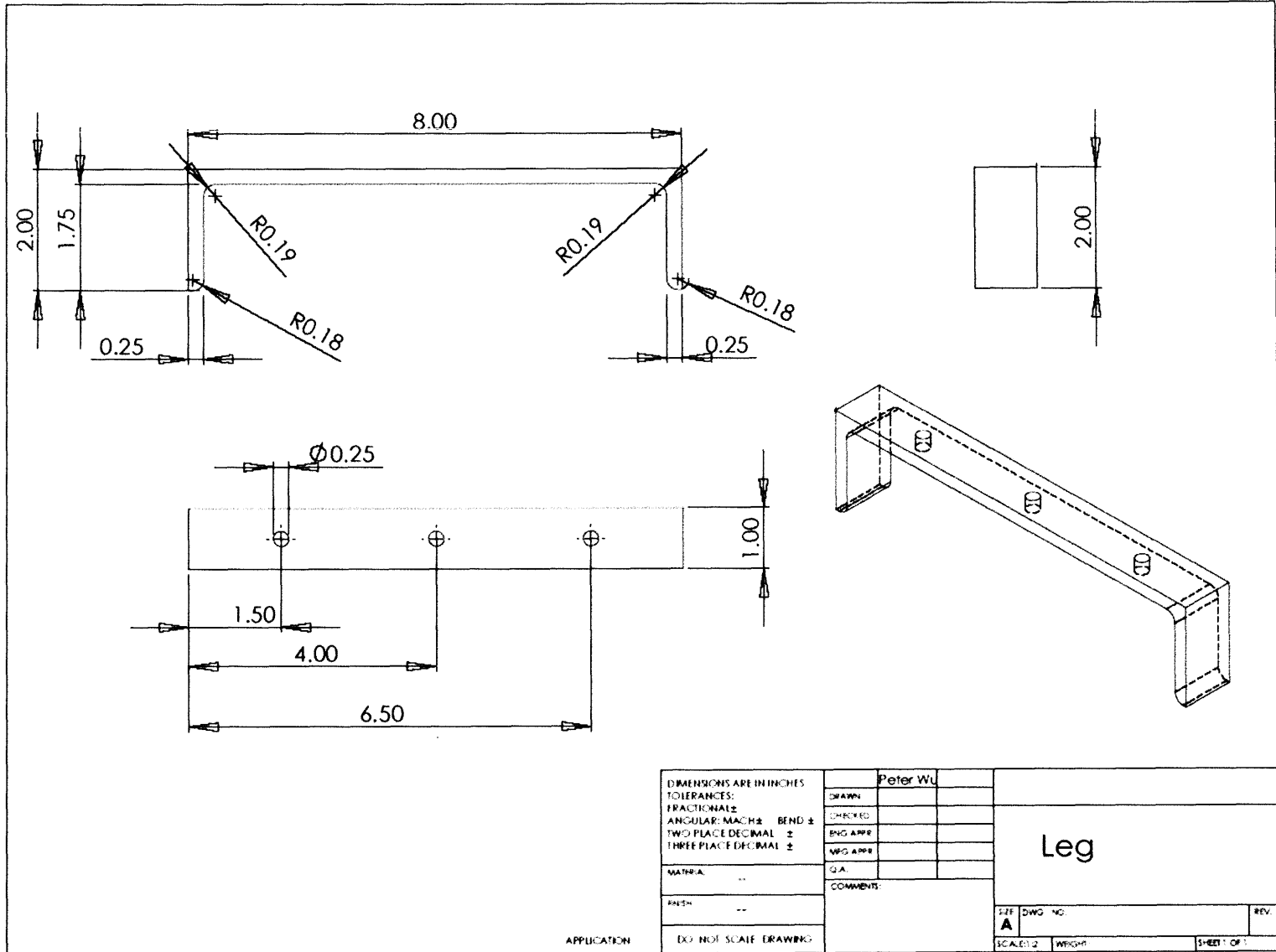
		DIMENSIONS ARE IN INCHES		Peter Wu	
		TOLERANCES:		DRAWN	
		FRACTIONAL: 1/16		CHECKED	
		ANGULAR: MACH 1/2 BEND 1/2		ENG APPR.	
		TWO PLACE DECIMAL 2		MFG APPR.	
		THREE PLACE DECIMAL 2		D.A.	
		MATERIAL --		COMMENTS:	
		FINISH --			
NEXT ASSY	USED ON			SIZE A	
APPLICATION		DO NOT SCALE DRAWING		DWG. NO.	
				SCALE: 1:2	
				WIDOW:	
				SHEET 1 OF 1	
				REV.	

Perpendicular Ballast on Dynamic Loading System



PROPRIETARY AND CONFIDENTIAL
 THE INFORMATION CONTAINED IN THIS
 DRAWING IS THE SOLE PROPERTY OF
 <INSERT COMPANY NAME HERE>. ANY
 REPRODUCTION IN PART OR AS A WHOLE
 WITHOUT THE WRITTEN PERMISSION OF
 <INSERT COMPANY NAME HERE> IS
 PROHIBITED.

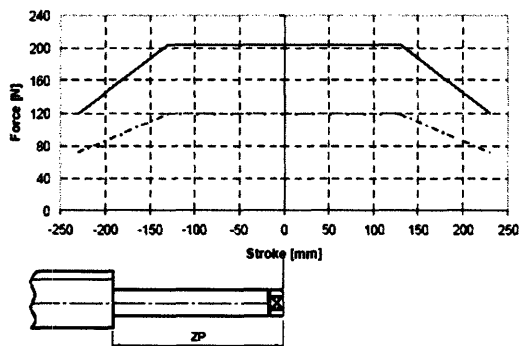
		DIMENSIONS ARE IN INCHES	Peter Wu	
		TOLERANCES:	DESIGN	
		FRACTIONAL: ±	CHECKED	
		ANGULAR: MACH ± BEND ±	ENG APPR	
		TWO PLACE DECIMAL ±	MFG APPR	
		THREE PLACE DECIMAL ±	QA	
		MATERIAL: --	COMMENTS:	
		FINISH: --		
NEXT ASSY	USED ON			
APPLICATION	DO NOT SCALE DRAWING			
			Ballast - Perpendicular	
SIZE	DWG. NO.			REV.
A				
SCALE: 1:2	WEIGHT:			SHEET 1 OF 1



APPENDIX C: MOTOR SPECIFICATIONS

Linmot® Linear Motor Specifications

Linear Motor	<i>LinMot® P01-37x240/60x260</i>
Servo Controller	<i>E100-MT</i>
Power Supply	48VDC, 150W
Peak Force, Fp	120N (27lbf)
Continuous Force, Fc	55N (12.4lbf)
Limit Force, Fb	72N (16.2lbf)
Force Constant, cF	40N/A (9lbf/A)
Maximum Stroke, s	260mm (10.2in)
Shortened Stroke, SS	60mm (2.4in)
Zero Position, ZP	75mm (3in)
Max. Acceleration, a	144m/s ² (5700in/s ²)
Max. Velocity, v	1.3m/s (51in/s)
Position Repeatability	± 0.1mm (± 0.004in)
Linearity	± 0.3%
Slider Mass, mS	829g (1.83lb)
Slider Length, lS	395mm (15.6in)



Servo Controller:

- Series 1000
supply voltage 72 V DC
phase current 5.0 A
- - - Series 100
supply voltage 48 V DC
phase current 3.0 A